

DESIGN OF LOG-PERIODIC DIPOLE ARRAY FEED  
AND  
WIDE BAND REFLECTOR ANTENNA SYSTEM

A THESIS SUBMITTED TO  
THE GRADUATE SCHOOL OF NATURAL AND APPLIED SCIENCES  
OF  
MIDDLE EAST TECHNICAL UNIVERSITY

BY

FATMA MÜGE TANYER

IN PARTIAL FULFILLMENT OF THE REQUIREMENTS  
FOR  
THE DEGREE OF MASTER OF SCIENCE  
IN  
ELECTRICAL AND ELECTRONICS ENGINEERING

MARCH 2005

Approval of the Graduate School of Natural and Applied Sciences

---

Prof. Dr. Canan ÖZGEN  
Director

I certify that this thesis satisfies all the requirements as a thesis for the degree of Master of Science and quality, as a thesis for the degree of Master.

---

Prof. Dr. İsmet ERKMEN  
Head of Department

This is to certify that we have read this thesis and that in our opinion it is fully adequate, in scope and quality, as a thesis for the degree of Master of Science.

---

Prof. Dr. Altuncan HIZAL  
Supervisor

**Examining Committee Members**

Prof. Dr. Tuncay BİRAN (METU, EE)

---

Prof. Dr. Altuncan HIZAL (METU, EE)

---

Prof. Dr. Nilgün GÜNALP (METU, EE)

---

Assoc. Prof. Dr. Gülbin DURAL (METU, EE)

---

Erdal SAYGINER M.S.E.E (ASELSAN)

---

**I hereby declare that all information in this document has been obtained and presented in accordance with academic rules and ethical conduct. I also declare that, as required by these rules and conduct, I have fully cited and referenced all material and results that are not original to this work.**

Name, Last name: Fatma Müge TANYER

Signature :

# **ABSTRACT**

## **DESIGN OF LOG-PERIODIC DIPOLE ARRAY FEED AND WIDE BAND REFLECTOR ANTENNA SYSTEM**

**TANYER, Fatma Müge**

**M.S., Department of Electrical and Electronics Engineering  
Supervisor: Prof. Dr. Altunkan HIZAL**

**March 2005, 165 pages**

The introduction of broadband systems to communication and radar technologies has demanded the design of broadband antennas. In this thesis, broadband log-periodic dipole antennas and reflector antennas are investigated. A dual polarized log-periodic dipole antenna and a reflector antenna are designed and analyzed within the frequency band of 0.4-18 GHz.

Basic theory and calculations about mutual coupling between the linear antenna elements are given. The currents at the bases of dipoles of the log-periodic antenna are found and these currents are used as inputs for the design of the reflector antenna. After the simulations made with MATLAB® and FORTRAN, a prototype single polarized log-periodic antenna is produced. Developments on the prototype antenna are performed, both to improve the electrical characteristics of the antenna and to make the final design realizable. After the performance of the

single polarized log-periodic antenna is found satisfactory, dual polarized antenna is produced.

Performances of both single and dual polarized log-periodic antennas are measured in the anechoic chamber at ASELSAN<sup>®</sup> Inc. After the measurements of the antenna, using the currents at the bases of the dipoles, a reflector antenna is designed using “MIR” program written in FORTRAN, which is based on physical optics method. A method to calculate the aperture blockage of the reflector is developed. Simulation results of reflector antenna are given.

**Keywords:** Log-Periodic Antenna, Mutual Coupling, Reflector Antenna

# ÖZ

## LOG-PERİYODİK DİPOL İLE BESLENEN GENİŞ BANTLI REFLEKTÖR ANTEN TASARIMI

**TANYER, Fatma Müge**

**Yüksek Lisans, Elektrik ve Elektronik Mühendisliği Bölümü  
Tez Yöneticisi: Prof. Dr. Altunkan HIZAL**

**Mart 2005, 165 sayfa**

Geniş bantlı sistemlerin, iletişim ve radar teknolojilerinde kullanılmaya başlanması, geniş bantlı antenlerin tasarımını gerektirmiştir. Bu tezde, geniş bantlı logaritmik periyodik ve reflektör antenlerin 0.4-18 GHz frekans bandında analizi ve tasarımı yapıldı.

Lineer anten elemanlarının arasındaki karşılıklı etkileşimlerle ilgili temel teori ve hesaplamalar verildi. Logaritmik periyodik antenin her bir dipol girişlerindeki akımlar bulundu ve bu akımlar, reflektör anten tasarımında girdi olarak kullanıldı. MATLAB® ve FORTRAN ile yapılan simülasyonlar sonucunda, tek polarizasyonlu bir ilk örnek logaritmik periyodik anten üretildi. İlk örnek anten üzerinde, antenin elektriksel özelliklerini iyileştirecek ve son tasarımı üretilebilir hale getirecek geliştirmeler yapıldı. Tek polarizasyonlu logaritmik periyodik antenin performansı tatmin edici bulunduktan sonra, çift polarizasyonlu anten üretildi.

Tek polarizasyonlu ve çift polarizasyonlu logaritmik periyodik antenlerin performansları, ASELSAN® A.Ş.'deki yankısız odada ölçüldü. Antenin ölçümlerinden sonra, FORTRAN'da yazılmış olan ve fiziksel optik metoduna dayanan "MIR" programını ve dipol girişlerindeki akımları kullanarak reflektör anten tasarımı yapıldı. Reflektör antenin açıklık blokajını hesaplamak için bir metot geliştirildi. Reflektör antenin simülasyon sonuçları verildi.

**Anahtar kelimeler:** Logaritmik Periyodik Anten, Karşılıklı Etkileşim, Reflektör Anten.

*To my family*

## **ACKNOWLEDGEMENTS**

The author wishes to express her sincere gratitude to her advisor Prof. Dr. Altunkan Hızal for his supervision, valuable guidance, helpful suggestions and tolerance.

Valuable friendship, help and support of all of the RF Design Group members, and the continued interest of Erdal Saygıner, Serhat Erzin, Ali Günay Yıldız and R. Fırat Tiğrek are particularly appreciated. The practical realization of this work would not have been possible without Murat Mutluol, for his efforts the author is grateful. The author would also like to thank to ASELSAN<sup>®</sup> Inc. for providing the facilities for the completion of this thesis.

Special appreciation and gratitude are also due to family of author, especially her brother, Dr. Ali Murat Tanyer, for their encouragement, endless love and understanding of her spending lots of time on this work.

# TABLE OF CONTENTS

<b>PLAGIARISM</b>	<b>iii</b>
<b>ABSTRACT</b>	<b>iv</b>
<b>ÖZ</b>	<b>vi</b>
<b>ACKNOWLEDGEMENTS</b>	<b>ix</b>
<b>TABLE OF CONTENTS</b>	<b>x</b>
<b>LIST OF TABLES</b>	<b>xiv</b>
<b>LIST OF FIGURES</b>	<b>xv</b>
<b>LIST OF ABBREVIATIONS</b>	<b>xx</b>
<b>CHAPTER</b>	
<b>1. INTRODUCTION</b>	<b>1</b>
1.1. RESEARCH AIMS	2
1.2. RESEARCH OBJECTIVES	2
1.3. GUIDE TO THE THESIS	2
<b>2. ADMITTANCE MATRIX APPROACH TO LOG-PERIODIC ANTENNAS</b>	<b>5</b>
2.1. INTRODUCTION	5
2.2. CHARACTERIZATION OF A TWO-PORT MICROWAVE NETWORK	6
2.3. ADMITTANCE MATRIX APPROACH	7
2.3.1. TRANSMISSION-MATRIX REPRESENTATION	8
2.3.1.1. TWO ANTENNAS CONNECTED BY A TRANSMISSION LINE	9

2.3.1.2. THREE ANTENNAS CONNECTED BY TWO TRANSMISSION LINES.....	12
2.3.1.3. FOUR ANTENNAS CONNECTED BY THREE TRANSMISSION LINES.....	16
2.3.1.4. N ANTENNAS CONNECTED BY N-1 TRANSMISSION LINES.....	18
<b>3. MUTUAL IMPEDANCE BETWEEN LINEAR ELEMENTS .....</b>	<b>20</b>
3.1. ANALYSIS OF DIPOLE ANTENNA.....	21
3.2. ANALYSIS OF THE SELF AND MUTUAL IMPEDANCE OF LINEAR ELEMENTS.....	22
3.2.1. CHECK-UP CALCULATIONS .....	27
3.2.2. SELF IMPEDANCES OF LINEAR ANTENNAS.....	31
3.2.3. MUTUAL COUPLING FOR DUAL POLARIZED LOG- PERIODIC ANTENNAS .....	35
3.2.3.1. CALCULATION OF MUTUAL COUPLING OF THE ORTHOGONAL ANTENNAS .....	37
3.2.4. CHECK-UP CALCULATIONS FOR CURRENTS OF LOG- PERIODIC ANTENNA.....	41
3.3. FAR FIELD PATTERNS OF LOG PERIODIC ANTENNA....	48
3.3.1. GENERALIZATION FOR THE FAR-FIELDS OF THE ANTENNA .....	50
<b>4. ANALYSIS AND DESIGN OF THE LOG-PERIODIC DIPOLE ANTENNA (LPDA) .....</b>	<b>52</b>
4.1. INTRODUCTION.....	52
4.2. DESCRIPTION OF LOG-PERIODIC ANTENNA .....	53
4.2.1. LOADED TRANSMISSION LINE REGION .....	55
4.2.2. ACTIVE REGION .....	59
4.2.3. INACTIVE (REFLECTIVE) REGION.....	60
4.3. EFFICIENCY OF LPDA.....	60
4.4. DESIGN OF LOG-PERIODIC DIPOLE ANTENNAS .....	62

4.4.1. FEEDING OF THE LOG-PERIODIC ANTENNA.....	65
4.4.2. DESIGNING FOR GIVEN INPUT IMPEDANCE.....	67
4.4.2.1. FEED SEPARATION FOR A DUAL POLARIZED LOG PERIODIC ANTENNA .....	70
4.5. DUAL POLARIZED LOG-PERIODIC ANTENNA DESIGN .	72
4.5.1. DESIGN PROCEDURE.....	74
4.5.2. PRODUCTION PROCESS .....	83
<b>5. ANALYSIS AND DESIGN OF THE REFLECTOR ANTENNA .....</b>	<b>84</b>
5.1. INTRODUCTION.....	84
5.2. FRONT FED PARABOLIC REFLECTORS.....	84
5.2.1. RADIATION FROM PARABOLOIDAL REFLECTORS.....	86
5.2.1.1. APERTURE INTEGRATION TECHNIQUE .....	87
5.2.1.2. INDUCED CURRENT APPROACH (PHYSICAL OPTICS).....	88
5.2.2. APERTURE EFFICIENCY AND DIRECTIVITY .....	89
5.2.3. FEED DESIGN .....	93
5.3. <i>MIR</i> PROGRAM.....	93
5.3.1. EFFICIENCY AND BLOCKAGE EFFECTS OF A REFLECTOR ANTENNA .....	96
5.3.1.1. CURVE FIT TO $F(\Psi, \xi)$ .....	97
<b>6. IMPLEMENTATIONS, MEASUREMENTS AND SIMULATIONS OF LPDA AND REFLECTOR ANTENNA .....</b>	<b>100</b>
6.1. INTRODUCTION.....	100
6.2. MEASUREMENTS OF A SINGLE POLARIZED LOG- PERIODIC ANTENNA.....	103
6.3. MEASUREMENTS OF THE DUAL POLARIZED LOG- PERIODIC ANTENNA.....	113

6.3.1. RADIATION PATTERNS OF DUAL POLARIZED LOG-PERIODIC ANTENNA.....	119
6.3.1.1. 0.4-4 GHZ FREQUENCY BAND .....	119
6.3.1.2. 4-12 GHZ FREQUENCY BAND .....	122
6.3.1.3. 12-18 GHZ FREQUENCY BAND .....	126
6.3.1.4. CROSS POLARIZED RADIATION PATTERNS.....	132
6.4. SIMULATIONS OF THE REFLECTOR ANTENNA DESIGNED USING MIR.....	134
6.4.1. EFFICIENCY AND BLOCKAGE CALCULATIONS .....	144
<b>7. CONCLUSIONS .....</b>	<b>147</b>
<b>REFERENCES .....</b>	<b>150</b>
<b>APPENDICES</b>	
<b>A. MATLAB<sup>®</sup> CODE WHICH CALCULATES THE CURRENTS AT THE BASES OF DIPOLES AND E AND H-PLANE PATTERNS OF A LPDA.....</b>	<b>153</b>
<b>B. MATLAB<sup>®</sup> CODE WHICH CALCULATES SELF AND MUTUAL IMPEDANCES OF LINEAR ELEMENTS.</b>	<b>157</b>
<b>C. FORTRAN CODE WHICH CALCULATES SELF AND MUTUAL IMPEDANCES OF LINEAR ELEMENTS.</b>	<b>158</b>
<b>D. MATLAB<sup>®</sup> CODE WHICH CALCULATES MUTUAL IMPEDANCES BETWEEN ORTHOGONAL ELEMENTS .....</b>	<b>162</b>
<b>E. TEST REPORT OF MECHANICAL STRENGTH OF THE LOG PERIODIC ANTENNA .....</b>	<b>163</b>
<b>F. SPECIFICATION OF THE COAXIAL CABLE USED IN THE CONSTRUCTION OF LPDA .....</b>	<b>164</b>

# LIST OF TABLES

## TABLES

<b>3.1</b> Mutual impedances between half wave-length dipoles with different spacing between them [3].....	28
<b>3.2</b> Mutual impedances between successive dipoles calculated in FORTRAN.	30
<b>3.3</b> Mutual impedances between successive dipoles calculated in MATLAB®.	31
<b>3.4</b> Self impedances of dipoles calculated in FORTRAN.....	33
<b>3.5</b> Self impedances of dipoles calculated in MATLAB® .....	33
<b>3.6</b> Simple formulas for the input resistance of dipoles [7] .....	34
<b>3.7</b> Self impedances of dipoles calculated by using formulas in Table 3.6 .....	34
<b>4.1</b> Dimensions of the log-periodic antenna (all dimensions are in mm.) .....	82
<b>5.1</b> Minimum gain requirements for the reflector antenna.....	94
<b>5.2</b> Values of the electrical fields for different $\Psi$ and $\xi$ angles. ....	98
<b>5.3</b> Values of the field magnitudes, $ F(\Psi, \xi) $ for different $\Psi$ and $\xi$ angles... ..	98
<b>6.1</b> Comparison of HPBW's calculated using MATLAB and MIR program..	134
<b>6.2</b> Summary information about the simulated patterns .....	143
<b>6.3</b> Gains and efficiencies considering blockage and no blockage effects .....	144
<b>6.4</b> Gain loss due to efficiency and blockage effects.....	145

# LIST OF FIGURES

## FIGURES

2.1 Log-periodic dipole array [2].....	5
2.2 A two port network .....	6
2.3 Transmission line segment .....	8
2.4 Transmission line segment with cross over of lines.....	9
2.5 Two antennas connected by a transmission line .....	10
2.6 Three antennas connected by two transmission lines .....	13
2.7 Four antennas connected by three transmission lines .....	16
2.8 Detailed view of $A_1$ , $A_2$ , $A_3$ and $A_4$ .....	16
3.1 Transmission line with an antenna and with an equivalent impedance [1] .....	20
3.2 Geometry for the analysis of dipole antenna .....	21
3.3 Two port network and its T-equivalent [2].....	22
3.4 Position of two dipole antennas used in the analysis of self and mutual impedances.....	24
3.5 Self resistance and reactance of dipole antenna [2] .....	26
3.6 Variation of mutual impedance between two parallel dipoles $\lambda/2$ long as a function of the separation $d/\lambda$ [4] .....	29
3.7 Log-periodic antenna used in calculation of mutual impedances between dipoles.....	30
3.8 Geometry used in calculation of the self impedance [5] .....	32
3.9 Two antennas connected by a transmission line in a dual polarized log-periodic antenna .....	35
3.10 Detailed view of dipole antennas which are perpendicular to each other. ....	36
3.11 Approximations on Figure 3.9(a).....	36
3.12 Two dipole antennas orthogonal to each other .....	37
3.13 Two dipole antennas orthogonal to each other with no assumption of zero wire radius of the second antenna.....	38
3.14 Detailed view of the cross-section of the second antenna in Figure 3.13 .....	38

<b>3.15</b> Absolute values of currents given in Joachim [6] (left) versus calculated ones in MATLAB <sup>®</sup> at frequencies 100 MHz, 150 MHz and 200 MHz from top to bottom respectively .....	42
<b>3.16</b> Phases of currents given in Joachim [6] (left) versus calculated ones in MATLAB <sup>®</sup> at frequencies 100 MHz, 150 MHz and 200 MHz from top to bottom respectively.....	43
<b>3.17</b> Dipole base currents for the log periodic antenna given in Stutzman and Gary [7].....	44
<b>3.18</b> Calculated dipole base currents in MATLAB <sup>®</sup> .....	45
<b>3.19</b> Dipole base currents for the log periodic antenna given in Balanis [2] (left) versus calculated ones in MATLAB <sup>®</sup> at the frequency where element number 10 is $\frac{\lambda}{2}$ .....	46
<b>3.20</b> Phases of currents given in Balanis [2] (left) versus calculated ones in MATLAB <sup>®</sup> at the frequency where element number 10 is $\frac{\lambda}{2}$ .....	47
<b>3.21</b> Finite dipole geometry.....	48
<b>3.22</b> Zoomed view of Figure 3.21 where dipoles are in xz plane (on the page) ....	49
<b>3.23</b> Orientation of a log-periodic antenna on the Cartesian coordinate system....	50
<b>3.24</b> Zoomed view of Figure 3.21 where dipoles are in xz plane (into the page) ..	51
<b>4.1</b> Main regions of a log-periodic dipole antenna [8].....	55
<b>4.2</b> Feeder field for a log-periodic antenna [5].....	56
<b>4.3</b> Radiation field for a log-periodic antenna [5] .....	56
<b>4.4</b> Voltage distribution for log periodic antenna composed of 13 elements [2] ...	57
<b>4.5</b> $Vt/c$ versus $\sigma$ for $\tau = 0.8$ and $0.97$ with $Z_0 / Z_a = 0.33$ [5].....	58
<b>4.6</b> Element currents for the array given in Figure 4.4 [2].....	59
<b>4.7</b> Radiating efficiency of active region vs. relative length of longest element [5] .....	61
<b>4.8</b> Radiating efficiency of the active region vs. feeder impedance and $\tau$ [5].....	62
<b>4.9</b> Computed contours of constant directivity versus $\tau$ and $\sigma$ for log periodic dipole arrays [2] .....	63
<b>4.10</b> Unsuccessful method of feeding the antenna [5] .....	65
<b>4.11</b> Successful method of feeding the antenna [2].....	66

<b>4.12</b>	Energizing dipoles by using coaxial line [5] .....	66
<b>4.13</b>	Relative characteristic impedance of feeder vs. relative characteristic impedance of dipole element for different values of $\sigma'$ [2] .....	68
<b>4.14</b>	$R_0$ vs. $\sigma$ for $Z_0=100$ and $Z_a=350$ for two values of $\tau$ [5].....	69
<b>4.15</b>	Top view of feeder line configuration .....	70
<b>4.16</b>	Top view of a pair of feed lines for a dual polarized log periodic antenna ....	71
<b>4.17</b>	Two feeder conductors from Figure 4.16 .....	71
<b>4.18</b>	Detailed view of a of feed line and the positioning of the dipoles on the transition regions .....	77
<b>4.19</b>	Modified form of detailed view of a of feed line and the positioning of the dipoles on the transition regions.....	79
<b>4.20</b>	Final form of detailed view of a of feed line and the positioning of the dipoles on the transition regions.....	81
<b>5.1</b>	The surface geometry of a paraboloidal reflector .....	84
<b>5.2</b>	Parabolic reflector taper and spillover efficiencies as a function of reflector angular aperture.....	92
<b>5.3</b>	Scaled down version of the reflector antenna designed using “MIR” .....	95
<b>5.4</b>	Geometrical parameters for the paraboloidal reflector [18] .....	96
<b>5.5</b>	Blocked region of the reflector antenna .....	99
<b>6.1</b>	Top View of the Anechoic Chamber in ASELSAN <sup>®</sup> Inc. [9] .....	101
<b>6.2</b>	Antenna Measurement Setup in Anechoic Chamber .....	102
<b>6.3</b>	First production of single polarized log periodic antenna .....	103
<b>6.4</b>	Input Return Loss of the Antenna given in Figure 6.3.....	104
<b>6.5</b>	Coaxial cable construction on the top part of the log-periodic antenna.....	104
<b>6.6</b>	Modification of the coaxial cable construction given in Figure 6.5 .....	105
<b>6.7</b>	Zoom to the tip of the tuned antenna with a small piece of metal.....	106
<b>6.8</b>	$S_{11}$ improvement with small piece of metal.....	106
<b>6.9</b>	Comparison of the H plane patterns when the coaxial cable construction differs in Figure 6.5 and Figure 6.6 at frequencies 12 GHz (a), 16.08 GHz (b), 16.44 GHz (c) and 18 GHz (d). .....	108
<b>6.10</b>	Thinnest part of the antenna.....	109
<b>6.11</b>	Modified form of the thinnest part of the antenna .....	110

<b>6.12</b>	Comparison of the H plane patterns when the top parts of the antennas are different as seen in Figure 6.7 and Figure 6.11 at frequencies 12 GHz (a), 16.08 GHz (b), 16.44 GHz (c) and 18 GHz (d).....	112
<b>6.13</b>	$S_{11}$ comparison between the tuned antenna and the final design of the single polarized antenna.....	113
<b>6.14</b>	Full drawing of 0.4-18 GHz dual polarized LPDA.....	114
<b>6.15</b>	Full photo of 0.4-18 GHz dual polarized LPDA.....	115
<b>6.16</b>	Return loss of dual polarized log periodic antenna.....	116
<b>6.17</b>	Comparison of the return losses of dual polarized and single polarized log periodic antennas .....	116
<b>6.18</b>	Top and smallest part of the full drawing given in Figure 6.14.....	117
<b>6.19</b>	Practical realization of the smallest part of the antenna given in Figure 6.18 .....	118
<b>6.20</b>	Connectors at the bottom of the antenna .....	118
<b>6.21</b>	E and H plane patterns of dual polarized log periodic antenna measured from two ports of the antenna at frequencies 0.76 GHz (a), 1.12 GHz (b), 2.056 GHz (c), 2.992 GHz (d) and 4 GHz (e) respectively .....	121
<b>6.22</b>	E and H plane patterns of dual polarized log periodic antenna measured from two ports of the antenna at frequencies 4 GHz (a), 4.96 GHz (b), 6.08 GHz (c), 7.04 GHz (d), 8.16 GHz (e), 8.96 GHz (f), 10.08 GHz (g) and 11.04 GHz (h) respectively.....	126
<b>6.23</b>	E and H plane patterns of dual polarized log periodic antenna measured from two ports of the antenna at frequencies 12 GHz (a), 13.08 GHz (b), 14.88 GHz (c-1, c-2), 15.96 GHz (d-1, d-2), 17.04 GHz (e-1, e-2) and 18 GHz (f-1, f-2) respectively .....	131
<b>6.24</b>	Cross polarized patterns measured from the vertical port of the dual polarized log periodic antenna at various frequencies between 0.76-4 GHz (a), 5.12-10.08 GHz (b) and 12-18 GHz(c).....	133
<b>6.25</b>	Simulated E plane pattern at 0.4 GHz .....	135
<b>6.26</b>	Simulated H plane pattern at 0.4 GHz.....	135
<b>6.27</b>	Simulated E plane pattern at 2 GHz.....	136
<b>6.28</b>	Simulated H plane pattern at 2 GHz.....	136
<b>6.29</b>	Simulated E plane pattern at 7 GHz.....	137

<b>6.30</b>	Simulated H plane pattern at 7 GHz.....	137
<b>6.31</b>	Zoomed simulated E plane pattern at 7 GHz.....	138
<b>6.32</b>	Zoomed simulated H plane pattern at 7 GHz .....	138
<b>6.33</b>	Simulated E plane pattern at 12 GHz .....	139
<b>6.34</b>	Simulated H plane pattern at 12 GHz.....	139
<b>6.35</b>	Zoomed simulated E plane pattern at 12 GHz.....	140
<b>6.36</b>	Zoomed simulated H plane pattern at 12 GHz.....	140
<b>6.37</b>	Simulated E plane pattern at 18 GHz .....	141
<b>6.38</b>	Simulated H plane pattern at 18GHz.....	141
<b>6.39</b>	Zoomed simulated E plane pattern at 18 GHz.....	142
<b>6.40</b>	Zoomed simulated H plane pattern at 18 GHz.....	142
<b>6.41</b>	Gain of the reflector antenna calculated using Kraus's formula.....	143
<b>6.42</b>	Gain of the reflector calculated from the Kraus's formula and net gain after the losses due to efficiency and blockage are taken into account .....	145
<b>6.43</b>	Perspective and side views of the reflector antenna together with feed.....	146

## **LIST OF ABBREVIATIONS**

LPDA	Log Periodic Dipole Array
MIR	Microwave Reflector
HPBW	Half Power Beam Width

# CHAPTER I

## INTRODUCTION

The introduction of broadband systems to communication and radar technologies has demanded the design of broadband antennas. Log-Periodic antennas are widely used for applications where a large frequency band is needed. At any frequency, only a small part of the whole structure is active. Electrical properties of a log-periodic antenna such as input impedance, pattern, directivity, side lobe level, beamwidth variations are periodic with the logarithm of the frequency. Antennas obtained from this principle are called log-periodic. Successive dipole lengths, dipole diameters and distance of the successive dipoles from the apex of the antenna are related by the constant  $\tau$ . If  $\tau$  is selected very close to 1, the variations over the frequency band will be small. In practice, even with  $\tau$  which is not very close to 1, good frequency-independent characteristics are observed. Horn antennas and spiral antennas are the other examples for wide band antennas.

The first log-periodic antenna which is bidirectional was introduced by Isbell and DuHammel [5]. Later, Isbell could obtain a unidirectional pattern by using a nonplanar arrangement of the two halves of the antenna. Then he introduced the most commonly used antenna, log-periodic dipole array.

In long distance radio communication and high resolution radar applications, antennas with high gain are required. Reflector antennas are the most widely used and the cheapest large aperture (high gain) antennas. They have gains over 30 dB above S-band (2-4 GHz). When an antenna at its focus feed the reflector, reflector collimates the power into a large aperture plane, which is the projected area of the reflector. The reflector has theoretically zero degree beamwidth therefore it practically has very high gain. Phased array antennas are another alternative to get high gain, but they are very expensive compared to reflector antennas. Therefore, a reflector antenna with log periodic feed antenna may be used for a very wide

band and high gain antenna application. To get both vertical and horizontal polarizations, dual polarized feed antenna can be used instead of a single polarized one.

### **1.1. RESEARCH AIMS**

The aims of this research are:

- To design a dual polarized log periodic antenna with a frequency range of 0.4-18 GHz.
- To construct a dual polarized log periodic antenna from the design above.
- To simulate the pattern of the log periodic antenna.
- Using the pattern of the log periodic feed antenna as incident field, to design a reflector antenna with required gain characteristics.

### **1.2. RESEARCH OBJECTIVES**

The objectives of this research are:

- To investigate previous log periodic dipole antenna design methods.
- To model and simulate the LPDA
- To construct and measure all the electrical characteristics of the LPDA and to make necessary improvements on the antenna
- To construct the dual polarized LPDA and make all the measurements related to it.
- To simulate the reflector antenna using the physical dimensions and the pattern of the LPDA

### **1.3. GUIDE TO THE THESIS**

Chapter 1 gives an introduction to the thesis. Research aims and objectives are stated.

In Chapter 2, admittance matrix approach to log-periodic antenna is given. A general rule to find the currents at the bases of the dipoles of a log-periodic antenna composed of N dipoles is stated. This approach is based on finding the self and mutual impedances of the dipoles in the log-periodic antenna.

Chapter 3 is devoted to mutual impedance between linear antenna elements. First, basic information about mutual coupling then some theoretical analyses are given. Then, the mutual couplings are calculated by MATLAB<sup>®</sup> and FORTRAN simulations. These results are compared with each other to see if both programs give approximately the same results, and these results are also compared with other examples given in literature [1], [3]. In Chapter 3, mutual coupling between orthogonal elements is also discussed and programmed in MATLAB<sup>®</sup>. Then, a MATLAB<sup>®</sup> program utilizing the mutual coupling matrices is used to find the absolute values and phases of the currents of the antenna and these results are compared with the ones given in literature. [2], [6], [7]. At the end of this chapter E and H-plane patterns of a log-periodic antenna, using the currents calculated by MATLAB<sup>®</sup> are discussed and also programmed.

Analysis and design procedure of a log-periodic antenna are given in Chapter 4. First of all, basic information about log-periodic antennas and different regions in a log-periodic antenna are discussed. Then, some design parameters for a single polarized log-periodic antenna are given. In designing a dual polarized antenna some additional parameters are needed. These are also given in Chapter 4. At the end of this chapter, the design of a dual polarized antenna which will be one of the products of this thesis is given step by step. Practical realizations of the designed antennas are also discussed. Some drawings and the production processes of the antennas are also given in this chapter.

In Chapter 5, analysis and design techniques of reflector antennas are discussed. First, brief information, then some analysis techniques about reflector antennas are given. The design of a reflector antenna which is another product of this thesis is accomplished. The feed of the reflector antenna is the dual polarized log-periodic antenna which is the first product of this thesis. The currents at the bases of the

dipoles of the log-periodic antenna are used as input for the reflector antenna design. Far field patterns of the reflector are calculated by the MIR program which is written in FORTRAN. In this chapter, gain reduction of the designed reflector antenna due to efficiency of the antenna and the blocked region are calculated using the output file of the MIR program and also programmed in MATLAB<sup>®</sup>. Dimensions related to the designed LPDA and the reflector antenna are given also in this chapter.

Implementations and measurements of LPDA and reflector antenna are given in Chapter 6. Some photos and drawings, related to the final form of LPDA and the reflector antenna, are given in this Chapter. Improvement of the two designed LPDA is discussed. SWR, E and H-plane patterns of the antenna and simulated E and H-planes of the reflector antenna together with half-power beamwidths are also given.

Chapter 7 is devoted to the conclusions of the results obtained from all of the simulations and measurements done throughout the thesis. New ideas and possible future works are given also in this chapter.

Finally in Appendices, MATLAB<sup>®</sup> codes to find the currents at the bases of a log-periodic dipole antenna, E and H-plane patterns of the antenna, mutual impedances between the linear and orthogonal antenna elements are given. FORTRAN codes which calculates mutual impedances between the linear antenna elements and which calculates the far field pattern of a reflector antenna are also given in appendices. Test report to specify the mechanical strength of the LPDA produced in the scope of this thesis and physical and mechanical properties of the coaxial cable used in the construction of LPDA takes place in this section.

## CHAPTER II

### ADMITTANCE MATRIX APPROACH TO LOG-PERIODIC ANTENNAS

#### 2.1. INTRODUCTION

The log periodic antenna, described in Figure 2.1, consists of parallel linear dipole elements arranged side by side in a plane and forming a coplanar array. Currents at the bases of the dipoles are used to determine the pattern of the log periodic antenna. To calculate the dipole base currents, admittance matrix approach to LPDA, which uses the mutual couplings between the dipoles, is utilized. Admittance matrix approach to LPDA will be detailed in this chapter. Dipole base currents will be used for the design of the reflector antenna which will be designed in the scope of this thesis

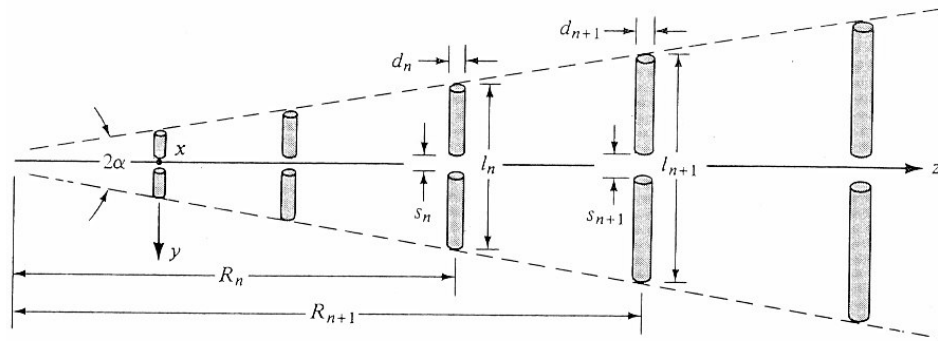


**Figure 2.1** Log-periodic dipole array [2]

## 2.2. CHARACTERIZATION OF A TWO-PORT MICROWAVE NETWORK

The ABCD parameters can be used to characterize a two-port microwave network.

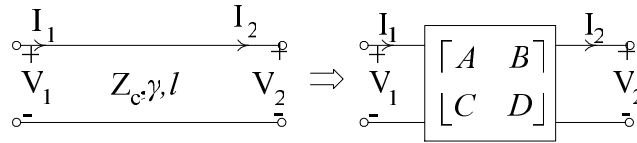


**Figure 2.2** A two port network

Definitions of some parameters in Figure 2.2 are as follows:

$Z_c$  is the characteristic impedance of the transmission line,

$\gamma$  is the propagation constant,

$$\gamma = \alpha + j\beta \text{ where}$$

$\alpha$  is attenuation constant (Np/m) and

$\beta$  is the phase constant (rad/m),

$l$  is the length of the transmission line.

For Figure 2.2, ABDC matrix of the transmission line in terms of currents and voltages can be written as follows:

$$\begin{bmatrix} V_1 \\ I_1 \end{bmatrix} = \begin{bmatrix} A & B \\ C & D \end{bmatrix} \begin{bmatrix} V_2 \\ I_2 \end{bmatrix} \quad \text{Equation 2.1}$$

where  $A = \text{Cosh} \gamma l = D$

$$B = Z_c \text{Sinh} \gamma l \text{ and}$$

$$C = \frac{1}{Z_c} \text{Sinh} \gamma l$$

For lossless transmission lines,  $\alpha = 0 \Rightarrow \text{Cosh} \alpha l = 1$  and  $\text{Sinh} \alpha l = 0$  since

$$\text{Cosh} \gamma l = \text{Cosh}(\alpha + j\beta)l = \text{Cosh} \alpha l \cdot \text{Cosh} j\beta l + \text{Sinh} \alpha l \cdot \text{Sinh} j\beta l = \text{Cosh} j\beta l = \text{Cos} \beta l$$

and

$$\text{Sinh} \gamma l = \text{Sinh}(\alpha + j\beta)l = \text{Sinh} \alpha l \cdot \text{Cosh} j\beta l + \text{Sinh} j\beta l \cdot \text{Cosh} \alpha l = \text{Sinh} j\beta l = j \text{Sin} \beta l$$

Thus, the new forms of A, B, C and D are:

$$A = \text{Cos} \beta l = D, \quad B = Z_c j \text{Sin} \beta l \text{ and } C = \frac{1}{Z_c} j \text{Sin} \beta l \quad \text{Equation 2.2}$$

### 2.3. ADMITTANCE MATRIX APPROACH

In this section, an admittance matrix approach to find the currents at the bases of the dipole elements of a log periodic dipole antenna will be given. First, currents for the antenna composed of two dipoles will be investigated and then the procedure for the antenna with two dipoles will be extended to a procedure for an antenna composed of three and four dipoles respectively. Finally, a procedure to find the current at the bases of the dipoles will be summarized for a log periodic antenna composed of N dipoles. Similar procedure is presented in Stutzman and Thiele [7].

### 2.3.1. TRANSMISSION-MATRIX REPRESENTATION

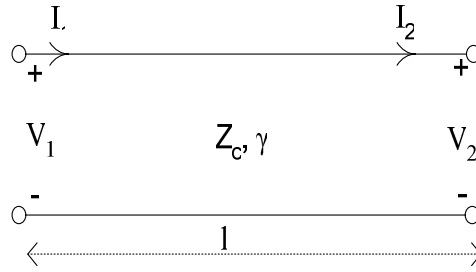


**Figure 2.3** Transmission line segment

For Figure 2.3, voltages and currents can be related as follows:

Substituting Equation 2.2 into Equation 2.1 gives:

$$I_1 = I_2 \cos \beta l + jY_c V_2 \sin \beta l \quad \text{Equation 2.3-a}$$

$$V_1 = V_2 \cos \beta l + jY_c^{-1} I_2 \sin \beta l \quad \text{Equation 2.3-b}$$

Rewriting the equations above in matrix form, we get:

$$\begin{bmatrix} V_1 \\ I_1 \end{bmatrix} = \begin{bmatrix} \cos \beta l & jY_c^{-1} \sin \beta l \\ jY_c \sin \beta l & \cos \beta l \end{bmatrix} \begin{bmatrix} V_2 \\ I_2 \end{bmatrix} \quad \text{Equation 2.4}$$

For the log periodic antenna, transmission lines between the dipole elements are crisscrossed and connected to each other. This crisscrossing of the lines is represented in Figure 2.4 as follows:

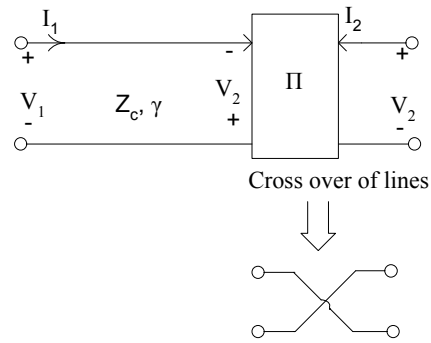


**Figure 2.4** Transmission line segment with cross over of lines

Considering the crisscrossing of the lines, Equations 2.3.a and 2.3.b takes the following form:

$$I_1 = I_2 \cos \beta l - jY_c V_2 \sin \beta l \quad \text{Equation 2.5-a}$$

$$V_1 = -V_2 \cos \beta l + jY_c^{-1} I_2 \sin \beta l \quad \text{Equation 2.5-b}$$

$$\text{Let } C = \cos \beta l \text{ and } S = \sin \beta l \quad \text{Equation 2.6}$$

### 2.3.1.1. TWO ANTENNAS CONNECTED BY A TRANSMISSION LINE

In this section, the current relation between the two antennas connected by a transmission line will be investigated.

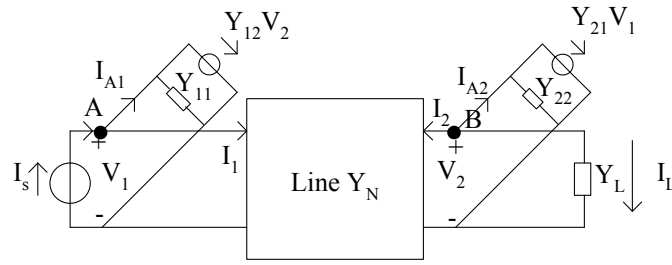


**Figure 2.5** Two antennas connected by a transmission line

In Figure 2.5, the excitation current is represented by  $I_s$ , the self admittances of the two antennas are represented by  $Y_{11}$  and  $Y_{22}$  and the mutual admittances of the antennas are represented by  $Y_{12}$  and  $Y_{21}$ .  $Y_L$  is the load admittance.  $Y_N$  is an admittance matrix for the transmission line between the two antennas and defined as:

$$[Y_N] = \frac{Y_c}{jS} \begin{bmatrix} C & 1 \\ 1 & C \end{bmatrix}, Y_c = Z_c^{-1} \quad \text{Equation 2.7}$$

In Figure 2.5, applying Kirchoff's current law at nodes A and B:

$$I_s = I_{A1} + I_1 \quad \text{Equation 2.8}$$

$$I_{A2} + I_2 + I_L = 0 \Rightarrow I_{A2} + I_2 + Y_L \cdot V_2 = 0 \quad \text{Equation 2.9}$$

Rewriting Equation 2.5.b by using Equation 2.6:

$$V_1 + V_2 \cdot C = jY_c^{-1} \cdot S \cdot I_2 \Rightarrow I_2 = \frac{Y_c}{j \cdot S} (V_1 + V_2 \cdot C) \quad \text{Equation 2.10}$$

Replacing Equation 2.10 into Equation 2.5-a:

$$I_1 = \frac{Y_c}{j.S}(V_1 + V_2.C).C - j.Y_c.V_2.S$$

$$\Rightarrow I_1 = \frac{Y_c}{j.S}.C.V_1 + \left(\frac{Y_c}{j.S}.C^2 - j.Y_c.S\right).V_2$$

$$\Rightarrow I_1 = \frac{Y_c}{j.S}.C.V_1 + \frac{Y_c}{jS}\left(C^2 - j.Y_c.S.\frac{j.S}{Y_c}\right).V_2$$

Since  $\text{Cos}^2 \beta l + \text{Sin}^2 \beta l = 1$  ( $C^2 + S^2 = 1$ ), then:

$$I_1 = \frac{Y_c}{j.S}(C.V_1 + V_2) \quad \text{Equation 2.11}$$

Rewriting Equation 2.10 and Equation 2.11 in matrix form:

$$\begin{bmatrix} I_1 \\ I_2 \end{bmatrix} = \frac{Y_c}{jS} \begin{bmatrix} C & 1 \\ 1 & C \end{bmatrix} \begin{bmatrix} V_1 \\ V_2 \end{bmatrix} \text{ and using Equation 2.7} \Rightarrow$$

$$\begin{bmatrix} I_1 \\ I_2 \end{bmatrix} = [Y_N] \begin{bmatrix} V_1 \\ V_2 \end{bmatrix} \quad \text{Equation 2.12}$$

Rewriting Equation 2.8 and Equation 2.9 in matrix form:

$$\begin{bmatrix} I_S \\ 0 \end{bmatrix} = \begin{bmatrix} I_{A1} \\ I_{A2} \end{bmatrix} + \begin{bmatrix} I_1 \\ I_2 \end{bmatrix} + \begin{bmatrix} 0 \\ Y_L.V_2 \end{bmatrix} \quad \text{Equation 2.13}$$

where

$$\begin{bmatrix} I_{A1} \\ I_{A2} \end{bmatrix} = [Y_A] \begin{bmatrix} V_1 \\ V_2 \end{bmatrix} \text{ and } [Y_A] = [Z_A]^{-1} \quad \text{Equation 2.14}$$

In Equation 2.14,  $[Z_A]$  is a matrix which is composed of the self impedances of the dipole elements and the mutual impedances between the dipole elements. For example for an antenna composed of two dipoles,

$$[Z_A] = \begin{bmatrix} Z_{11} & Z_{12} \\ Z_{21} & Z_{22} \end{bmatrix} \text{ where;}$$

$Z_{11}$  is the self impedance of the first dipole,

$Z_{22}$  is the self impedance of the second element,

$Z_{12}=Z_{21}$  is the mutual impedance between two dipoles.

Replacing Equation 2.12 and Equation 2.14 into Equation 2.13:

$$\begin{bmatrix} I_s \\ 0 \end{bmatrix} = [Y_A] \begin{bmatrix} V_1 \\ V_2 \end{bmatrix} + [Y_N] \begin{bmatrix} V_1 \\ V_2 \end{bmatrix} + \begin{bmatrix} 0 & 0 \\ 0 & Y_L \end{bmatrix} \begin{bmatrix} V_1 \\ V_2 \end{bmatrix} \Rightarrow$$

$$\begin{bmatrix} I_s \\ 0 \end{bmatrix} = \left( [Y_A] + [Y_N] + \begin{bmatrix} 0 & 0 \\ 0 & Y_L \end{bmatrix} \right) \begin{bmatrix} V_1 \\ V_2 \end{bmatrix} \quad \text{Equation 2.15}$$

For a given excitation current,  $I_s$  (for example  $I_s=1$  ampere),  $\begin{bmatrix} V_1 \\ V_2 \end{bmatrix}$  can be solved.

Finally the currents at the bases of the dipoles can be found using Equation 2.14.

### 2.3.1.2. THREE ANTENNAS CONNECTED BY TWO TRANSMISSION LINES

Let us consider three antennas connected to each other by two transmission lines. The current relations on the dipoles can be related through the similar procedure which is described above.

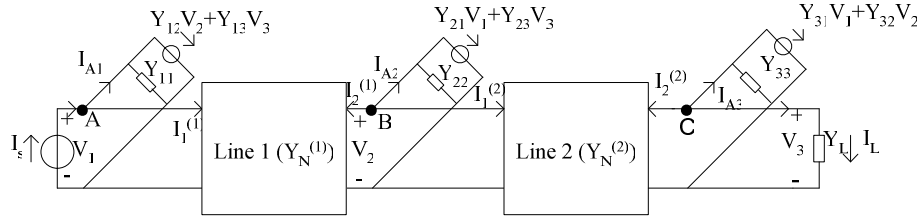


**Figure 2.6** Three antennas connected by two transmission lines

In Figure 2.6,  $I_s$  represents the excitation current,  $Y_{11}$ ,  $Y_{22}$  and  $Y_{33}$  represent the self admittances of the antennas and the mutual admittances of the antennas are represented by  $Y_{12}$ ,  $Y_{21}$ ,  $Y_{13}$ ,  $Y_{31}$ ,  $Y_{23}$ ,  $Y_{32}$ .  $Y_N^{(1)}$  and  $Y_N^{(2)}$  are admittance matrices for the transmission lines between the dipoles and  $Y_L$  is the load admittance.

In Figure 2.6, applying Kirchoff's current law at node A, B and C:

$$I_s = I_{A1} + I_1^{(1)} \quad \text{Equation 2.16}$$

$$0 = I_{A2} + I_2^{(1)} + I_1^{(2)} \quad \text{Equation 2.17}$$

$$0 = I_{A3} + I_2^{(2)} + Y_L \cdot V_3 \quad \text{Equation 2.18}$$

where the superscripts on I's show the line number.

Rewriting the Equation 2.16, Equation 2.17 and Equation 2.18 in matrix form:

$$\begin{bmatrix} I_s \\ 0 \\ 0 \end{bmatrix} = \begin{bmatrix} I_{A1} \\ I_{A2} \\ I_{A3} \end{bmatrix} + \begin{bmatrix} I_1^{(1)} \\ I_2^{(1)} \\ 0 \end{bmatrix} + \begin{bmatrix} 0 \\ I_1^{(2)} \\ I_2^{(2)} \end{bmatrix} + \begin{bmatrix} 0 \\ 0 \\ Y_L \cdot V_3 \end{bmatrix} \quad \text{Equation 2.19}$$

where

$$\begin{bmatrix} I_1^{(1)} \\ I_2^{(1)} \\ 0 \end{bmatrix} = \begin{bmatrix} Y_N^{(1)} \\ 0 \end{bmatrix} \cdot \begin{bmatrix} V_1 \\ V_2 \end{bmatrix} \text{ and } \begin{bmatrix} 0 \\ I_1^{(2)} \\ I_2^{(2)} \end{bmatrix} = \begin{bmatrix} 0 \\ Y_N^{(2)} \end{bmatrix} \cdot \begin{bmatrix} V_2 \\ V_3 \end{bmatrix}$$

$$\text{Let } Y_N^{(1)} = \begin{bmatrix} a^{(1)} & b^{(1)} \\ b^{(1)} & a^{(1)} \end{bmatrix} \text{ and } Y_N^{(2)} = \begin{bmatrix} a^{(2)} & b^{(2)} \\ b^{(2)} & a^{(2)} \end{bmatrix},$$

$$\text{Then; } Y_N^{(1)} \cdot \begin{bmatrix} V_1 \\ V_2 \end{bmatrix} = \begin{bmatrix} a^{(1)} & b^{(1)} \\ b^{(1)} & a^{(1)} \end{bmatrix} \cdot \begin{bmatrix} V_1 \\ V_2 \end{bmatrix} = \begin{bmatrix} a^{(1)} \cdot V_1 + b^{(1)} V_2 \\ b^{(1)} \cdot V_1 + a^{(1)} V_2 \end{bmatrix} \text{ and}$$

$$Y_N^{(2)} \cdot \begin{bmatrix} V_2 \\ V_3 \end{bmatrix} = \begin{bmatrix} a^{(2)} & b^{(2)} \\ b^{(2)} & a^{(2)} \end{bmatrix} \cdot \begin{bmatrix} V_2 \\ V_3 \end{bmatrix} = \begin{bmatrix} a^{(2)} \cdot V_2 + b^{(2)} V_3 \\ b^{(2)} \cdot V_2 + a^{(2)} V_3 \end{bmatrix}$$

Thus;

$$\begin{bmatrix} I_1^{(1)} \\ I_2^{(1)} \\ 0 \end{bmatrix} + \begin{bmatrix} 0 \\ I_1^{(2)} \\ I_2^{(2)} \end{bmatrix} = \begin{bmatrix} a^{(1)} V_1 + b^{(1)} V_2 \\ b^{(1)} V_1 + a^{(1)} V_2 \\ 0 \end{bmatrix} + \begin{bmatrix} 0 \\ a^{(2)} V_2 + b^{(2)} V_3 \\ b^{(2)} V_2 + a^{(2)} V_3 \end{bmatrix}$$

$$= \begin{bmatrix} a^{(1)} V_1 + b^{(1)} V_2 \\ b^{(1)} V_1 + a^{(1)} V_2 + a^{(2)} V_2 + b^{(2)} V_3 \\ b^{(2)} V_2 + a^{(2)} V_3 \end{bmatrix}$$

$$= \begin{bmatrix} a^{(1)} & b_{(1)} & 0 \\ b^{(1)} & a^{(1)} + a^{(2)} & b^{(2)} \\ 0 & b_{(2)} & a^{(2)} \end{bmatrix} \cdot \begin{bmatrix} V_1 \\ V_2 \\ V_3 \end{bmatrix}$$

Equation 2.20

Combining Equation 2.19 and Equation 2.20:

$$\begin{bmatrix} I_S \\ 0 \\ 0 \end{bmatrix} = \begin{bmatrix} I_{A1} \\ I_{A2} \\ I_{A3} \end{bmatrix} + \begin{bmatrix} a^{(1)} & b_{(1)} & 0 \\ b^{(1)} & a^{(1)} + a^{(2)} & b^{(2)} \\ 0 & b_{(2)} & a^{(2)} \end{bmatrix} \begin{bmatrix} V_1 \\ V_2 \\ V_3 \end{bmatrix} + \begin{bmatrix} 0 & 0 & 0 \\ 0 & 0 & 0 \\ 0 & 0 & Y_L \end{bmatrix} \begin{bmatrix} V_1 \\ V_2 \\ V_3 \end{bmatrix} \quad \text{Equation 2.21}$$

Where

$$\begin{bmatrix} I_{A1} \\ I_{A2} \\ I_{A3} \end{bmatrix} = Y_A \begin{bmatrix} V_1 \\ V_2 \\ V_3 \end{bmatrix} \quad \text{Equation 2.22}$$

Rewriting Equation 2.21 by combining it with Equation 2.22:

$$\begin{bmatrix} I_S \\ 0 \\ 0 \end{bmatrix} = Y_A \begin{bmatrix} V_1 \\ V_2 \\ V_3 \end{bmatrix} + \begin{bmatrix} a^{(1)} & b_{(1)} & 0 \\ b^{(1)} & a^{(1)} + a^{(2)} & b^{(2)} \\ 0 & b_{(2)} & a^{(2)} \end{bmatrix} \begin{bmatrix} V_1 \\ V_2 \\ V_3 \end{bmatrix} + \begin{bmatrix} 0 & 0 & 0 \\ 0 & 0 & 0 \\ 0 & 0 & Y_L \end{bmatrix} \begin{bmatrix} V_1 \\ V_2 \\ V_3 \end{bmatrix}$$

$$= (Y_A + Y_N + \begin{bmatrix} 0 & 0 & 0 \\ 0 & 0 & 0 \\ 0 & 0 & Y_L \end{bmatrix}) \begin{bmatrix} V_1 \\ V_2 \\ V_3 \end{bmatrix} \quad \text{Equation 2.23}$$

where

$$Y_N = \begin{bmatrix} a^{(1)} & b^{(1)} & 0 \\ b^{(1)} & a^{(1)} & 0 \\ 0 & 0 & 0 \end{bmatrix} + \begin{bmatrix} 0 & 0 & 0 \\ 0 & a^{(2)} & b^{(2)} \\ 0 & b^{(2)} & a^{(2)} \end{bmatrix} = \begin{bmatrix} [Y_N^{(1)}] & 0 \\ 0 & 0 \\ 0 & 0 \end{bmatrix} + \begin{bmatrix} 0 & 0 & 0 \\ 0 & [Y_N^{(2)}] \\ 0 & 0 & 0 \end{bmatrix}$$

In Equation 2.23,  $Y_A$  represents the inverse of the  $Z_A$ , impedance matrix which is formed by the self and mutual impedances of the dipole elements, as explained in 1.3.1.1.

For a given  $I_s$ ,  $\begin{bmatrix} V_1 \\ V_2 \\ V_3 \end{bmatrix}$  can be solved. Finally the currents on the dipoles can be found using Equation 2.22.

### 2.3.1.3. FOUR ANTENNAS CONNECTED BY THREE TRANSMISSION LINES

Let us consider four antennas connected to each other by three transmission lines. The current relations at the bases of the dipoles can be related through the similar procedure which is described above.

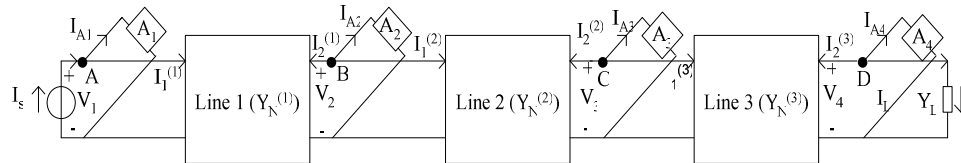


**Figure 2.7** Four antennas connected by three transmission lines

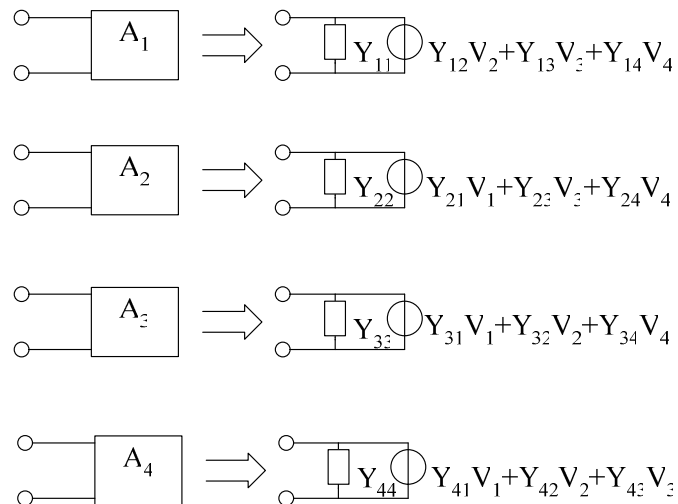


**Figure 2.8** Detailed view of  $A_1$ ,  $A_2$ ,  $A_3$  and  $A_4$

In Figure 2.7, applying Kirchoff's current law at node A, B, C and D:

$$I_S = I_{A1} + I_1^{(1)} \quad \text{Equation 2.24}$$

$$0 = I_{A2} + I_2^{(1)} + I_1^{(2)} \quad \text{Equation 2.25}$$

$$0 = I_{A3} + I_2^{(2)} + I_1^{(3)} \quad \text{Equation 2.26}$$

$$0 = I_{A4} + I_2^{(3)} + Y_L V_4 \quad \text{Equation 2.27}$$

where the superscripts on I's show the line number.

Rewriting the Equation 2.24, Equation 2.25, Equation 2.26 and Equation 2.27 in matrix form:

$$\begin{bmatrix} I_S \\ 0 \\ 0 \\ 0 \end{bmatrix} = \begin{bmatrix} I_{A1} \\ I_{A2} \\ I_{A3} \\ I_{A4} \end{bmatrix} + \begin{bmatrix} I_1^{(1)} \\ I_2^{(1)} \\ 0 \\ 0 \end{bmatrix} + \begin{bmatrix} 0 \\ I_1^{(2)} \\ I_2^{(2)} \\ 0 \end{bmatrix} + \begin{bmatrix} 0 \\ 0 \\ I_1^{(3)} \\ I_2^{(3)} \end{bmatrix} + \begin{bmatrix} 0 \\ 0 \\ 0 \\ Y_L V_4 \end{bmatrix}$$

After some manipulations:

$$\begin{bmatrix} I_S \\ 0 \\ 0 \\ 0 \end{bmatrix} = \left( Y_A + \begin{bmatrix} [Y_N^{(1)}] & 0 & 0 \\ 0 & 0 & 0 \\ 0 & 0 & 0 \\ 0 & 0 & 0 \end{bmatrix} + \begin{bmatrix} 0 & 0 & 0 & 0 \\ 0 & [Y_N^{(2)}] & 0 & 0 \\ 0 & 0 & 0 & 0 \\ 0 & 0 & 0 & 0 \end{bmatrix} + \begin{bmatrix} 0 & 0 & 0 & 0 \\ 0 & 0 & 0 & 0 \\ 0 & 0 & [Y_N^{(3)}] & 0 \\ 0 & 0 & 0 & 0 \end{bmatrix} \right) +$$

Equation 2.28

$$\begin{bmatrix} 0 & 0 & 0 & 0 \\ 0 & 0 & 0 & 0 \\ 0 & 0 & 0 & 0 \\ 0 & 0 & 0 & Y_L \end{bmatrix} \begin{bmatrix} V_1 \\ V_2 \\ V_3 \\ V_4 \end{bmatrix}$$

where  $[Y_N^{(i)}]$ 's are 2x2 line matrix.

For a given  $I_S$ ,  $\begin{bmatrix} V_1 \\ V_2 \\ V_3 \\ V_4 \end{bmatrix}$  can be solved. Finally the currents at the bases of the dipoles

can be found using

$$\begin{bmatrix} I_{A1} \\ I_{A2} \\ I_{A3} \\ I_{A4} \end{bmatrix} = Y_A \cdot \begin{bmatrix} V_1 \\ V_2 \\ V_3 \\ V_4 \end{bmatrix}. \quad \text{Equation 2.29}$$

#### 2.3.1.4. N ANTENNAS CONNECTED BY N-1 TRANSMISSION LINES

For a log-periodic dipole antenna consisting of N dipole elements, the procedure to find the currents at the bases of the dipole elements is as follows:

- $Y_A$  matrix which is the inverse of the  $Z_A$  should be formed. If there are N dipole elements on the log-periodic dipole antenna,  $Z_A$  is an N-by-N matrix. The diagonal entries of  $Z_A$  are the self impedances of the dipole elements and the off-diagonal elements are the mutual impedances between the dipole elements. For example,  $Z_A(2,4)=Z_A(4,2)$  is the mutual impedance between the second and the fourth dipole elements.
- For the transmission lines between the dipole elements,  $[Y_N^{(i)}]$  2-by-2 line matrices should be formed.
- Load admittance,  $Y_L$ , should be specified and should be placed into the last entry of the N-by-N matrix as seen in Equation 2.28.
- As one can see in Equation 2.28,  $[Y_N^{(i)}]$  2-by-2 line matrices should be placed into the diagonal and sub-diagonal parts of the N-by-N matrix. When all 2-by-2 matrices are placed in the N-by-N matrix, the last entry of the first  $Y_N$  matrix is summed up with the first entry of the second  $Y_N$  matrix and this procedure is repeated up to the last  $Y_N$  matrix as one can

see in Equation 2.21. At the end, the last entry of the last  $Y_N$  matrix is summed with the load admittance,  $Y_L$ .

- Following Equation 2.28, the voltage values on the dipole elements should be found for a given excitation current,  $I_s$ .
- By multiplying these voltage matrix and  $Y_A$  matrix, one can get the current values at the bases of the dipoles as seen in Equation 2.29.

A program to find the currents at the bases of the dipoles of a log-periodic dipole antenna is written in MATLAB<sup>®</sup> which is given in Appendix A. In the program “admittance matrix approach to LPDA” explained above is used. Tau, sigma, characteristic impedance of the feeder element, length of the dipoles and the spacing between the dipoles are the inputs for the program. Currents at the bases of the dipoles and using the currents E and H-plane patterns of the antenna are the outputs of the program.

In the MATLAB<sup>®</sup> program where currents at the bases of the dipoles are found, a code which forms the  $Z_A$  matrix is also used which is given in Appendix B. In the following section mutual coupling theory and related calculations are given.

## CHAPTER III

### MUTUAL IMPEDANCE BETWEEN LINEAR ELEMENTS

The input impedances of antennas are calculated when they radiate into an unbounded medium. The impedance of an antenna which is connected to a transmission line can be represented by an impedance as shown in Figure 3.1. This impedance,  $Z$ , is called the driving-point impedance. To match any antenna, this driving-point impedance must be matched. If the antenna is isolated, i.e. there are not any nearby objects; driving-point impedance is called the self-impedance of the antenna. The real part of this self-impedance is called the self-reactance (radiation resistance), and the imaginary part is called the self-reactance [1].

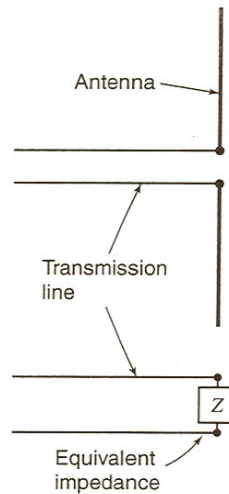


**Figure 3.1** Transmission line with an antenna and with an equivalent impedance

[1]

The presences of a nearby object, which can be another linear antenna, alter the current distribution, the radiated field and the input impedance. The current

distribution on one is affected by the field radiated by the other one. These mutual effects between the antennas should also be taken into account in designing the antennas. The driving-point impedance of an antenna in the presence of other elements depends on the self-impedance of the antenna and the mutual impedance between the antenna and the other element.

### 3.1. ANALYSIS OF DIPOLE ANTENNA

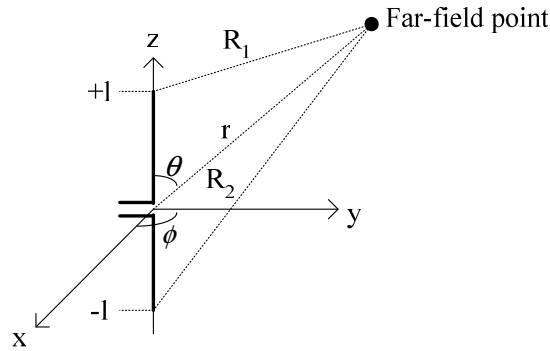


**Figure 3.2** Geometry for the analysis of dipole antenna

In Figure 3.2, the current distribution on the dipoles, which are assumed to be center-fed, can be written as:

$$I(x=0, y=0, z') = \begin{cases} \hat{a}_z \cdot I_0 \cdot \text{Sin}[k(l-z')] & , 0 \leq z' \leq l \\ \hat{a}_z \cdot I_0 \cdot \text{Sin}[k(l+z')] & , -l \leq z' \leq 0 \end{cases}$$

For the dipole configuration in Figure 3.2, magnetic field radiated by the dipole is

$$H = \hat{a}_\phi H_\phi = \frac{1}{\mu} \nabla \times A = \hat{a}_\phi \frac{1}{\mu} \frac{dA_z}{d\rho} \Rightarrow$$

$$H = -\hat{a}_\phi \frac{I_0}{4\pi j} \frac{1}{y} [e^{-jkR_1} + e^{-jkR_2} - 2\text{Cos}(kl)e^{-jkr}]$$

where

$$\begin{aligned}
r &= \sqrt{\rho^2 + z^2} \\
R_1 &= \sqrt{\rho^2 + (z-l)^2} \\
R_2 &= \sqrt{\rho^2 + (z+l)^2} \\
\rho^2 &= x^2 + y^2.
\end{aligned}
\tag{Equation 3.1}$$

The electric field can be found using Maxwell equations:

$E = \frac{1}{j\omega\epsilon} \nabla \times H$ . After some analytical details, two components of electrical field can be found [2]. These are the  $-y$  and the  $-z$  components of the electrical field and are equal to:

$$E_z = -j \frac{\eta I_0}{4\pi} \left[ \frac{e^{-jkR_1}}{R_1} + \frac{e^{-jkR_2}}{R_2} - 2 \cos(kl) \frac{e^{-jkr}}{r} \right]
\tag{Equation 3.2}$$

$$E_y = \frac{j\eta I_0}{4\pi y} \left[ (z-l) \frac{e^{-jkR_1}}{R_1} + (z+l) \frac{e^{-jkR_2}}{R_2} - 2z \cos(kl) \frac{e^{-jkr}}{r} \right]
\tag{Equation 3.3}$$

### 3.2. ANALYSIS OF THE SELF AND MUTUAL IMPEDANCE OF LINEAR ELEMENTS

A system consisting of two linear antennas can be represented by T-equivalent form of a two-port (four terminals) network as shown in Figure 3.3.

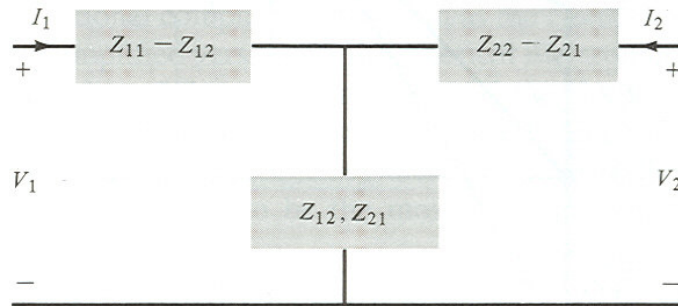


**Figure 3.3** Two port network and its T-equivalent [2]

The voltage current relations for Figure 3.3 are as follows:

$$\begin{aligned} V_1 &= Z_{11}I_1 + Z_{12}I_2 \\ V_2 &= Z_{21}I_1 + Z_{22}I_2 \end{aligned} \quad \text{Equation 3.4}$$

where  $Z_{11}$  and  $Z_{22}$  are the self impedances of the antennas,

$$Z_{12} = \left. \frac{V_1}{I_2} \right|_{I_1=0}$$

is the mutual impedance at port 1 due to the current at port

2 (with port 1 is open circuited),

$$Z_{21} = \left. \frac{V_2}{I_1} \right|_{I_2=0}$$

is the mutual impedance at port 2 due to the current at port

1 (with port 2 is open circuited).

For reciprocal networks  $Z_{12} = Z_{21}$ .

The driving-point impedances of the antennas can be written using Equation 3.4 as follows:

$$\begin{aligned} Z_{1d} &= \frac{V_1}{I_1} = Z_{11} + Z_{12} \left( \frac{I_2}{I_1} \right) \\ Z_{2d} &= \frac{V_2}{I_2} = Z_{22} + Z_{21} \left( \frac{I_1}{I_2} \right) \end{aligned} \quad \text{Equation 3.5}$$

Equation 3.5 shows that, driving-point impedance of an antenna depends on the self-impedance of the antenna itself, mutual impedance between the two antennas and the current ratios.

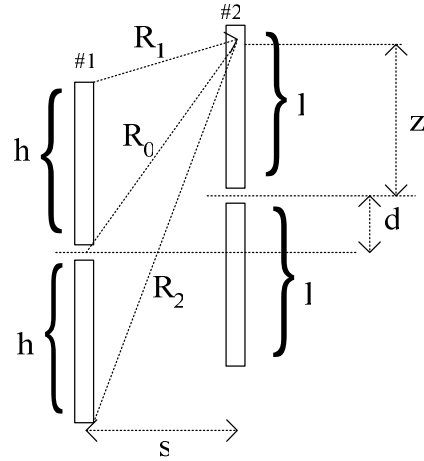


**Figure 3.4** Position of two dipole antennas used in the analysis of self and mutual impedances

More complex techniques can be used in the analysis of mutual coupling between the antennas, but here simplified models will be used by the help of induced emf method [2]. The following equation can be written for Figure 3.4:

$$V_{21} = -\frac{1}{I_{2i}} \int_{-l}^l E_{z21}(z') I_2(z') dz' \quad \text{Equation 3.6}$$

where

$V_{21}$  is the induced open-circuit voltage in antenna 2, referred to its current at the input terminals, due to the radiation from antenna 1,

$I_{2i}$  is the input current of antenna 2,

$E_{z21}(z')$  is the E-field component due to antenna 1, which is parallel to antenna 2,

$I_2(z')$  is the current distribution along antenna 2.

The mutual impedance between two antennas can be defined as follows:

$$Z_{21} = \frac{V_{21}}{I_{i1}} = -\frac{1}{I_{i1}I_{2i-1}} \int_{-l}^l E_{z21}(z')I_2(z')dz' \quad \text{Equation 3.7}$$

Equation 3.7 can be written also in the following form:

$$Z_{21} = \frac{V_{21}}{I_{i1}} = j \frac{\eta I_{1m} I_{2m}}{4\pi I_{i1} I_{2i-1}} \int_{-l}^l \sin[k(l-|z'|)] \left[ \frac{e^{-jkR_1}}{kR_1} + \frac{e^{-jkR_2}}{kR_2} - 2\cos(kh) \cdot \frac{e^{-jkR_0}}{kR_0} \right] dz' \quad \text{Equation 3.8}$$

where

$$kR_1 = \sqrt{(ks)^2 + (kz + kd - kh)^2},$$

$$kR_2 = \sqrt{(ks)^2 + (kz + kd + kh)^2},$$

$$kR_0 = \sqrt{(ks)^2 + (kz + kd)^2},$$

$$\eta = \sqrt{\frac{\mu}{\epsilon}} = 120\pi \text{ is the intrinsic impedance of free space.}$$

For a very thin dipole with length  $2l$ , the current at input terminals,  $I_i$ , can be related to the maximum current,  $I_m$  as follows:

$$I_i = I_m \sin(kl) \quad \text{Equation 3.9}$$

Replacing Equation 3.9 into Equation 3.8, the following equation can be obtained:

$$Z_{21} = \frac{j.30}{(\sin(kh))(\sin(kl))} \int_{-l}^l \left( \frac{e^{-jkR_1}}{kR_1} + \frac{e^{-jkR_2}}{kR_2} - 2\cos(kh) \cdot \frac{e^{-jkR_0}}{kR_0} \right) \cdot \sin(k(l-|z'|)) dz' \quad \text{Equation 3.10}$$

One can notice that when  $h$  (or  $l$ ), which is the half length of the dipole antenna, is approximately equal to  $k\left(\frac{\lambda}{2}\right)$ ,  $\text{Sin}(kh) = \text{Sin}\left(\frac{2\pi}{\lambda} k \frac{\lambda}{2}\right) = \text{Sin}(k\pi)$ ,  $k = 1, 2, 3 \dots n$ , so one can expect very high values of  $Z_{21}$ . In the second row of Table 3.5, when  $l = 0.1395m = 0.93\frac{\lambda}{2}$ , the corresponding self impedance is,  $R + jX = 4428 + j3509$ . In Figure 3.5, self resistance and reactance of dipole antenna can be seen. In Figure 3.5, the dipoles are  $l$  length, therefore when  $l$  is approximately equal to  $\lambda$ , self impedance takes very high values.

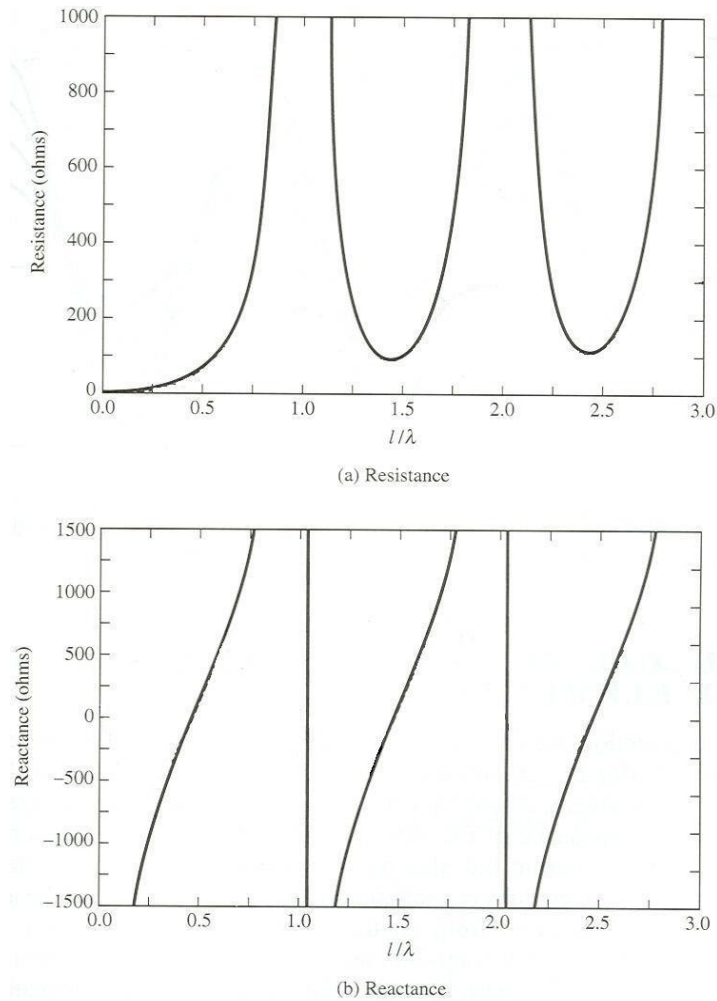


**Figure 3.5** Self resistance and reactance of dipole antenna [2]

Equation 3.10 is solved in MATLAB<sup>®</sup> to find the self and mutual impedances of the antenna elements. The MATLAB<sup>®</sup> program is given in Appendix B.

A program written in FORTRAN given in Appendix C and an appendix in Markov [3] are taken as references to check the results of the self and mutual impedances calculated by the MATLAB<sup>®</sup> program.

### 3.2.1. CHECK-UP CALCULATIONS

First, the impedances calculated in FORTRAN program are compared with the ones given in the appendix of Markov [3] in order to check the consistency of the references.

- Input of FORTRAN Program:

The input file is in the following form:

```
“HL= 0.612 LL= 0.465 SL= .49 DL= .00
```

```
50”
```

HL and LL are the half-length of dipoles in wave-length; SL is the spacing between the dipoles in wave-length. DL is the offset between the centers of the dipoles in again wavelength and, DL is the same with “d” in Figure 3.4.

50 is the number of gauss points which should be even. When number of gauss points increase, the result converges the actual result more.

- Appendix of Markov [3]:

In the appendix, definitions of HL, LL, SL and DL are the same with the notation used in FORTRAN program. HL and LL are taken as 0.25, and the spacing between the dipoles vary from 0 to 3.90.

In the check-up calculations, HL and LL are taken as 0.25, DL is taken as 0 and SL varies from 0 to 3, gauss number and  $\lambda$  are taken as 50 and 0.3 meter respectively.

The results are as follows:

**Table 3.1** Mutual impedances between half wave-length dipoles with different spacing between them [3]

SL	MARKOV		FORTRAN	
	$R_{12}(\Omega)$	$X_{12}(\Omega)$	$R_{12}(\Omega)$	$X_{12}(\Omega)$
0.00	73.1	42.5	73.13	42.54
0.02	72.9	35.1	72.89	35.09
0.04	72.3	27.8	72.19	27.82
0.20	51.4	-19.2	51.4	-19.17
0.40	6.2	-37.5	6.217	-37.43
0.80	-18.5	12.2	-18.49	12.26
0.90	-7.5	18.5	-7.49	18.55
2	1.1	9.4	1.08	9.36
3	0.5	6.3	0.48	6.31

Inspection of Table 3.1 shows that the real parts,  $R_{12}$ , and the imaginary parts,  $X_{12}$ , of the mutual impedances of each reference are almost equal.

The Figure 3.6 shows the variation of mutual impedance between two parallel half-wave length dipoles as a function of the separation  $d/\lambda$ . In Table 3.1, SL is in terms of wavelength, therefore the values in the first column of Table 3.1, can be considered as x axis values in Figure 3.6, and the corresponding real and imaginary parts of the mutual impedances can be compared with the results in Table 3.1. Comparison shows that the values are consistent with each other.

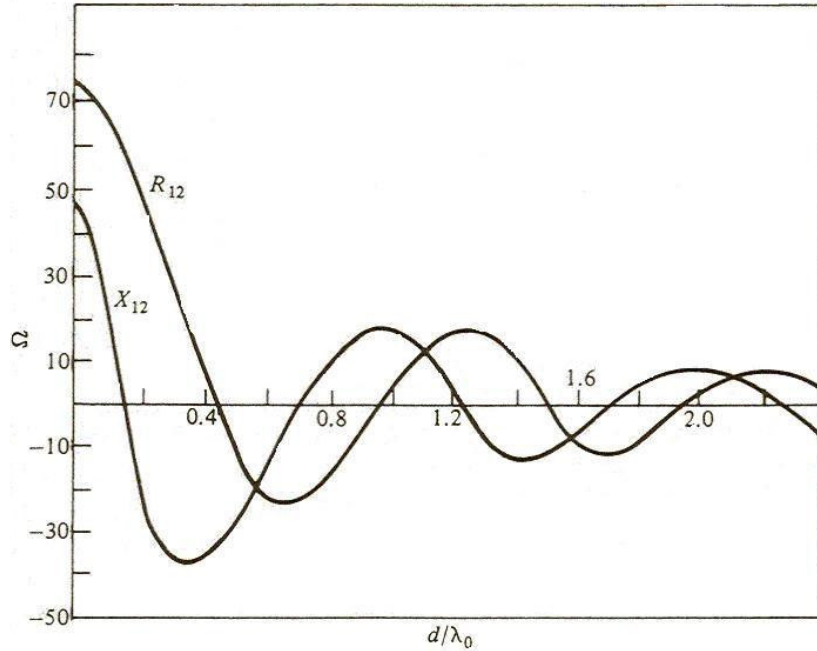


**Figure 3.6** Variation of mutual impedance between two parallel dipoles  $\lambda/2$  long as a function of the separation  $d/\lambda$  [4]

Second, the impedances calculated in FORTRAN are compared with the ones calculated in MATLAB<sup>®</sup> in order to check the consistency of two programs written in FORTRAN and MATLAB<sup>®</sup>. In the check-up calculations, a simple log-periodic antenna consisting of eight dipoles is designed as shown in Figure 3.7. Mutual couplings between the successive dipoles are calculated with FORTRAN and MATLAB<sup>®</sup>. Input file for FORTRAN was defined previously. Figure 3.4 is taken as reference for MATLAB<sup>®</sup> program, “h” and “l” represents the half-lengths of the dipoles and “s” represents the spacing between them in meters.  $\lambda$  is taken as 0.3 meter. Results are in the following:

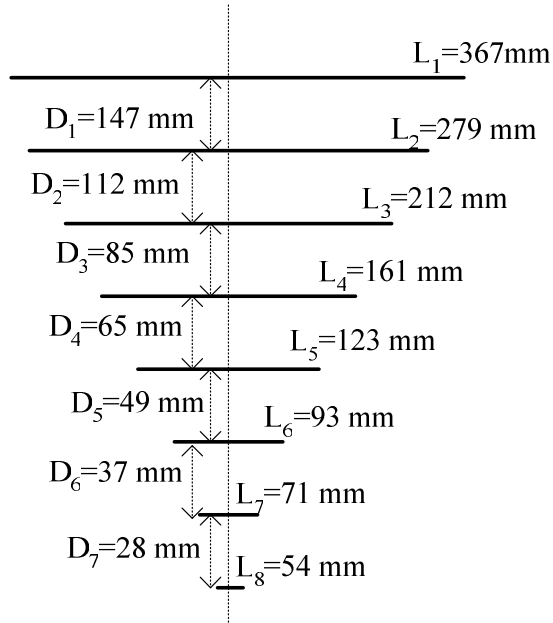


**Figure 3.7** Log-periodic antenna used in calculation of mutual impedances between dipoles

**Table 3.2** Mutual impedances between successive dipoles calculated in FORTRAN

FORTRAN					
<b>n</b>	<b>HL</b>	<b>LL</b>	<b>SL(n and (n+1))</b>	<b><math>R_{n,n+1}(\Omega)</math></b>	<b><math>X_{n,n+1}(\Omega)</math></b>
1	0.612	0.465	0.526	330.4	295,8
2	0.465	0.353	0.405	29.76	-535
3	0.353	0.268	0.31	55.41	-72.1
4	0.268	0.205	0.236	37.24	-22.42
5	0.205	0.155	0.1783	23.16	-9.824
6	0.155	0.118	0.135	13.81	-9.154
7	0.118	0.09	0.1016	8.189	-13.66

**Table 3.3** Mutual impedances between successive dipoles calculated in  
MATLAB®

MATLAB®					
<b>n</b>	<b>h(m)</b>	<b>l(m)</b>	<b>l(n and (n+1)) (m)</b>	<b>R<sub>n,n+1</sub>(Ω)</b>	<b>X<sub>n,n+1</sub>(Ω)</b>
1	0.1835	0.1395	0.158	332.59	295.68
2	0.1395	0.106	0.1215	29,798	-536.32
3	0.106	0.0805	0.093	55.6414	-72.401
4	0.0805	0.0615	0.071	37.1863	-22.548
5	0.0615	0.0465	0.0535	23.1588	-9.8255
6	0.0465	0.0355	0.0405	13.8496	-9.1646
7	0.0355	0.027	0.0305	8.2124	-13.637

The last two columns of Table 3.2 and Table 3.3 show the real and imaginary parts of the mutual couplings between successive dipoles for the log periodic antenna given in Figure 3.7. Inspection of Table 3.2 and Table 3.3 shows that, mutual impedances of each program are almost equal.

### 3.2.2. SELF IMPEDANCES OF LINEAR ANTENNAS

In determining self impedances, thickness of the dipole is important. The thickness of the dipole is taken into account by approximating the self impedance of two dipole having the same length and radius of the dipole apart from each other. In other words, self impedance of each dipole is calculated from the same formula as mutual coupling between two elements. Sinusoidal current distribution over each dipole element assumption is still valid.

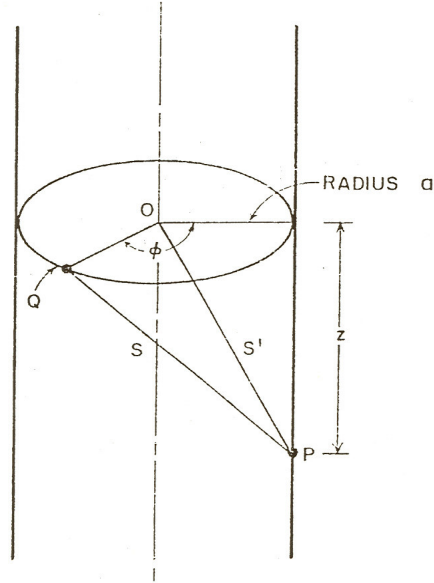


**Figure 3.8** Geometry used in calculation of the self impedance [5]

Referring to Figure 3.8, current is assumed to be concentrated at the center. Distance  $s$  can be found by:

$$s = \sqrt{2a^2(1 - \cos\phi) + z^2} = \sqrt{2a^2 + z^2} \cdot \sqrt{1 - \frac{2a^2}{2a^2 + z^2} \cdot \cos\phi} \quad \text{Equation 3.11}$$

For very thin dipoles,  $z \gg a$ , so  $s \approx \sqrt{2a^2 + z^2}$

Comparing with Equation 3.8, spacing,  $s$  can be replaced by  $\sqrt{2}a$ , so the self impedance of a dipole can be approximated by finding a mutual coupling between two dipoles having same length which are  $\sqrt{2}a$  apart from each other where  $a$  is the radius of the dipole [5].

Self impedances calculated in FORTRAN program are compared with the ones calculated in MATLAB<sup>®</sup> program in order to check the consistency of two programs. Calculating the self impedances, dimensions of the log-periodic antenna given in Figure 3.7 are used. Radii of the dipoles of the antenna are 4.24mm,

3.53mm, 3.18mm, 2.47mm, 1.76mm, 1.41mm, 1.06mm and 0.7mm starting from the longest dipole. In FORTRAN program “HL and SL” are the half-length of the dipoles in wave-length as explained before and in MATLAB® program “l” is the half length of the dipoles and r is the radius of the dipoles in meters. In both programs spacing is taken as the radius of the dipoles as explained before and  $\lambda$  is taken as 0.3 meter. Calculated values in both programs are given in the following:

**Table 3.4** Self impedances of dipoles calculated in FORTRAN

<b>FORTRAN</b>				
<b>n</b>	<b>HL</b>	<b>SL</b>	<b>R<sub>nn</sub>(Ω)</b>	<b>X<sub>nn</sub>(Ω)</b>
1	0.612	0.02	274.7	-164.7
2	0.465	0.0166	4428	3516
3	0.353	0.015	266.18	324.4
4	0.268	0.0116	90.29	75.86
5	0.205	0.00833	42.51	-53.34
6	0.155	0.00666	21.70	-164.1
7	0.118	0.005	11.86	-280.2
8	0.09	0.0033	6,679	-438.1

**Table 3.5** Self impedances of dipoles calculated in MATLAB®

<b>MATLAB®</b>				
<b>n</b>	<b>l(m)</b>	<b>r(m)</b>	<b>R<sub>nn</sub>(Ω)</b>	<b>X<sub>nn</sub>(Ω)</b>
1	0.1835	0.006	276.63	-165.17
2	0.1395	0.005	4428	3509
3	0.106	0.0045	266.18	325.8
4	0.0805	0.0035	90.63	76.48
5	0.0615	0.0025	42.50	-53.31
6	0.0465	0.002	21,698	-164.04
7	0.0355	0.0015	11,932	-279.27
8	0.027	0.001	6.6792	-436.28

Inspection of Table 3.4 and Table 3.5 shows that, self impedances of each program are almost equal.

As a second check, calculating the self-impedance of a half-wave dipole, one can find resistance and reactance values of self-impedance,  $R_{11} + jX_{11} = (73.12 + j41.29)\Omega$  using both MATLAB® and FORTRAN programs.

Some simple and approximate formulas exist in the literature [7] to calculate the input resistance of the dipoles. These are stated as follows:

**Table 3.6** Simple formulas for the input resistance of dipoles [7]

Length, L	Input resistance Rin(ohms)
$0 < L < \frac{\lambda}{4}$	$20\pi^2 \left(\frac{L}{\lambda}\right)^2$
$\frac{\lambda}{4} < L < \frac{\lambda}{2}$	$24.7 \left(\pi \frac{L}{\lambda}\right)^{2.4}$
$\frac{\lambda}{2} < L < 0.637\lambda$	$11.14 \left(\pi \frac{L}{\lambda}\right)^{4.17}$

Using Table 3.6, Rnn( $\Omega$ ) columns in Table 3.4 and Table 3.5 are calculated again. Result of computation is as follows:

**Table 3.7** Self impedances of dipoles calculated by using formulas in Table 3.6

N	Total length, L(m)	Rnn( $\Omega$ )
1	0.367	
2	0.279	
3	0.212	
4	0.161	98.37
5	0.123	45.34
6	0.093	23.18
7	0.071	11.05
8	0.054	6.395

Inspection of Table 3.7 shows that, real parts of the self impedances given in Table 3.6 are approximately equal with the values given in Table 3.4 and Table 3.5. Since  $\frac{L}{\lambda} > 0.637$  for the first three dipoles, first three rows of Table 3.7 cannot be filled out.

### 3.2.3. MUTUAL COUPLING FOR DUAL POLARIZED LOG-PERIODIC ANTENNAS

In a dual polarized log periodic antenna, there are two half wave dipole elements perpendicular to each other for a frequency. In this section, mutual coupling between these perpendicular elements will be investigated.

In Figure 2.5, two antennas connected by a transmission line are given. For this configuration current-voltage relations are investigated and the result is generalized to N antennas connected by N-1 transmission lines. When two perpendicular antennas are considered, as a starting point the following figure can be considered:

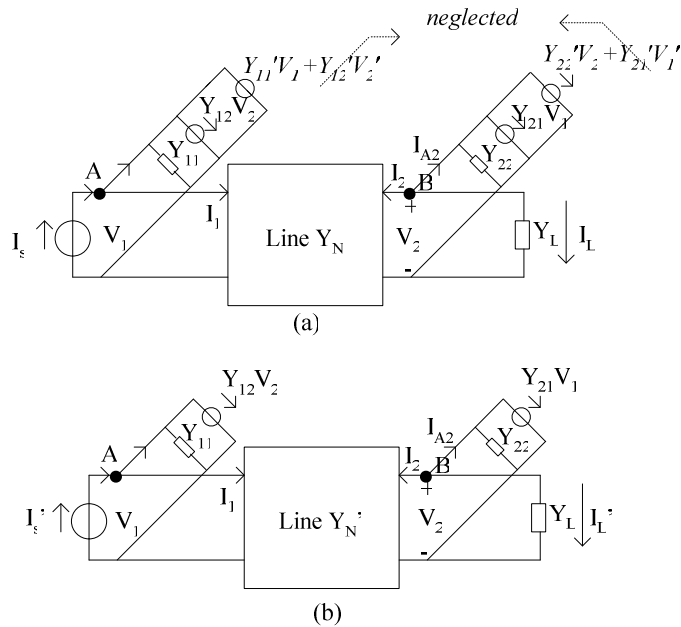


**Figure 3.9** Two antennas connected by a transmission line in a dual polarized log-periodic antenna

In Figure 3.9(a), the symbols written in “italic”, show the effect of the dipole antenna which is perpendicular to it and shown in Figure 3.9(b).  $Y_{11}'$  is the mutual admittance of the dipole antennas which are perpendicular to each other and which are at the same level.  $Y_{12}'$  is the mutual admittance of the first and the second dipole antennas which are perpendicular to each other as shown in Figure 3.10.  $V_1$  and  $V_1'$  are not necessarily equal. But if the coming signal, forms a  $45^\circ$  angle with the two antennas, then  $V_1 = V_1'$ .

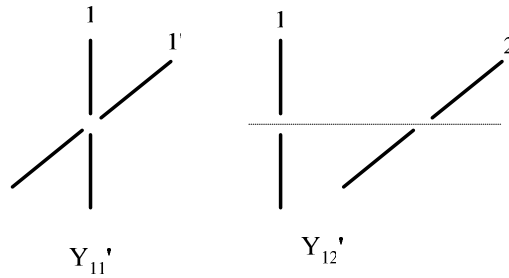


**Figure 3.10** Detailed view of dipole antennas which are perpendicular to each other.

In Figure 3.9(a), it is obvious that  $Y_{11} \gg Y_{11}'$ ,  $Y_{12} \gg Y_{12}'$  as mutual coupling between orthogonal elements are small compared to one between elements in the same plane.  $Y_{12}'$  is expected to be very small as compared with  $Y_{11}'$ . Therefore in Figure 3.9(a),  $Y_{12}'$  is neglected among  $Y_{11}, Y_{12}$  and  $Y_{11}'$ .

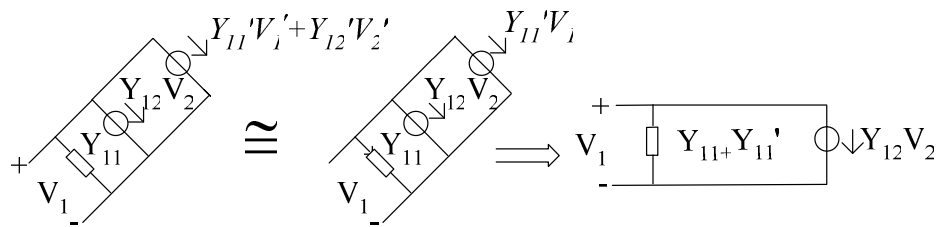


**Figure 3.11** Approximations on Figure 3.9(a)

In section 2.3.1, it is stated that, the diagonal entries of  $Z_A$ , which is the inverse of  $Y_A$  matrix, are the self impedances of the dipole elements. Considering the effect of orthogonal elements and making some approximations stated above, the diagonal entries of  $Y_A$  matrix will be  $Y_{11}+Y_{11}'$  instead of  $Y_{11}$  only. So, the next job is to find  $Y_{11}'$  and compare it with  $Y_{11}$ .

### 3.2.3.1. CALCULATION OF MUTUAL COUPLING OF THE ORTHOGONAL ANTENNAS

To calculate the mutual coupling between two orthogonal antennas, first, electric field component which is parallel to antenna 2 due to antenna 1 should be found which is the y component of the electric field. To find  $E_y$ , considering Figure 3.12, when  $z=x=0$ , Equation 3.3 is turned out to be:

$$E_y = \frac{j\eta I_0}{4\pi y} \left[ (-l) \frac{e^{-jkR_1}}{R_1} + (l) \frac{e^{-jkR_2}}{R_2} \right] \quad \text{Equation 3.12}$$

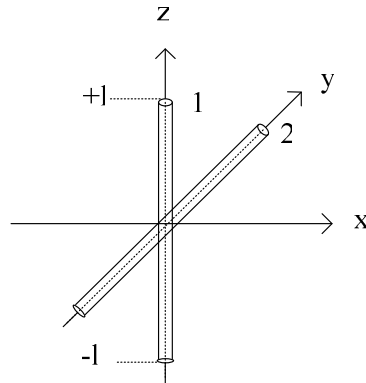


**Figure 3.12** Two dipole antennas orthogonal to each other

Since  $z=0$ , from Equation 3.1,  $R_1 = R_2 = \sqrt{\rho^2 + l^2}$ . Therefore from Equation 3.12,  $E_y$  is turned to be 0, assuming the wire radius is very small. Since  $E_y$  is zero, from Equation 3.7,  $Z_{21}=0$ .

If we don't assume the radius of the second dipole is zero, i.e., the dipole is not very thin, corresponding figure is as follows:

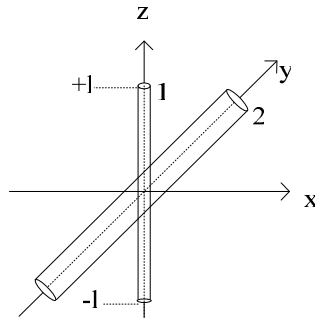


**Figure 3.13** Two dipole antennas orthogonal to each other with no assumption of zero wire radius of the second antenna

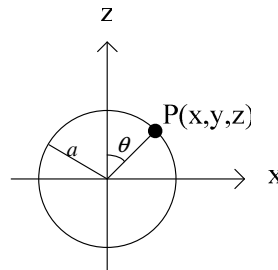


**Figure 3.14** Detailed view of the cross-section of the second antenna in Figure 3.13

In Figure 3.14,  $x^2 + z^2 = a^2$

where

$$x = a \sin \theta$$

$$z = a \cos \theta$$

Equation 3.13

Equation 3.1 is turned out to be

$$\begin{aligned}
\rho &= \sqrt{x^2 + y^2} = \sqrt{a^2 \sin^2 \theta + y^2} \\
R_1 &= \sqrt{\rho^2 + (a \cos \theta - h)^2} \\
R_2 &= \sqrt{\rho^2 + (a \cos \theta + h)^2} \\
r &= \sqrt{\rho^2 + (a \cos \theta)^2}
\end{aligned}
\tag{Equation 3.14}$$

Substituting Equation 3.13 and Equation 3.14 into Equation 3.3, one gets:

$$\begin{aligned}
E_y &= \frac{j\eta I_0}{4\pi y} \left[ (a \cos \theta - l) \frac{e^{-jk\sqrt{\rho^2 + (a \cos \theta - h)^2}}}{\sqrt{\rho^2 + (a \cos \theta - h)^2}} + (a \cos \theta + l) \frac{e^{-jk\sqrt{\rho^2 + (a \cos \theta + h)^2}}}{\sqrt{\rho^2 + (a \cos \theta + h)^2}} \right. \\
&\quad \left. - 2a \cos \theta \cos(kl) \frac{e^{-jk\sqrt{\rho^2 + (a \cos \theta)^2}}}{\sqrt{\rho^2 + (a \cos \theta)^2}} \right]
\end{aligned}
\tag{Equation 3.15}$$

$$Z_{21} = \frac{V_{21}}{I_{1i}} = -\frac{1}{I_{1i} I_{2i}} \int_{-l}^{+l} E_y(y) I_2(y) dy$$

$$\text{Assuming } I_{1i} \text{ and } I_{2i} \text{ are 1 and } J_2(y) = \frac{I_2(y)}{2\pi a}$$

$$Z_{21} = -\int_0^{2\pi} \int_{-l}^{+l} E_y(y) \frac{I_2(y)}{2\pi a} dy \cdot a d\theta
\tag{Equation 3.16}$$

Substitution of Equation 3.15 into Equation 3.16 gives the mutual coupling between two orthogonal antennas. Equation 3.16 is solved using MATLAB<sup>®</sup> to find the mutual coupling between two orthogonal antennas. The MATLAB<sup>®</sup> program is given in Appendix D

Assuming a sinusoidal current distribution on antenna 2, mutual coupling between two orthogonal elements is found to be  $-1.6000 \times 10^{-17} + j1.7984 \times 10^{-16} \Omega$ , absolute value of which is equal to  $1.8055 \times 10^{-16} \Omega$ . One can consider an impedance matrix as follows:

$$Z = \begin{bmatrix} Z_{11} & Z_{12} \\ Z_{21} & Z_{22} \end{bmatrix}$$

where  $Z_{11}$  and  $Z_{22}$  are the self impedances of two orthogonal antennas

$Z_{12} = Z_{21}$  are the mutual impedances between two orthogonal antennas.

To find the mutual admittance between two orthogonal antennas, inverse of the  $Z$  matrix should be found.

$$Y = Z^{-1} = \frac{1}{\Delta} \begin{bmatrix} Z_{22} & -Z_{21} \\ -Z_{12} & Z_{11} \end{bmatrix}$$

where  $\Delta = Z_{11}Z_{22} - Z_{12}Z_{21}$

So the mutual admittance between the orthogonal antennas is:

$$Y_{11}' = \frac{-Z_{21}}{\Delta}.$$

From Equation 3.8, the self impedances of the dipoles of the antenna given in Figure 3.7 can be calculated. The self impedance of the first dipole is found to be  $276.63 - j165.17\Omega$ , absolute value of which is equal to  $322.18\Omega$ . So the calculated mutual admittance between two orthogonal dipoles is:

$$Y_{11}' = 1.591128 \times 10^{-21} - j6.8232 \times 10^{-22} \Omega$$

Now,  $Y_{11}'$  can be compared with  $Y_{11}$  in Figure 3.11.  $Y_{11}$  can be found first by forming the  $Z$  matrix of the log periodic antenna given in Figure 3.7 by using Table 3 and 5 and second taking the inverse of this  $Z$  matrix.  $Y_{11}$  is found to be as  $0.0024 + j0.0019\Omega$  with an absolute value of  $0.0031\Omega$ . When  $Y_{11}'$  and  $Y_{11}$  are compared, it can be easily seen that,  $Y_{11}'$  is much smaller than  $Y_{11}$ , therefore  $Y_{11} + Y_{11}'$  can be approximated as  $Y_{11}$  in Figure 3.11. Thus, all the mutual impedances are calculated considering the single polarized antenna.

In the admittance matrix approach, using the mutual impedance, ZA matrix, it was stated that currents at the bases of the dipoles can be found. At this point calculated currents should be checked to verify the accuracy of the MATLAB<sup>®</sup> program.

#### **3.2.4. CHECK-UP CALCULATIONS FOR CURRENTS OF LOG-PERIODIC ANTENNA**

Current distributions given in literature for several log-periodic antennas are also calculated by MATLAB<sup>®</sup> to verify the accuracy of the program. These verifications are summarized as follows:

1) In Joachim [6], absolute values and phases of currents at the bases of dipoles are given for a log-periodic antenna composed of 12 elements and with  $\tau = 0.9$  at three different frequencies. Same graphs are sketched using MATLAB<sup>®</sup>. These graphs are given as follows for comparison.

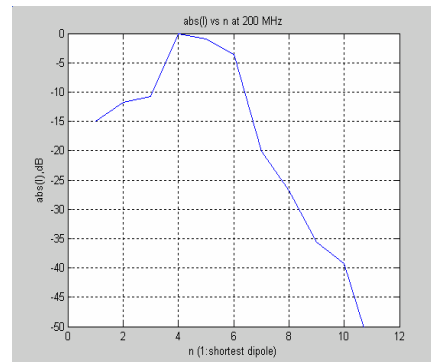
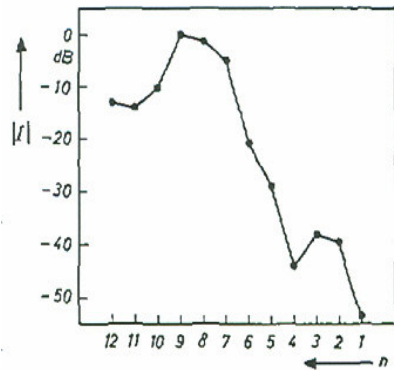
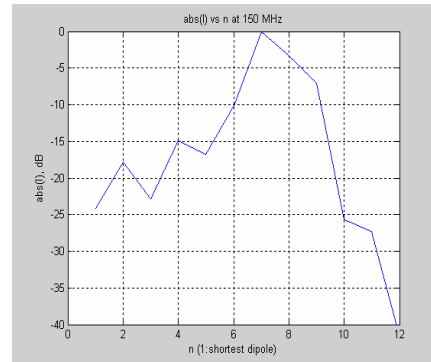
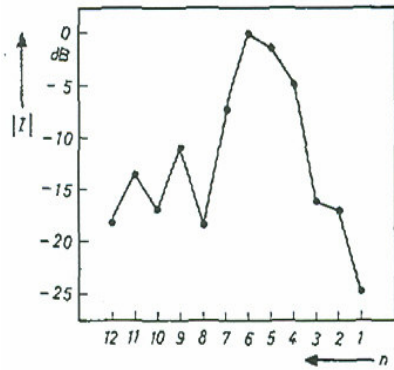
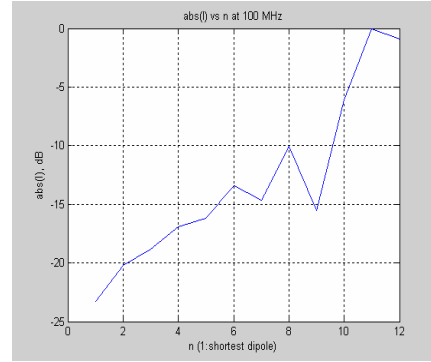
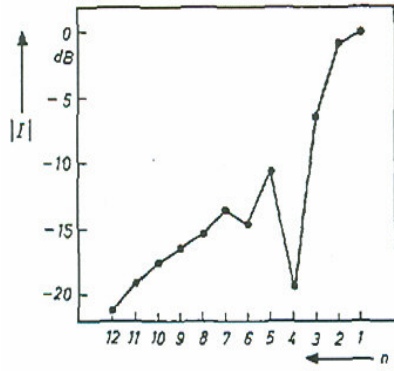


**Figure 3.15** Absolute values of currents given in Joachim [6] (left) versus calculated ones in MATLAB<sup>®</sup> at frequencies 100 MHz, 150 MHz and 200 MHz from top to bottom respectively

Inspection of Figure 3.15, the graphs at the right show the MATLAB<sup>®</sup> results, the ones at the left are the ones given in Joachim [6]. First, second and third rows

correspond to the frequencies of 100 MHz, 150 MHz and 200 MHz respectively. In the MATLAB<sup>®</sup> graphs, on the x-axis “1” represents the shortest dipole, while in the graphs at the left side of the MATLAB<sup>®</sup> graphs, “1” represents the longest dipole. These are also true for the phase graphs. Comparison of two graphs at three frequencies shows that these graphs are sufficiently similar.

The phases of the currents are given in Figure 3.16. The graphs at the right show the MATLAB<sup>®</sup> results as before, while the ones at the left are taken from Joachim [6].

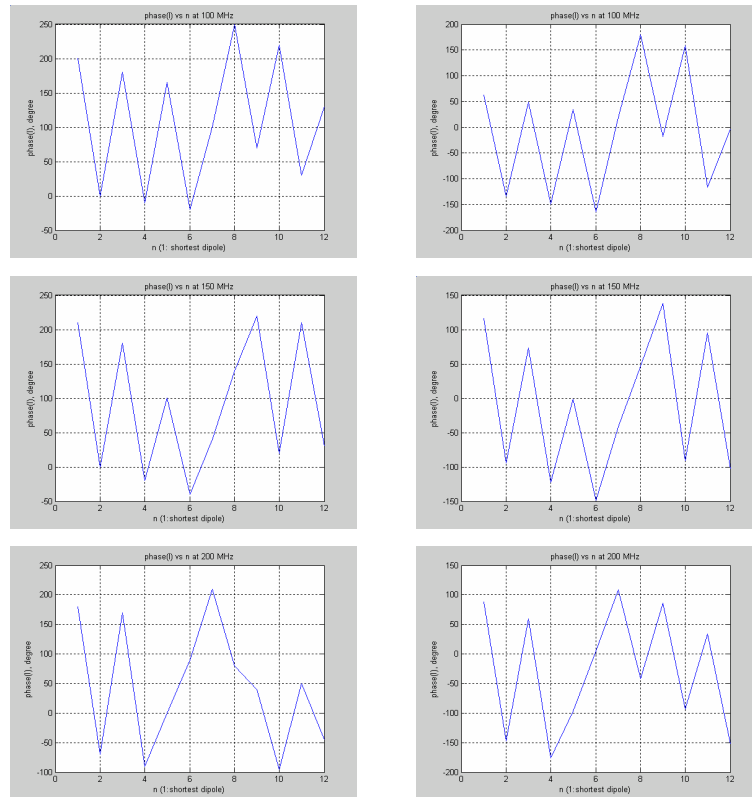


**Figure 3.16** Phases of currents given in Joachim [6] (left) versus calculated ones in MATLAB<sup>®</sup> at frequencies 100 MHz, 150 MHz and 200 MHz from top to bottom respectively

Comparison of two graphs at three frequencies shows that these graphs are sufficiently similar. The curves at the same frequency have the same slopes.

2) In Stutzman and Gary [7], relative dipole terminal current amplitudes at the bases of dipoles are given for a log-periodic antenna composed of 18 elements and with  $\tau = 0.917$  and  $\sigma = 0.169$  at three different frequencies. Same graphs are sketched using MATLAB<sup>®</sup>. These graphs are given as follows for comparison.

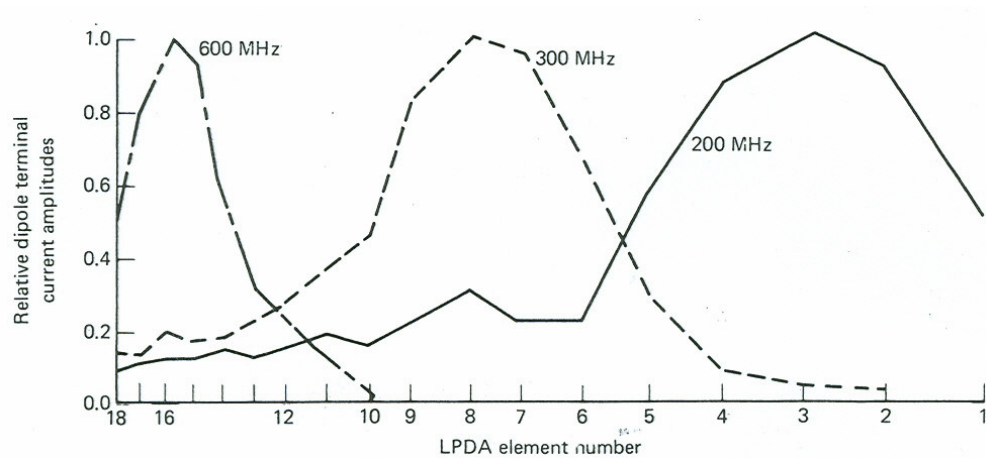


**Figure 3.17** Dipole base currents for the log periodic antenna given in Stutzman and Gary [7]

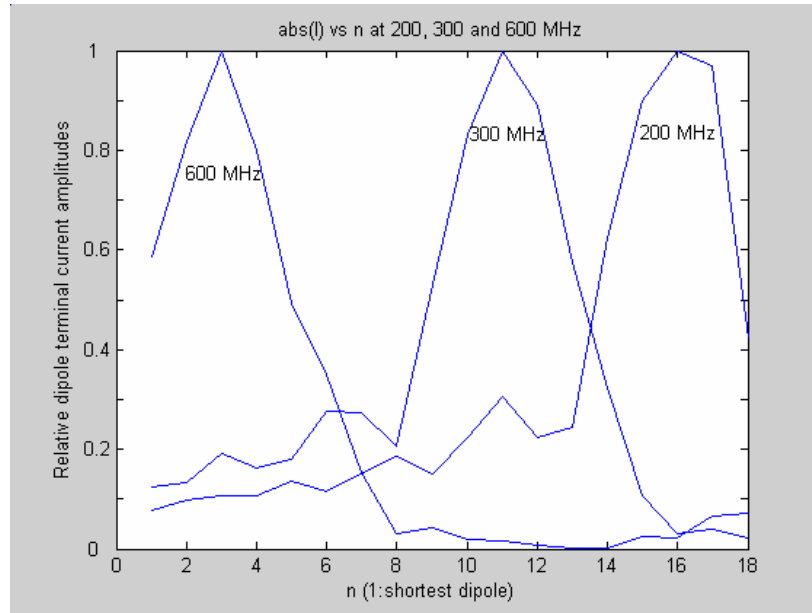


**Figure 3.18** Calculated dipole base currents in MATLAB®

In Figure 3.18, on the x-axis “1” represents the shortest dipole, while in Figure 3.17, “1” represents the longest dipole. Relative dipole terminal current amplitudes at 200, 300 and 600 MHz are quite similar in Figure 3.17 and Figure 3.18.

3) In Balanis [2], absolute values of currents at the bases of the dipoles are given for a log-periodic antenna composed of 13 elements and with  $\tau = 0.95$  and  $\sigma = 0.0564$  at the frequency where element No.10 is  $\frac{\lambda}{2}$ . Same graph is sketched using MATLAB®. These graphs are given as follows for comparison.

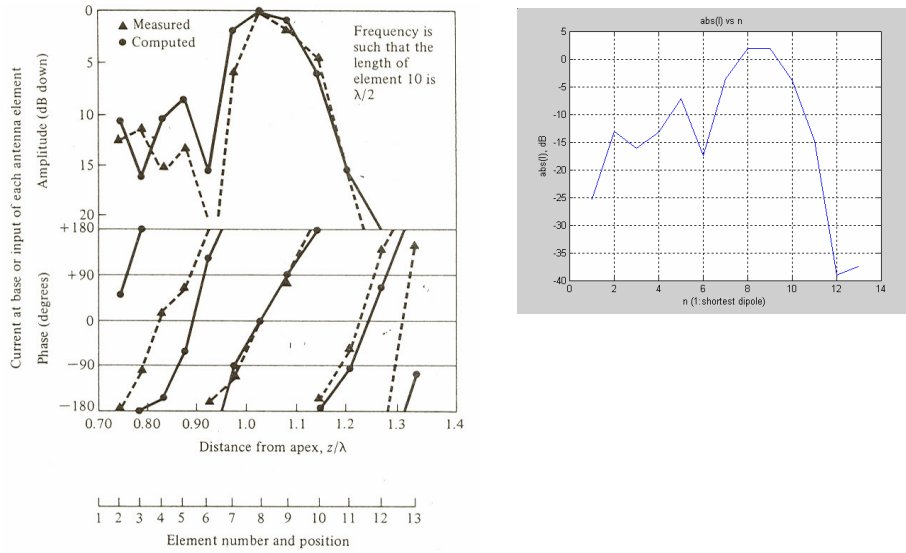


**Figure 3.19** Dipole base currents for the log periodic antenna given in Balanis [2] (left) versus calculated ones in MATLAB<sup>®</sup> at the frequency where element number

$$10 \text{ is } \frac{\lambda}{2}$$

Inspection of Figure 3.19, similarity between the two graphs can be noticed.

The phases of the currents are given in Figure 3.20. The graph at the right show the MATLAB<sup>®</sup> results, while the one at the left are taken from Balanis [2]. Comparison of two graphs shows that these graphs are sufficiently similar. The curves have the same slopes.

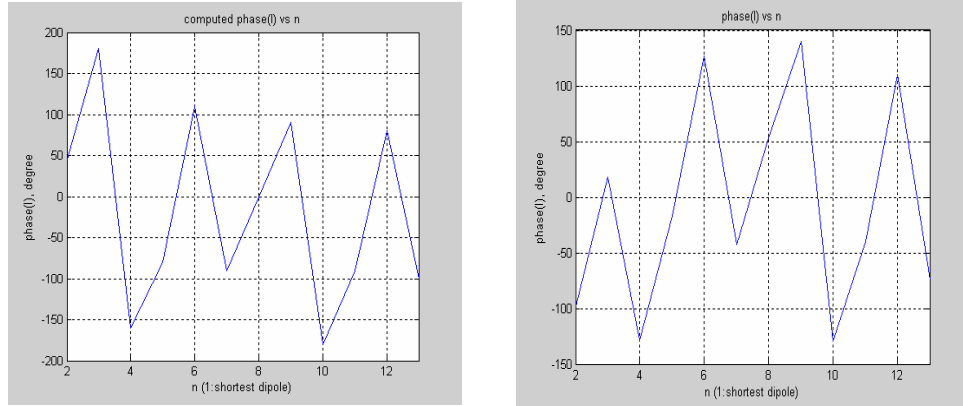


**Figure 3.20** Phases of currents given in Balanis [2] (left) versus calculated ones in

MATLAB<sup>®</sup> at the frequency where element number 10 is  $\frac{\lambda}{2}$

In section 1.3, it was stated that, after finding the currents at the bases of the dipoles, E and H-plane pattern of the log periodic antenna can also be calculated. In the following section far field patterns of a log periodic dipole antenna will be discussed.

### 3.3. FAR FIELD PATTERNS OF LOG PERIODIC ANTENNA

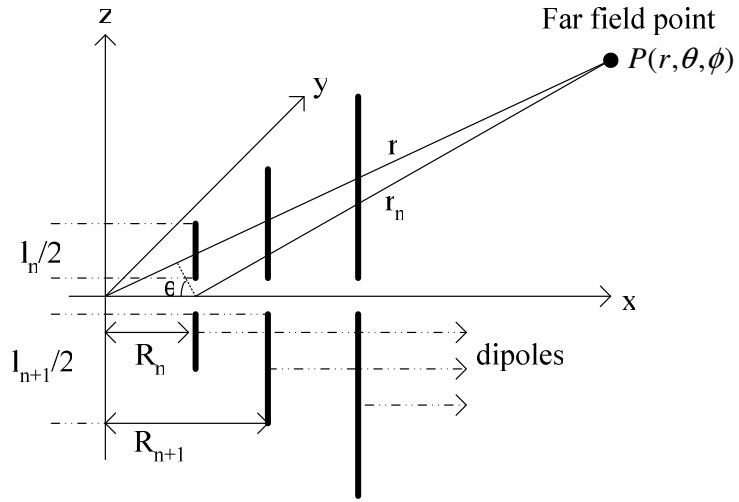


**Figure 3.21** Finite dipole geometry

In Figure 3.21, the current distribution on the dipoles, which are assumed to be center-fed, can be written as:

$$I(x=0, y=0, z') = \begin{cases} \frac{\hat{a}_z \cdot I_0 \cdot \text{Sin} \left[ k \left( \frac{l}{2} - z' \right) \right]}{\text{Sin} \left( k \frac{l}{2} \right)} & , 0 \leq z' \leq \frac{l}{2} \\ \frac{\hat{a}_z \cdot I_0 \cdot \text{Sin} \left[ k \left( \frac{l}{2} + z' \right) \right]}{\text{Sin} \left( k \frac{l}{2} \right)} & , -\frac{l}{2} \leq z' \leq 0 \end{cases}$$

Then the E field of a single dipole is:

$$E_{\theta_n} = j\eta \frac{I_{0n} e^{-jkr_n}}{2\pi r_n \cdot \text{Sin} \left( k \frac{l_n}{2} \right)} \left[ \frac{\text{Cos} \left( \frac{kl_n}{2} \text{Cos} \theta \right) - \text{Cos} \left( \frac{kl_n}{2} \right)}{\text{Sin} \theta} \right], [2] \quad \text{Equation 3.17}$$

In Equation 3.17, using Figure 3.22,  $r_n \approx r - R_n \sin \theta$ , which is the far field approximation for phase terms, in the numerator and  $r_n \approx r$ , which is the far field approximation for amplitude terms, in the denominator. Substituting these equality and approximation in Equation 3.17:

$$E_{\theta_n} = \frac{e^{-jkr}}{r} \cdot \frac{j\eta}{2\pi \cdot \sin(k \frac{l_n}{2})} \cdot I_{0n} \cdot e^{+jkR_n \sin \theta} \cdot F_n(\theta) \quad \text{Equation 3.18}$$

$$\text{where } F_n(\theta) = \left[ \frac{\cos\left(\frac{kl_n}{2} \cos \theta\right) - \cos\left(\frac{kl_n}{2}\right)}{\sin \theta} \right], [2]$$

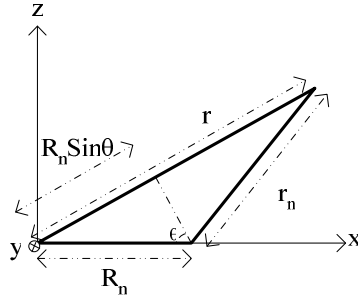


**Figure 3.22** Zoomed view of Figure 3.21 where dipoles are in xz plane (on the page)

Equation 3.18 is the  $E_{\theta_n}$  of one dipole. Total E plane pattern which is produced by N dipole:

$$E_{\theta} = \frac{e^{-jkr}}{r} \cdot \frac{j\eta}{2\pi \cdot \sin(k \frac{l_n}{2})} \cdot \sum_{n=1}^N I_{0n} \cdot e^{+jkR_n \sin \theta} \cdot F_n(\theta) \quad \text{Equation 3.19}$$

Equation 3.19 is the E-plane pattern of an antenna consisting of N dipole. In Figure 3.21, E-plane is the xz plane where  $\phi = 0$ . E-plane of an antenna is the plane where electric field lines occur.

### 3.3.1. GENERALIZATION FOR THE FAR-FIELDS OF THE ANTENNA

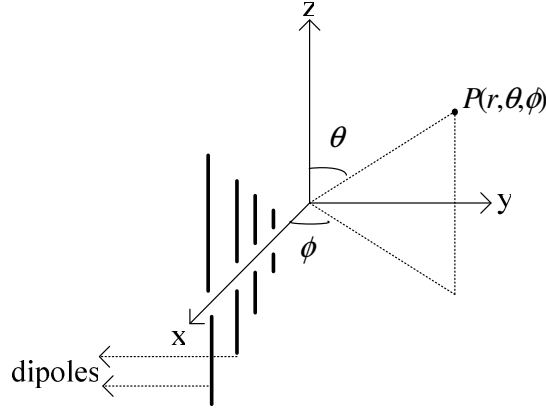


**Figure 3.23** Orientation of a log-periodic antenna on the Cartesian coordinate system

Referring Figure 3.23,

$$F_{ANT(\theta, \phi)} = \frac{j\eta}{2\pi r \cdot \text{Sin}(k \frac{l_n}{2})} \cdot e^{-jkr} \sum_{n=1}^N I_{0n} \cdot e^{+jk\hat{r}_n \cdot \hat{r}} \cdot F_n(\theta, \phi)$$

$$\text{where } F_n(\theta, \phi) = \left[ \frac{\text{Cos}\left(\frac{kl_n}{2} \text{Cos}\theta\right) - \text{Cos}\left(\frac{kl_n}{2}\right)}{\text{Sin}\theta} \right],$$

$r\hat{n}' = R_n \cdot \hat{a}_x$  and from rectangular-to-spherical transformation

$$\hat{r} = \text{Sin}\theta \cdot \text{Cos}\phi \cdot \hat{a}_x + \text{Sin}\theta \cdot \text{Sin}\phi \cdot \hat{a}_y + \text{Cos}\theta \cdot \hat{a}_z.$$

Finally,

$$F_{ANT}(\theta, \phi) = \frac{j\eta}{2\pi r \sin(k \frac{l_n}{2})} e^{-jkr} \sum_{n=1}^N I_{0n} e^{+jkR_n \sin\theta \cos\phi} F_n(\theta, \phi) \quad \text{Equation 3.20}$$

Using Equation 3.20, E and H plane patterns can be found. As explained before, E-plane, where the electric field lines occur, is the xz plane where  $\phi = 0$ . H-plane is the xy plane where  $\theta = 90^\circ$

In calculating the H-plane of the antenna, far field approximations also can be made by using Figure 3.24.  $r_n \approx r - R_n \cos\phi$ , which is the far field approximation for phase terms, in the numerator and  $r_n \approx r$ , which is the far field approximation for amplitude terms.

H plane pattern is,

$$E_\phi = \frac{e^{-jkr}}{r} \cdot \frac{j\eta}{2\pi \sin(k \frac{l_n}{2})} \sum_{n=1}^N I_{0n} e^{+jkR_n \cos\phi} F_n(\theta, \phi) \Big|_{\theta=90} \quad \text{Equation 3.21}$$

$$\text{where } F_n(\theta, \phi) \Big|_{\theta=90} = \left[ 1 - \cos\left(\frac{kl_n}{2}\right) \right]$$

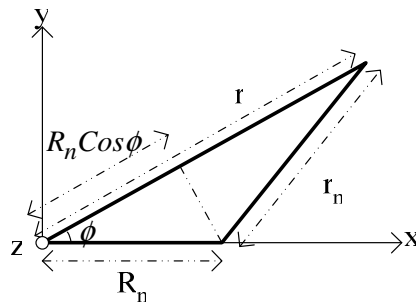


**Figure 3.24** Zoomed view of Figure 3.21 where dipoles are in xz plane (into the page)

## CHAPTER IV

### ANALYSIS AND DESIGN OF THE LOG-PERIODIC DIPOLE ANTENNA (LPDA)

#### 4.1. INTRODUCTION

In many applications an antenna should operate over a wide range of frequencies. An antenna with this feature is called a broadband antenna. If  $f_L$  and  $f_U$  are called lower and upper frequencies of operation for which satisfactory performance is obtained, then bandwidth can be defined as a ratio by  $\frac{f_U}{f_L}$ . Log periodic antenna can be one of the broadband antennas. Basic idea of a log-periodic antenna is using elements of varying lengths, which would resonate at different frequencies.

The properties of the log periodic antenna such as impedance, pattern, directivity, beamwidth, side lobe level at frequency  $f$ , will be repeated at all frequencies given  $f \cdot \tau^n$ , where  $n$  is integer. If  $\tau$  is not too far away from unity, the variations between these frequencies are quite small. When plotted on a logarithmic scale, these frequencies ( $f, \tau f, \tau^2 f \dots$ ) are equally spaced. That's to say, variations are periodic with logarithm of frequency. That's where "log-periodic" name comes from.

In a log periodic antenna, the lengths of the dipoles are half wavelength. When the antenna is operated at a wavelength within the design limits, that is approximately

$$2l_N < \lambda < 2l_1$$

where  $N$  is the total number of elements, a linearly polarized beam is observed in the direction of smaller elements. For any frequency within the design band, there are some elements, which are nearly half-wave length dimensions. The currents on these elements are large compared to the currents on the other elements. The elements with dimensions approximately half-wave lengths contribute most of the radiation so the region where these elements take place is called “active region”. As the frequency changes from  $f_{max}$  to  $f_{min}$ , the active region shifts from one group of elements to the next. The elements outside the active region act as parasitic elements. They do not contribute the radiation much.

## 4.2. DESCRIPTION OF LOG-PERIODIC ANTENNA

The log periodic antenna, described in Figure 2.1, consists of parallel linear dipole elements. The lengths of the dipole elements, the spacing from the virtual apex to the dipole elements, the wire radius of the dipole elements, the spacing between the quarter wave-length dipoles are proportional with the geometric scale factor,  $\tau$ , which is always smaller than 1. As shown in Figure 2.1, a wedge of enclosed angle  $2\alpha$  bounds the dipole lengths. The spacing factor,  $\sigma$  is defined as the distance between two dipole elements divided by the twice of the length of the larger dipole element. The relationship between the parameters shown in Figure 2.1 can be summarized as follows:

$$\frac{1}{\tau} = \frac{l_2}{l_1} = \frac{l_{n+1}}{l_n} = \frac{R_2}{R_1} = \frac{R_{n+1}}{R_n} = \frac{d_2}{d_1} = \frac{d_{n+1}}{d_n} = \frac{s_2}{s_1} = \frac{s_{n+1}}{s_n} \quad \text{Equation 4.1}$$

where

$\tau$  is the geometric ratio and  $\tau < 1$ ,

$l$  is the length of the dipole,

$R$  is the distance from apex to the dipole elements,

$d$  is the diameter of the dipole elements,

$s$  is the gap spacing at the dipole center,

$\alpha$  is the half of the apex angle.

In typical designs,  $\alpha$  takes values between  $10^\circ$  -  $45^\circ$  and  $\tau$  varies from 0.7 to 0.95.

Spacing factor, which relates distance between two adjacent elements with the length of the larger element, can be defined as:

$$\sigma = \frac{R_{n+1} - R_n}{2l_{n+1}} \quad \text{Equation 4.2}$$

In the design of log-periodic dipole arrays, fundamental design parameters can be related through the following equation:

$$\tan(\alpha) = \left( \frac{1 - \tau}{4\sigma} \right) \quad \text{Equation 4.3}$$

If two of the parameters are specified, the third one can be found through this equation. Using this equation, one can find that  $\sigma$  takes the values between 0.07 and 0.43 for typical designs.

Theoretically the ratio of the element length to the element radius should be same but in practice the dipole elements constituting a log-periodic dipole array are grouped into 3 different radii for the whole log-periodic antenna.

Main regions of a log periodic antenna can be summarized as follows:

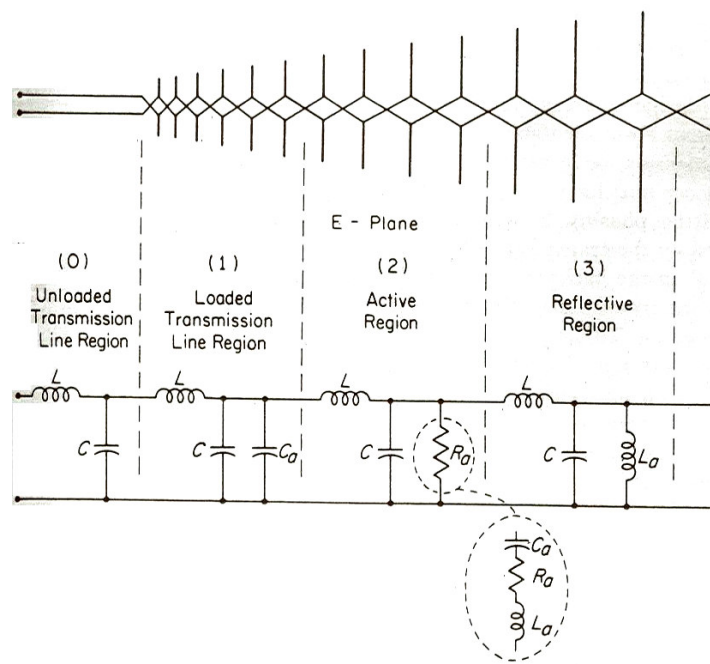


**Figure 4.1** Main regions of a log-periodic dipole antenna [8]

#### 4.2.1. LOADED TRANSMISSION LINE REGION

In this region dipoles are shorter than a half-wave length at a given frequency. Since elements are shorter than  $\lambda/2$ , the elements act as shunt capacitors. The small elements in this region are closely spaced and fed out of phase, so their contribution to the total radiated field is negligible.

The antenna is fed from the smallest dipole at this region. There are two types of fields along the structure. One originates at the feeder point and propagates in the direction of longer elements, which is called transmission field and given in Figure 4.2.

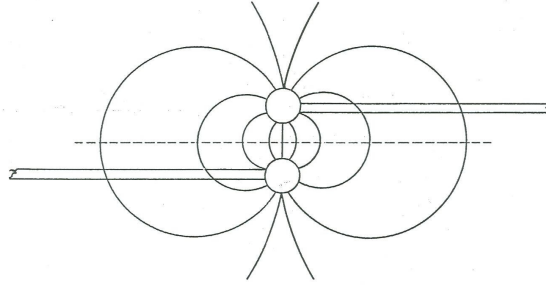


**Figure 4.2** Feeder field for a log-periodic antenna [5]

The other field originates around the dipole and propagates in the direction of shorter elements, which is called radiated field and given in Figure 4.3. Both fields are perpendicular to the axis of the antenna. When the antenna is fed from the smallest dipole, a TEM type wave is set-up and supported by the feeder line.

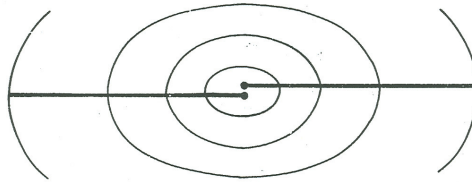


**Figure 4.3** Radiation field for a log-periodic antenna [5]

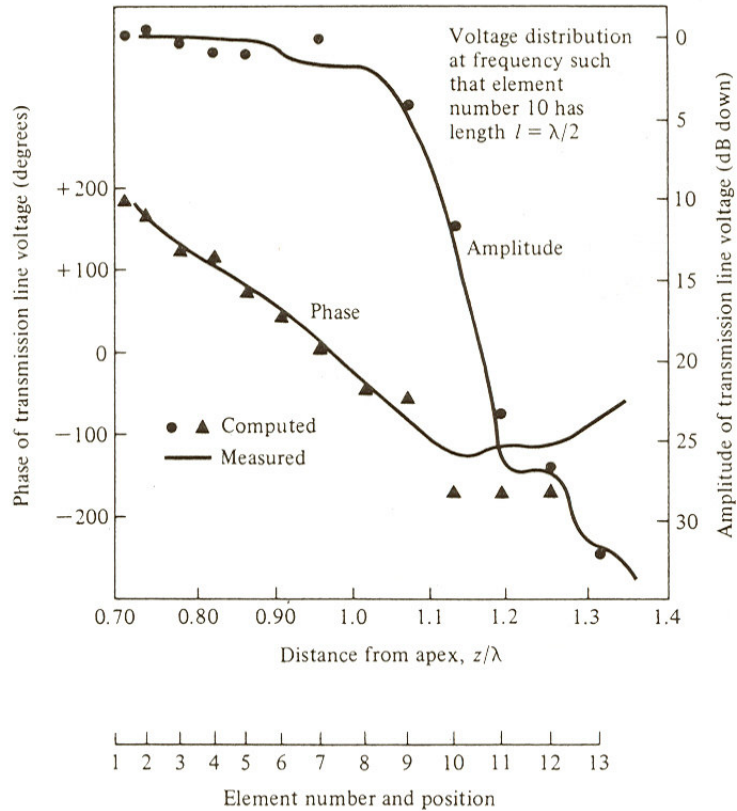


**Figure 4.4** Voltage distribution for log periodic antenna composed of 13 elements [2]

In Figure 4.4, one can see transmission line voltage versus distance from apex. In the graph, voltages are calculated at the bases of the dipoles. Inspection of Figure 4.4, the amplitude of the voltage is constant from the beginning of the feeder line up to the point where  $z/\lambda \approx 1$ , which shows there is very little attenuation or reflection when the wave travels in this part of the transmission line. In  $z/\lambda > 1$  region, the voltage drops rapidly since the energy is given to the elements, which are approximately half-wave length in the transmission region. Since the magnitude of voltage is almost constant and the phase is linear in the transmission line region, loading is said to be uniform and capacitive. The capacitance of a dipole is proportional to its length. The spacing between two dipoles is also proportional to its length, thus the added capacitance per unit length is constant [5].

In can be found in the literature [5], for low VSWR antennas, the slope of the phase of the voltage up to  $z/\lambda \approx 1$  point is proportional to the velocity of the propagation of the transmission wave,  $V_t$ , relative to the speed of light,  $c$ . When the slope of the line in reflective region is calculated in Figure 4.4,  $\tan \alpha = 0.68$ . One can notice that, the wave produced is a “slow wave” since  $V_t < c$ .  $V_t$  primarily depends on  $\sigma$ . It was found that when  $\sigma$  decreases, velocity of the transmission wave decreases. This can be observed in Figure 4.5 for two different values of  $\tau$ .

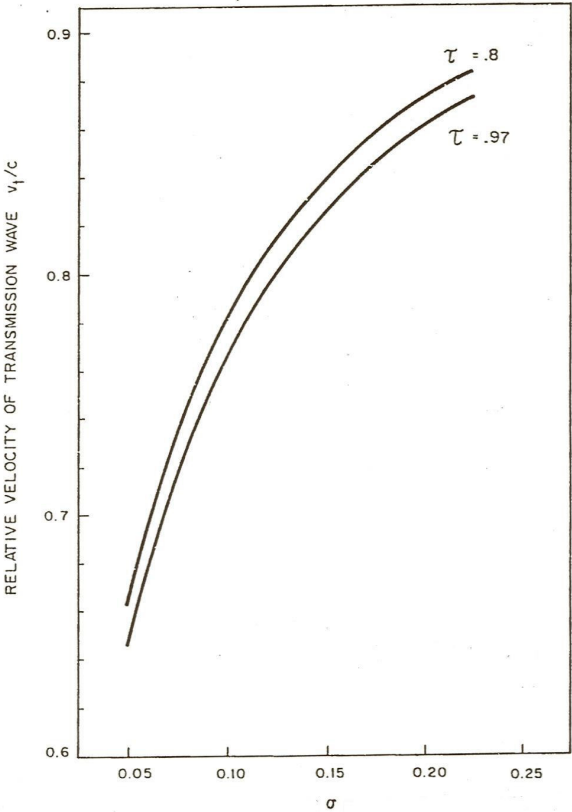


**Figure 4.5**  $V_t/c$  versus  $\sigma$  for  $\tau = 0.8$  and  $0.97$  with  $Z_0/Z_a = 0.33$  [5]

#### 4.2.2. ACTIVE REGION

In this region, dipoles are approximately half-wave length at a given frequency. Thus, dipole impedances have mainly resistive component. Radiation of antenna is determined mainly by this region.

Inspection of Figure 4.6, one sees the absolute value of current at the bases of each dipole and corresponding phases. As an important observation, amplitude of current is maximum at the base of dipole, which is a bit shorter than half-wave length. As frequency changes, maximum place of the current moves along the active region.

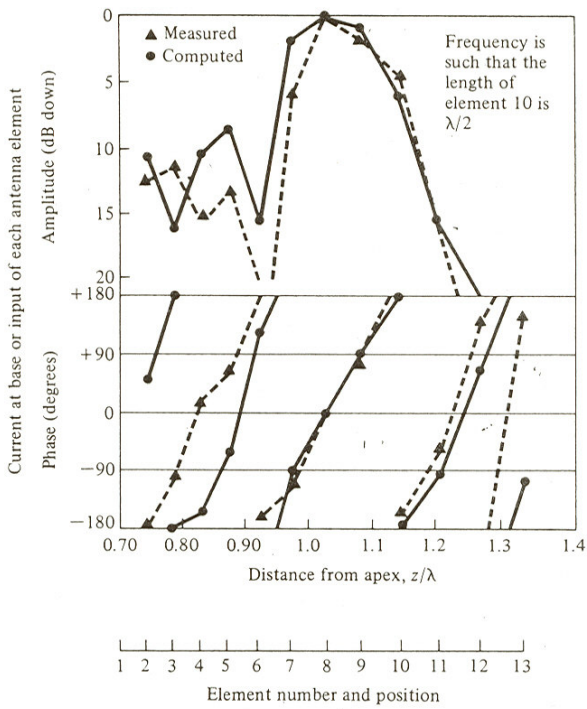


**Figure 4.6** Element currents for the array given in Figure 4.4 [2].

### 4.2.3. INACTIVE (REFLECTIVE) REGION

This region is also called “unexcited region”. In this region, dipoles are longer than half wave length at a given frequency. Inspection of Figure 4.6 reveals that, in the unexcited region, magnitude of the currents at the bases of the dipoles decrease rapidly because most of the incident power is radiated by the elements in the active region.

In this region, it was shown that [5], if enough power is delivered, elements which are approximately odd multiples of half wave length will radiate. The other elements do not radiate because the elements which are longer than a half wave length are not efficiently coupled to the feeder, due to a difference in impedance level.

### 4.3. EFFICIENCY OF LPDA

Efficiency of a log periodic antenna can be calculated from  $\eta = \frac{P_{IN} - P_T}{P_{IN}}$  where

$P_{IN}$  is the total input power and  $P_T$  is the power dissipated in a matched resistor at the large end of the antenna.

Computed results shown in Figure 4.7, show that, when the longest element is half wavelength, radiating efficiency is approximately 83% for a feeder impedance,  $Z_0$ , is equal to 100  $\Omega$ . This means approximately 83% of incident power is radiated by the active region.

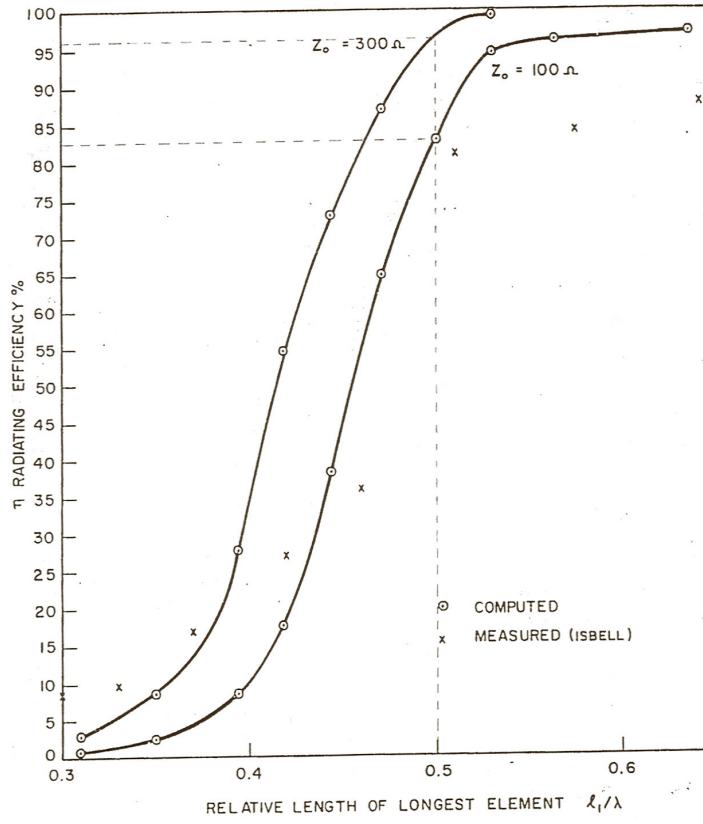


**Figure 4.7** Radiating efficiency of active region vs. relative length of longest element [5]

Inspection of Figure 4.7, it is observed that for  $Z_0 = 300 \Omega$ , efficiency increases from 80% to 95%. This is the result of the movement of the active region toward the apex of the antenna when  $Z_0$  is increased. [5]

Radiation efficiency varies with  $Z_0$  and  $\tau$ . This phenomenon can be observed in Figure 4.8.

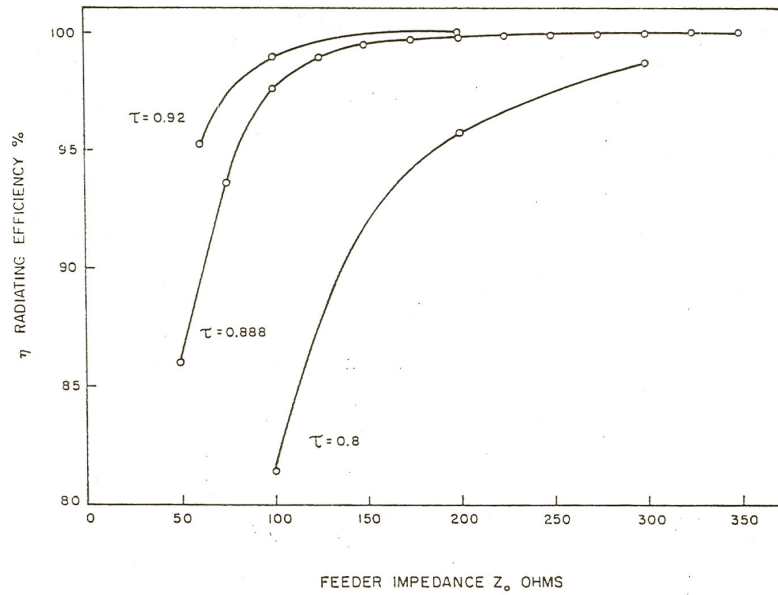


**Figure 4.8** Radiating efficiency of the active region vs. feeder impedance and  $\tau$  [5]

If the efficiency is less than 85%, the antenna is terminated by short circuit and some power is reflected back into the active region. In log periodic antennas having a feeder impedance,  $Z_0$ , less than 75  $\Omega$ , important amount of power can not be radiated by the active region, remains on the feeder at the part after the feeder region. This power is reflected back through the antenna by shorting the feeder at the large end, as is commonly done. In practice, feeder is terminated in a short circuit a distance of  $\lambda_{\max}/8$  or less behind the largest element, so that at the lowest frequency  $Z_T$  remains still inductive, assuming that the impedance  $Z_T$  terminates the feeder. [5]

#### 4.4. DESIGN OF LOG-PERIODIC DIPOLE ANTENNAS

In this section, first parameters will be reviewed. Then details about the feeding and input impedance of the antenna will be determined. Finally, physical and the electrical properties of the dual polarized log-periodic antenna, which is the first product of this thesis, will be detailed.

As the first step of the design procedure, fundamental design parameters  $\tau$  and  $\sigma$  should be chosen for a given directivity. For a given directivity, the relative spacing,  $\sigma$  and the geometric ratio,  $\tau$  can be related through the following figure:

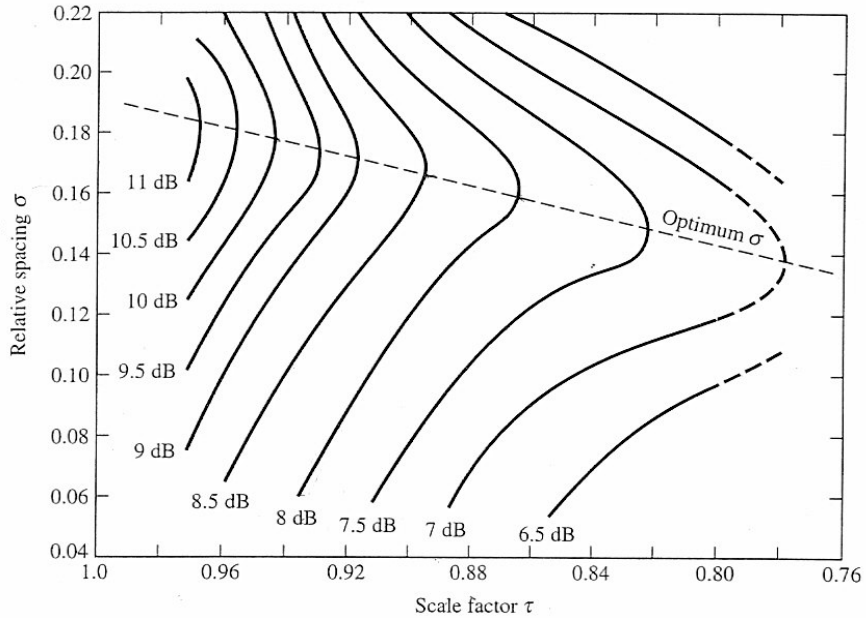


**Figure 4.9** Computed contours of constant directivity versus  $\tau$  and  $\sigma$  for log periodic dipole arrays [2]

Fundamental design parameters can be related through the Equation 4.3 which

is equal to:  $\tan(\alpha) = \left( \frac{1-\tau}{4\sigma} \right)$

In Figure 4.9, for a given directivity, corresponding  $\sigma$  and  $\tau$  can be found. For a certain  $\tau$ , if maximum directivity is desired,  $\sigma_{opt}$  should be chosen through the curves. Optimum  $\sigma$  in Figure 4.9 can be formulated as:

$$\sigma_{opt} = 0.258\tau - 0.066 \quad \text{Equation 4.4}$$

Gain of a log-periodic antenna is only slightly affected by the dipole thickness. It increases about 0.2 dB for a doubling of the dipole thickness. [7] One can use  $\sigma$  smaller than the optimum value of the  $\sigma$ ,  $\sigma_{opt}$ , but it shouldn't be smaller than 0.05 since the front to back ratio decreases and the directivity falls off rapidly. The latter is also valid for  $\sigma$  greater than  $\sigma_{opt}$ . When  $\sigma$  greater than  $\sigma_{opt}$  is chosen, side lobes appear.

After determining  $\sigma$ ,  $\tau$  and  $\alpha$ , bandwidth of the system which determines the longest and the shortest dipole elements can be calculated. Active region bandwidth,  $B_{ar}$  can be related with the fundamental design parameters by the following equation:

$$B_{ar} = 1.1 + 7.7(1 - \tau)^2 \cot \alpha \quad \text{Equation 4.5}$$

In practice a slightly larger structure bandwidth,  $B_s$  is usually designed to reach the desired bandwidth,  $B$ . These bandwidths are related by:

$$B_s = BB_{ar} = B(1.1 + 7.7(1 - \tau)^2 \cot \alpha) \quad \text{Equation 4.6}$$

where

$$B = \frac{f_{max}}{f_{min}}$$

Boom length of the structure is defined between the shortest dipole and longest dipole elements and is given by:

$$\frac{L}{\lambda_{max}} = \frac{1}{4} \left( 1 - \frac{1}{B_s} \right) \cot \alpha \quad \text{Equation 4.7}$$

where  $\lambda_{max} = 2l_{max} = \frac{v}{f_{min}}$

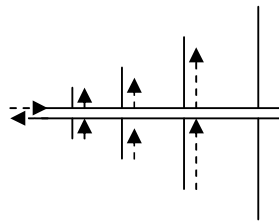
Number of the dipole elements is given by:

$$N = 1 + \frac{\log(B_s)}{\log\left(\frac{1}{\tau}\right)} \quad \text{Equation 4.8}$$

#### 4.4.1. FEEDING OF THE LOG-PERIODIC ANTENNA

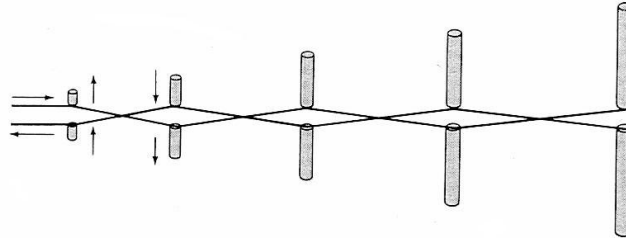
The elements are energized from a balanced, constant impedance feeder, adjacent elements being connected to the feeder in an alternating fashion and they are energized starting from the smallest dipole.

Figure 4.10 shows an unsuccessful method of exciting the antenna. The elements are closely spaced with a distance of approximately  $0.07\lambda$ . The phase progression along the array is such as to produce a beam to the right of the Figure 4.10. As longer elements, to the right of the active region, are in the beam and have not alternating phase, they produce interference effects to the pattern result.



**Figure 4.10** Unsuccessful method of feeding the antenna [5]

Figure 4.11 shows a successful method of exciting the antenna. Difference between the two method of exciting is, by criss-cross connection, a  $180^\circ$  phase is added to the terminal of each element.



**Figure 4.11** Successful method of feeding the antenna [2]

Little energy is radiated by the adjacent closely spaced short elements because the phase between these elements is almost in opposite so their interference effects are very small. The longer and the larger elements radiate at the same time. The mechanical phase reversal between these elements produces a phase progression so that energy is beamed to the left of the Figure 4.11, in the direction shorter elements.

Alternative to the crisscross connection, the antenna can be energized from a coaxial line. By this way, the  $180^\circ$  phase reversal between adjacent elements is obtained. The shield of the coax is inserted through the hollow of the one feeder line, and at the front of the antenna the central conductor of the coax is extended and connected to the other feeder line as shown in Figure 4.12.

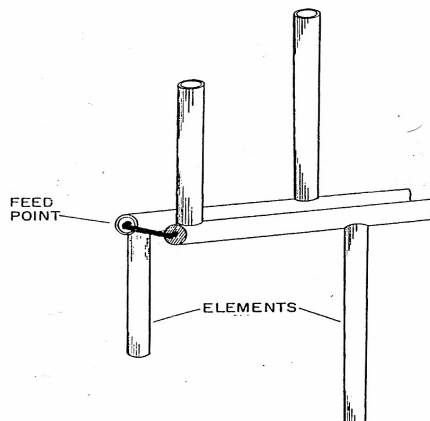


**Figure 4.12** Energizing dipoles by using coaxial line [5]

Using a coaxial cable as a feed line, provides a built-in broadband balun resulting in a balanced overall. The antenna is fed from the smallest dipole element. A 180° phase difference between two equal dipole arms is formed by using a coaxial cable as a feed line which is a balanced structure.

Ideally the feeder should be conical or stepped to preserve the exact scaling between the elements, but in practice, it is found that two parallel cylinders can successfully replace the cones as long as the radius of the cylinders remains small compared to the shortest wavelength of operation [5]. The element feeder configuration is shown in the Figure 4.12.

It is seen that the elements don't lie on the same plane exactly, the departure therefrom is equal to the feeder spacing which is always small.

#### 4.4.2. DESIGNING FOR GIVEN INPUT IMPEDANCE

Once the final values of  $\tau$  and  $\sigma$  are found, to get required input impedance  $R_0$ , the characteristic impedance of the feeder,  $Z_0$  must be determined. To accomplish this, first the average characteristic impedance of a dipole element  $Z_a$  should be defined as follows:

$$Z_a = 120(\ln(l_n / d_n) - 2.25) \quad [2] \quad \text{Equation 4.9}$$

where

$l_n$  is the length of the  $n^{\text{th}}$  dipole element

$d_n$  is the diameter of the  $n^{\text{th}}$  dipole element

The  $l_n / d_n$  ratio should be same for each element ideally. Practically, the element diameters can be scaled in two, three or more groups, and in the computation of the characteristic impedance of dipole elements the average  $l_n / d_n$  in a group should be used.

Characteristic impedance of the feeder line,  $Z_0$ , relative to the required input impedance  $R_0$ , which is real, can be given by:

$$\frac{Z_0}{R_0} = \frac{1}{8\sigma' \frac{Z_a}{R_0}} + \left[ \frac{1}{\left(8\sigma' \frac{Z_a}{R_0}\right)^2} + 1 \right]^{1/2} \quad [5] \quad \text{Equation 4.10}$$

where

$\frac{Z_a}{R_0}$  is the average characteristic impedance of a dipole element with respect to

the required input impedance  $R_0$

$\sigma'$  is the mean relative spacing,

$$\sigma' = \frac{\sigma}{\sqrt{\tau}} \quad [2] \quad \text{Equation 4.11}$$

A graph of Equation 4.10 is given in Figure 4.13:

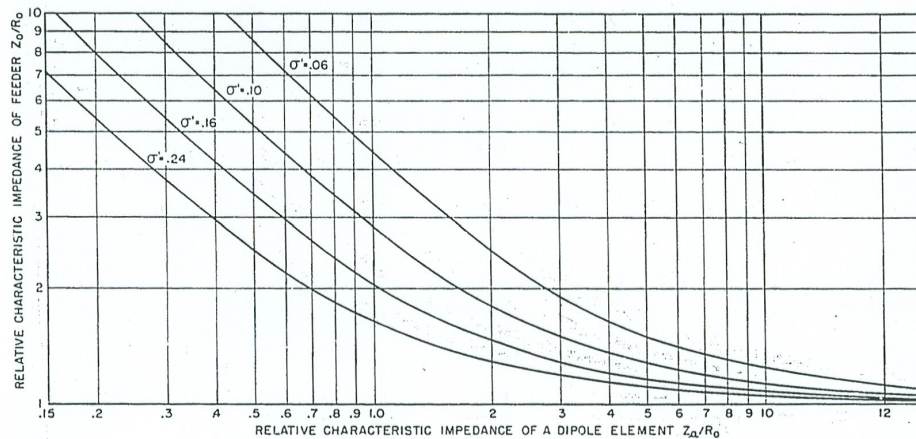


**Figure 4.13** Relative characteristic impedance of feeder vs. relative characteristic impedance of dipole element for different values of  $\sigma'$  [2]

Equation 4.10 can be inverted to the following form:

$$R_0 = \frac{Z_0}{\sqrt{\left(1 + \frac{Z_0 \sqrt{\tau}}{Z_a 4\sigma}\right)}} \quad \text{Equation 4.12}$$

Figure 4.14 is a graph of Equation 4.12 for  $Z_0=100$  and  $Z_a=350$  as a function of  $\sigma$ , for two values of  $\tau$ , 0.8 and 0.97. In this graph, for constant  $Z_0$  and  $Z_a$ , the effect of  $\tau$  can be viewed. It can be noted that, the dependence of  $\tau$  on the input impedance of a log-periodic dipole antenna,  $R_0$ , is not great. For a given  $Z_0$  and  $Z_a$ ,  $R_0$  primarily depends on the spacing  $\sigma$ . As  $\sigma$  increases, the added loading decreases, so  $R_0$  approaches to the  $Z_0$ .

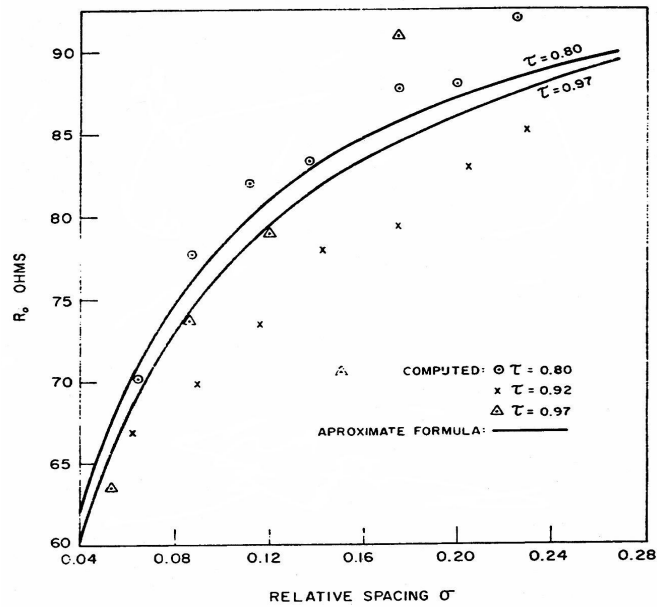


**Figure 4.14**  $R_0$  vs.  $\sigma$  for  $Z_0=100$  and  $Z_a=350$  for two values of  $\tau$  [5]

Feeder is spaced according to the following formula:

$$s = d \cosh\left(\frac{Z_0}{120}\right) \quad [2] \quad \text{Equation 4.13}$$

where

$s$  is the center-to-center spacing of the feeder conductors,

$d$  is the diameter of the feeder conductors and

$Z_0$  is the characteristic impedance of the feeder line.

In Figure 4.15, one can notice that center-to-center spacing between the feeder conductors,  $s$  should be greater than the diameter of the feeder conductor,  $d$ . Otherwise, two feeder conductors intersect with each other.

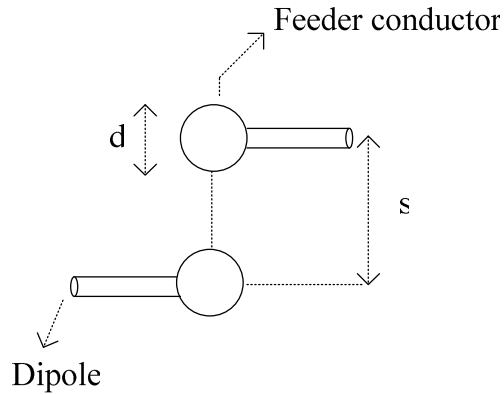


**Figure 4.15** Top view of feeder line configuration

#### 4.4.2.1. FEED SEPARATION FOR A DUAL POLARIZED LOG PERIODIC ANTENNA

For dual polarized log periodic antenna, there are 4 feeder conductors, two pairs of feed lines, as shown in Figure 4.16.

In Figure 4.16, feeder conductors 1 and 3 form a pair of transmission line, and an antenna. This is also valid for feeder conductors 2 and 4.

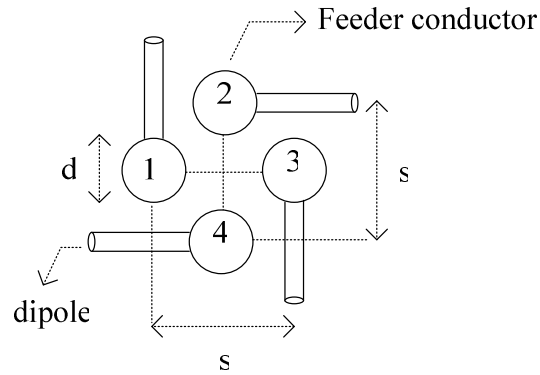


**Figure 4.16** Top view of a pair of feed lines for a dual polarized log periodic antenna

In Figure 4.16, as explained before, center-to-center spacing between the feeder conductors,  $s$  should be greater than the diameter of the feeder conductor,  $d$ . This condition is not sufficient for the feed section of dual polarized log periodic antenna. Conductors 1 and 2 also should not intersect with each other. From this condition, the following calculation can be made:

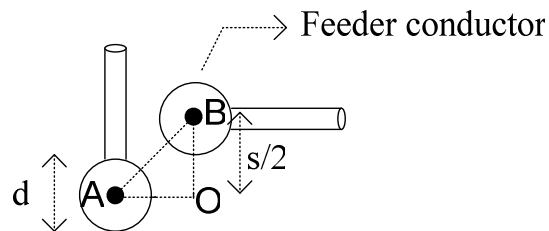


**Figure 4.17** Two feeder conductors from Figure 4.16

In Figure 4.17, from AOB triangle, distance from point A to point B is equal to  $s/\sqrt{2}$ .

$$s/\sqrt{2} \geq d \Rightarrow s \geq d\sqrt{2}$$

Using Equation 4.13,

$$d \cosh\left(\frac{Z_0}{120}\right) \geq d\sqrt{2} \Rightarrow \cosh\left(\frac{Z_0}{120}\right) \geq \sqrt{2} \Rightarrow$$

$$\frac{Z_0}{120} \geq 0.88 \Rightarrow$$

$$\boxed{Z_0 \geq 105.6}$$

This result tells us that, in order to make the feeder conductors 1 and 2 in Figure 4.16 non-intersecting, characteristic impedance of the feeder,  $Z_0$  should be greater than 105.6 Ohm.

In dual polarized log-periodic antennas, it is found that,  $Z_0$ , should be greater than 105.6Ω. From Equation 4.10,  $Z_0$  depends on  $\frac{8\sigma'Za}{R_0}$ . If we call  $\frac{8\sigma'Za}{R_0}$  as  $x$ ,

$$\text{then } \frac{Z_0}{R_0} = \frac{1}{x} + \sqrt{\frac{1}{x^2} + 1}.$$

To get a high  $Z_0$ ,  $\sigma'$  and  $Za$  should be small or  $R_0$  should be large. After some analysis it is found that, most effective thing is increasing  $R_0$  to get high feeder impedance greater than 100Ω. That's why in the design of dual-polarize log-periodic antenna required input impedance is taken as 100 Ω.

#### **4.5. DUAL POLARIZED LOG-PERIODIC ANTENNA DESIGN**

In this section, an example for a log-periodic antenna will be given. Design of a dual polarized log periodic antenna is one of the topics in the scope of this thesis. First, design procedure will be explained step by step. Second, some physical properties and some experiments about the physical properties of the antenna will be explained. Finally, electrical properties of the antenna will be given. To design a log-periodic antenna, one should have a starting point such as a desired gain,

desired input impedance, desired feeder line characteristic impedance etc. The antenna designed for this thesis has some limitations as following:

Size of the antenna should be small as possible as it can, since it will be used as a feed for a reflector antenna.

Characteristic impedance of the feeder line should be greater than 105.6 Ohm in order to make the feeder conductors non-intersecting.

In the design of the antenna the correlation between parameters and their effects, which are detailed in section 4.4, are taken into account. Some relations about some design parameters are given as follows:

- Number of elements is determined by  $\tau$ . As  $\tau$  increases, number of elements also increases.
- As  $\alpha$  increases, size of the antenna decreases and  $\sigma$  decreases.
- For constant  $\sigma$ , as  $\tau$  increases,  $\alpha$  decreases and size increases.
- For constant  $\tau$ , as  $\sigma$  increases,  $\alpha$  decreases and size increases.
- $R_0$  decreases with increasing  $\tau$  and increasing  $\sigma$ .
- As  $\sigma' = \frac{\sigma}{\sqrt{\tau}}$  increases  $R_0$  approaches to  $Z_0$ .
- To increase  $Z_0$ , one should decrease  $8\sigma' \frac{Z_a}{R_0}$ . There are three ways to decrease  $8\sigma' \frac{Z_a}{R_0}$ .
  - $\sigma' = \frac{\sigma}{\sqrt{\tau}}$  can be decreased. This means that,  $\sigma$  should be decreased or  $\tau$  should be increased.

- $Z_a$  can be decreased. This means that, from Equation 4.9,  $l_n / d_n$  ration should be decreased.
- $R_0$  should be increased.

$R_0$  is the most effective parameter in order to change the characteristic impedance of the feeder line,  $Z_0$ .

#### 4.5.1. DESIGN PROCEDURE

Antenna will cover the frequency band of 0.4 GHz- 18 GHz. Since the mutual coupling between two orthogonal elements is so small as explained in Section 3.2.3, antenna will be designed as if it is a single polarize antenna but considering the procedure explained in 4.4.2.1 since two single polarize antenna will constitute a dual polarized antenna. Design procedure explained in Section 4.4 is followed as follows:

1)  $\tau = 0.865$

For this  $\tau$ , if one wants to get a maximum directivity, from Equation 4.4,  $\sigma_{opt} = 0.157$ . Since the characteristic impedance of the feeder line,  $Z_0$ , should be greater than 105.6 Ohm, as explained in Section 4.4.2.1,  $\sigma_{opt}$  should be small but greater than 0.05.  $\sigma$  which is smaller than  $\sigma_{opt}$ , will decrease the directivity, but directivity is not the main concern in this antenna.

2)  $\sigma = 0.08$

3) From Equation 4.3,  $\alpha = 22.87^\circ$  which means that, the apex angle of the antenna is  $2\alpha = 45.74^\circ$ .

4) From Figure 4.9, one can notice that, the directivity of the antenna is approximately 6.9dB.

- 5) From Equation 4.5 and Equation 4.6 ,  $B_{ar} = 1.433$  and  $Bs = 64.47$  .
- 6) From Equation 4.7,  $L = 43.76cm$  where  $\lambda_{max} = 75cm$  . This is the distance between the smallest and the largest dipoles.
- 7) From Equation 4.8,  $N= 29.72$ , which means that number of elements should be approximately 30. Number of dipole elements is chosen as 33.

Next, average characteristic impedance of a dipole element,  $Z_a$  input impedance,  $R_0$  of the antenna and the characteristic impedance of the feeder line,  $Z_0$  should be defined.

- 8) From Equation 4.11,  $\sigma' = 0.086$  .
- 9)  $l_{max} = 464.13$  mm and  $l_{min} = 4.46$  mm
- 10) To calculate the characteristic impedance of the feeder,  $Z_0$  first the characteristic elements of the dipoles,  $Z_a$  should be calculated. To calculate  $Z_a$  , dipoles can be grouped into three. First group consists of 13 shorter dipoles, second group consists of 8 dipoles and the third group consists of 12 longer dipoles.

Average  $l_n / d_n$  ratios can be calculated for each group:

$$avg(l_n / d_n) = \begin{cases} 44.1 \\ 45.3 \\ 119.61 \end{cases} \begin{matrix} \rightarrow \text{for the 1}^{st} \text{ group} \\ \rightarrow \text{for the 2}^{nd} \text{ group} \\ \rightarrow \text{for the 3}^{rd} \text{ group} \end{matrix}$$

Using Equation 4.9, corresponding  $Z_a$  values for each group are as follows:

$$Z_a = \left\{ \begin{array}{l} 184.375\Omega \\ 187.59\Omega \\ 304.108\Omega \end{array} \right\}$$

Using Equation 4.10, corresponding  $Z_0$  values for each group are as follows:

$$Z_0 = \left\{ \begin{array}{l} 206.17\Omega \\ 204.04\Omega \\ 158.632\Omega \end{array} \right\}$$

10) Finally, feed line configuration should be determined. Using Equation 4.13;

For 1<sup>st</sup> group,  $s = 2.87d$

For 2<sup>nd</sup> group,  $s = 2.83d$  and

For 3<sup>rd</sup> group,  $s = 2d$

where  $s$  is the center-to-center spacing of the feeder conductors and  $d$  is the diameter of the feeder conductors.

Referring Figure 4.18,  $d$  is chosen as 1 mm, 1.8 mm and 4 mm for 1<sup>st</sup>, 2<sup>nd</sup> and 3<sup>rd</sup> groups respectively.

Transition regions are adjusted as distance between the 13<sup>th</sup> and 14<sup>th</sup> dipoles is divided into two equal parts by the transition line. This is also valid for 21<sup>st</sup> and 22<sup>nd</sup> dipoles. Detailed view of the transition region is also given in Figure 4.18. In Figure 4.18,  $x$  and  $y$  are adjusted such that they are small compared to wavelength.

$$\frac{x}{\lambda} = \frac{3.615mm}{55.03mm} = 0.0656 \quad \text{and} \quad \frac{y}{\lambda} = \frac{3.625mm}{175.59mm} = 0.02$$

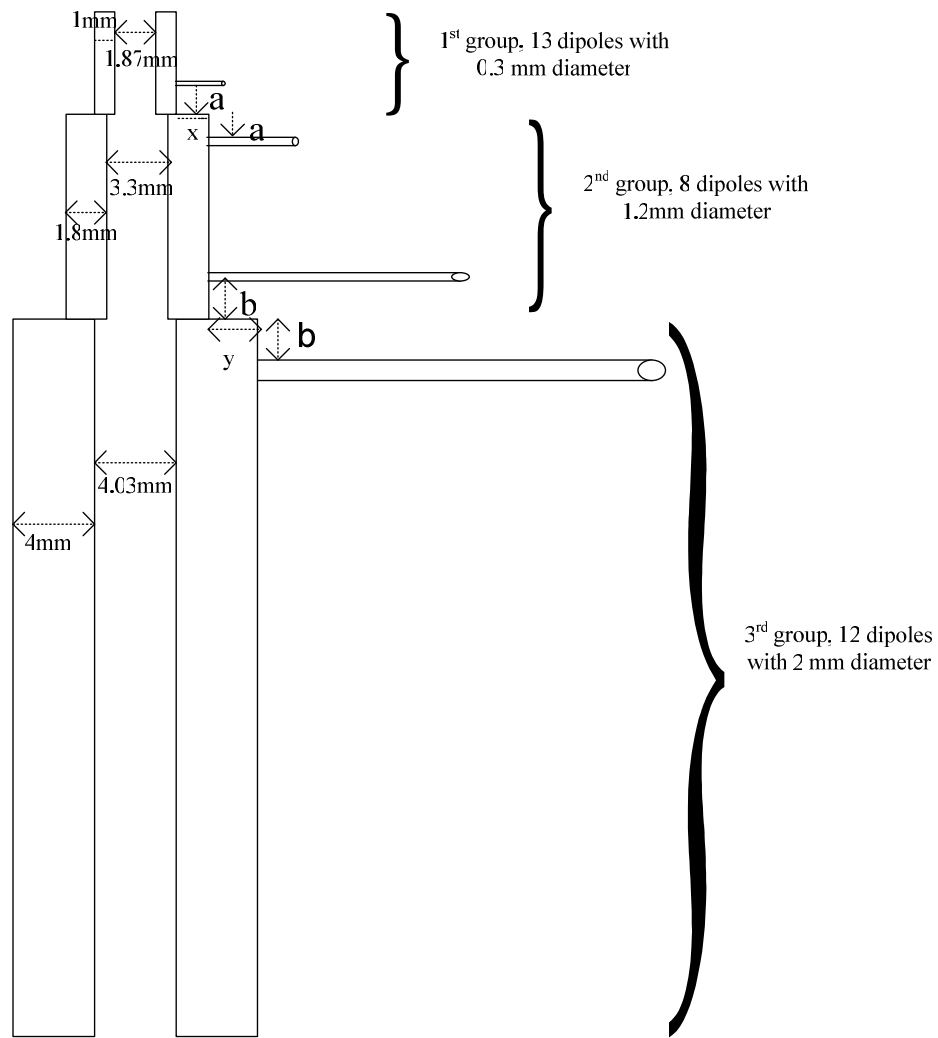


**Figure 4.18** Detailed view of a of feed line and the positioning of the dipoles on the transition regions

Structure given in Figure 4.18 is tried to be produced both in ASELSAN<sup>®</sup> and a company called Birikim Makine Sanayi ve Ticaret Ltd. Stepped transmission line is found to be very difficult and risky to be produced. Therefore the physical properties of the antenna had to be changed. Transmission lines are designed such that they have the same center. Production of centric transmission lines are very easy compared to production of off-centric transmission lines. Production of

centric transmission lines are very easy compared to production of off-centric transmission lines.

As a summary, for the new antenna:

$$\text{avg}(l_n / d_n) = \begin{cases} 47.43 \\ 108.74 \\ 299.02 \end{cases} \begin{array}{l} \rightarrow \text{for the 1}^{\text{st}} \text{ group} \\ \rightarrow \text{for the 2}^{\text{nd}} \text{ group} \\ \rightarrow \text{for the 3}^{\text{rd}} \text{ group} \end{array}$$

Corresponding  $Z_a$  values for each group are as follows:

$$Z_a = \begin{cases} 193.11\Omega \\ 292.67\Omega \\ 414.06\Omega \end{cases}$$

And finally, corresponding  $Z_0$  values for each group are as follows:

$$Z_0 = \begin{cases} 200.42\Omega \\ 161.32\Omega \\ 141.08\Omega \end{cases},$$

Feed line configuration is as follows:

For 1<sup>st</sup> group,  $s = 2.75d$

For 2<sup>nd</sup> group,  $s = 2.048d$  and

For 3<sup>rd</sup> group,  $s = 1.77d$

The modified detailed view of a pair of transmission lines is given in Figure 4.19.

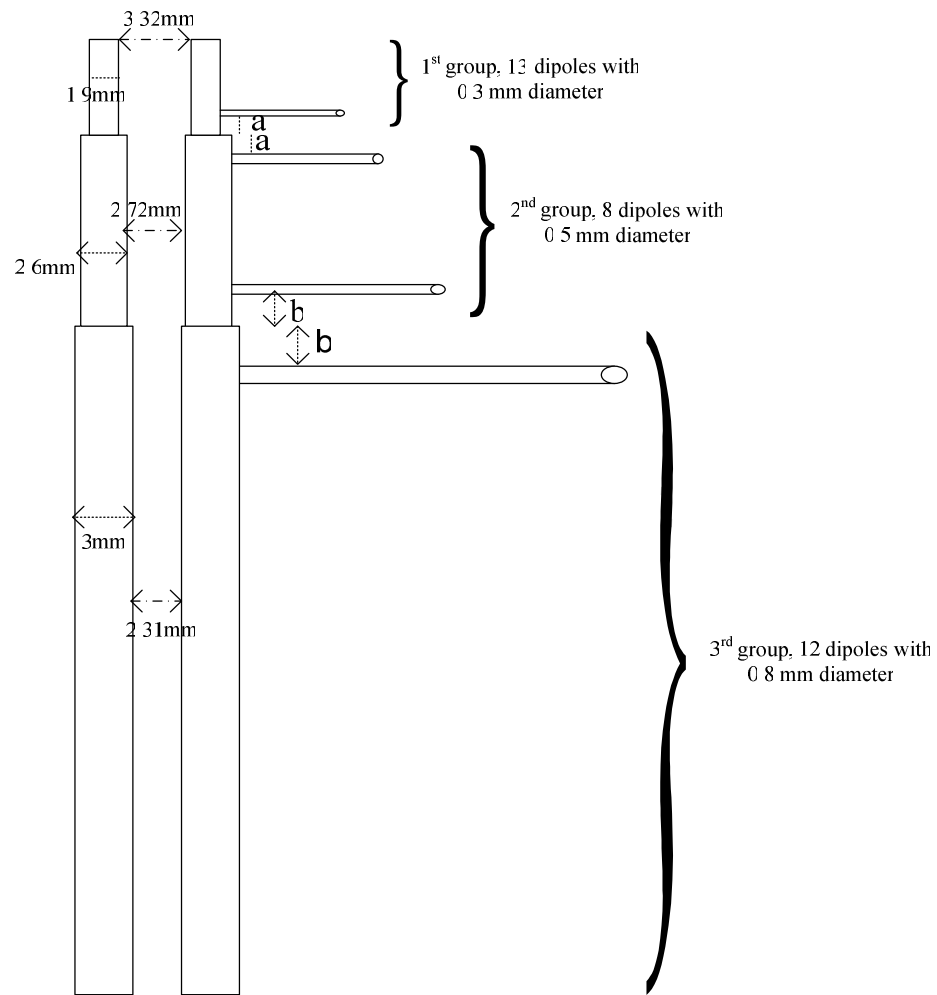


**Figure 4.19** Modified form of detailed view of a of feed line and the positioning of the dipoles on the transition regions

In the measurement process of the antenna given in Figure 4.19, the results are not satisfactory especially after 12 GHz. These results will be detailed in Chapter 6. It can be thought that, this is most probably because of the large distance in wavelengths between the transmission lines in the high frequency range. In Figure 4.19, the space of 3.32 mm makes  $0.3\lambda$  separation at 18 GHz. Thus in the next step, first group of transmission lines are tried to be placed closer to each other as

seen in Figure 4.20. Second and third parts of the transmission lines are same as in Figure 4.19. New parameters for the thinnest part of the antenna are as follows:

$$\text{avg}(l_n / d_n) = 44.09\text{mm},$$

$$Z_a = 184.366 \Omega,$$

$$Z_0 = 206.18 \Omega,$$

$$s = 2.8768d.$$

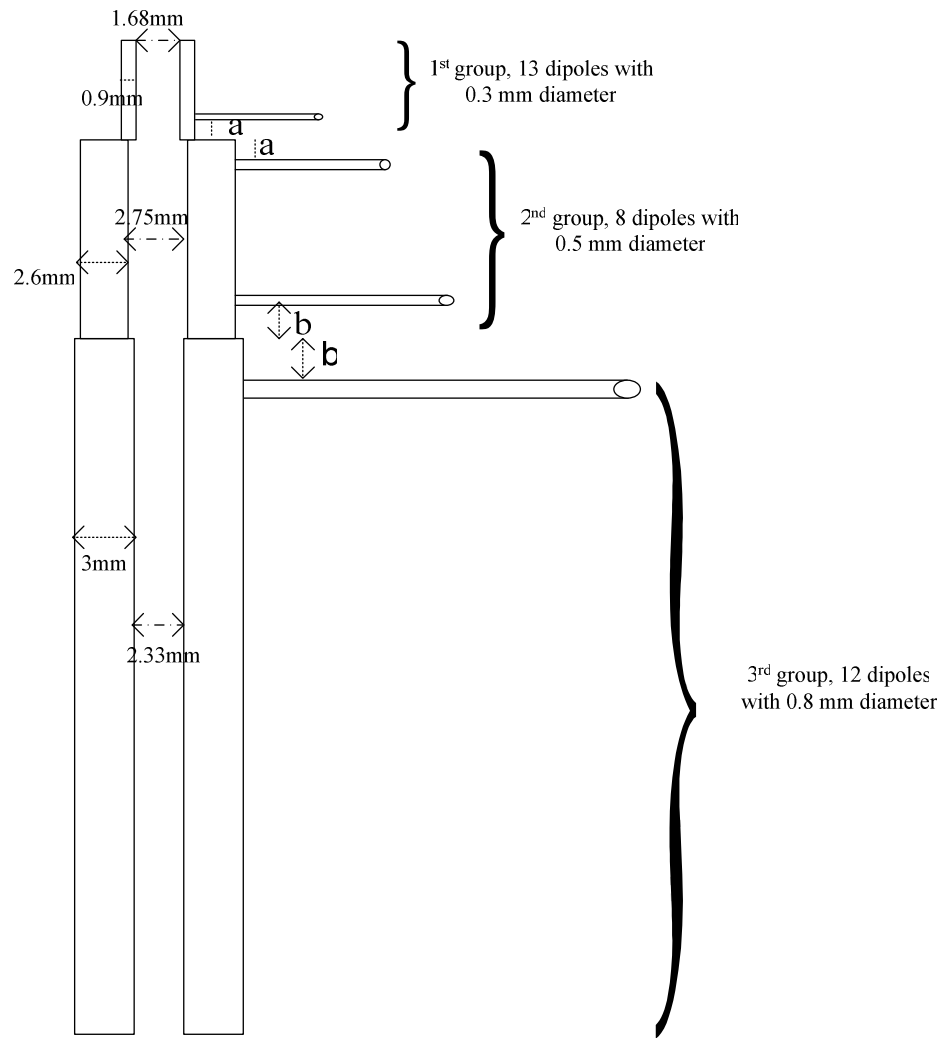


**Figure 4.20** Final form of detailed view of a of feed line and the positioning of the dipoles on the transition regions

**Table 4.1** Dimensions of the log-periodic antenna (all dimensions are in mm.)

# of dipoles	half length of dipoles	dim of TR line	R	dim of TR line	$\lambda/2+\text{dim TR line}$	$\lambda$	f(GHz)
1	2.23	0.3	4.29	0.9	5.36	10.72	27.985
2	2.58	0.3	4.96	0.9	6.06	12.12	24.752
3	2.99	0.3	5.73	0.9	6.8858	13.77	21.784
4	3.46	0.3	6.62	0.9	7.82	15.64	19.182
5	4	0.3	7.66	0.9	8.9	17.8	16.854
6	4.63	0.3	8.85	0.9	10.15	20.3	14.778
7	5.35	0.3	10.2	0.9	11.59	23.18	12.942
8	6.18	0.3	11.8	0.9	13.26	26.52	11.312
9	7.15	0.3	13.7	0.9	15.19	30.38	9.8749
10	8.26	0.3	15.8	0.9	17.42	34.84	8.6108
11	9.55	0.3	18.3	0.9	20	40	7.5
12	11.04	0.3	21.1	0.9	22.97	45.94	6.5303
13	12.77	0.3	24.4	0.9	26.43	52.86	5.6754
14	14.76	0.5	28.2	2.6	32.11	64.22	4.6714
15	17.06	0.5	32.7	2.6	36.71	73.42	4.0861
16	19.72	0.5	37.8	2.6	42.04	84.08	3.568
17	22.8	0.5	43.6	2.6	48.19	96.38	3.1127
18	26.36	0.5	50.5	2.6	55.31	110.6	2.712
19	30.47	0.5	58.3	2.6	63.53	127.1	2.3611
20	35.22	0.5	67.4	2.6	73.04	146.1	2.0537
21	40.72	0.5	77.9	2.6	84.04	168.1	1.7849
22	47.08	0.8	90.1	3	97.15	194.3	1.544
23	54.42	0.8	104	3	111.84	223.7	1.3412
24	62.92	0.8	120	3	128.83	257.7	1.1643
25	72.74	0.8	139	3	148.47	296.9	1.0103
26	84.09	0.8	161	3	171.17	342.3	0.8763
27	97.21	0.8	186	3	197.42	394.8	0.7598
28	112.38	0.8	215	3	227.76	455.5	0.6586
29	129.92	0.8	249	3	262.83	525.7	0.5707
30	150.2	0.8	287	3	303.39	606.8	0.4944
31	173.64	0.8	332	3	350.27	700.5	0.4282
32	200.74	0.8	384	3	404.47	808.9	0.3709
33	232.07	0.8	444	3	467.13	934.3	0.3211

#### **4.5.2. PRODUCTION PROCESS**

The antenna was produced at Özben Ltd. and Kalipsan Ltd. which are located at OSTIM, Ankara. Özben produced the transmission line part of the antenna. Kalipsan drilled the holes for mounting the dipoles with a special technique called “erosion”. In this technique, holes are drilled by electron bombardment. The smallest hole that can be drilled at Kalipsan with this technique has a diameter of 0.3 mm. Antenna is made of steel. There have been some experiments about the top and the thinnest part of the antenna details of which are given in Chapter 6. While these experiments are done, the thinnest part of the transmission line is made of copper with dipoles made of steel. The dipoles are soldered at ASELSAN<sup>®</sup> Inc. by Murat Mutluol. Then the whole structure is plated with nickel, copper, nickel, gold, with thicknesses of 3,5,5,2 microns respectively, to prevent rusting of the structure.

The prototype antenna is tested to check the mechanical strength of the dipoles at ASELSAN<sup>®</sup> Inc. As a result dipoles are broken off at a pulling strength of 14-15 kg. Test report is given in Appendix E.

## CHAPTER V

# ANALYSIS AND DESIGN OF THE REFLECTOR ANTENNA

### 5.1. INTRODUCTION

Reflector antennas have been used since the discovery of the em wave propagation in 1888 by Hertz but design and applications have been started to develop in the days of World War 2 when radar applications are involved. Reflector antennas are used in radio astronomy, microwave communication and satellite tracking. [2] Some of the most popular shapes of the reflector antennas are the plane, corner, and curved reflectors such as paraboloidal reflectors. In this chapter, as it is stated before, detailed information about front fed parabolic reflector antennas will be given. Then some information about the MIR program which is used to design the front feed parabolic reflector will be given.

### 5.2. FRONT FED PARABOLIC REFLECTORS

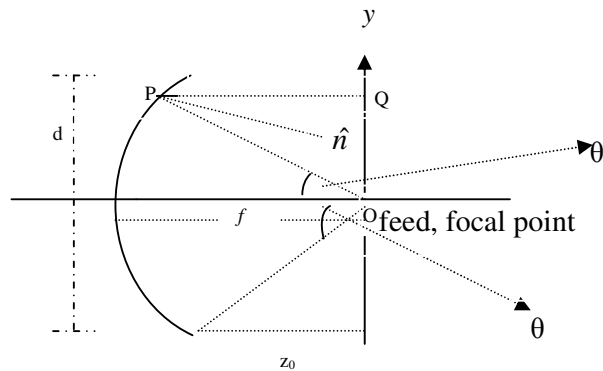


**Figure 5.1** The surface geometry of a paraboloidal reflector

The surface of a paraboloidal reflector is formed by revolving the parabolic curve about its axis. The antenna is illuminated by a small horn or a log-periodic dipole array locating at the focal distance,  $f$ , from the vertex. In Figure 5.1, the location of the feed is the point “O”. The paraboloidal surface has the property that all the rays coming from the focal point are reflected from the paraboloidal parallel to the axis. That means that the rays coming from the focal point are transformed into plane waves, i.e., reflected beams have a “zero” beamwidth. Referring Figure 5.1, total distance from point ‘O’ to ‘P’ plus the distance from ‘P’ to ‘Q’ is equal to the twice of the focal length,  $f$ .

If we call distance from point “O” to “P” as  $r'$ , and the angle between the z-axis and  $r'$  as  $\theta'$ ,

$$r'(1 + \cos \theta') = 2f \quad \text{Equation 5.1}$$

can be stated as the basic equation for the paraboloidal reflector. After some manipulations this equation can be written in a different form:

$$r' = f \times \sec^2(\theta'/2) \quad \text{Equation 5.2}$$

If one wants to write Equation 5.1 in terms of rectangular coordinates, that's:

$$r' + r' \cos \theta' = \sqrt{x'^2 + y'^2 + z'^2} + z' = 2 \times f \Rightarrow x'^2 + y'^2 = 4f(f - z') \quad [2]. \quad \text{Equation 5.3}$$

The unit vector which is normal to the surface at the reflection point,  $\hat{n}$ , divides the OPQ angle into two equal angles so each of these angles are  $\theta'/2$ . The unit vector is equal to the gradient of the surface equation divided by the magnitude of the surface equation, i.e.;  $\hat{n} = \hat{a}_r' \cos(\theta'/2) + \hat{a}_\theta' \sin(\theta'/2)$  where surface equation is:  $S = f - r' \cos^2(\theta'/2) = 0$  which is obtained from Equation 5.2.

Another important relation about the parabolic reflectors is the relation, which relates the subtended angle,  $\theta_0$  to the  $f/d$  ratio. Referring the Figure 5.1,  $\tan \theta_0 = \frac{d/2}{z_0}$ . From Equation 5.3, using  $x^2 + y^2 = (d/2)^2$  relation, which is simply a circle equation we get  $z_0 = f - d^2/16f$ . From the last two equations we get:

$$f = (d/4) \times \cot(\theta_0/2) \quad \text{Equation 5.4}$$

which is very important in designing the reflector antennas.

### 5.2.1. RADIATION FROM PARABOLOIDAL REFLECTORS

The two most commonly used techniques in analyzing the far field pattern of the antenna are aperture integration technique and the induced current approach. Both techniques lead to accurate results for radiated fields on the main beam and nearby minor lobes. In both methods some approximations are made such as:

- On the shadow region of the reflector, the current density is zero
- Discontinuity over the rim of the reflector is neglected
- Aperture blockage due to the feed and the direct radiation from the feed are neglected.

These approximations can lead to some errors in calculating the far minor lobes. Integration over the aperture plane is easier in the aperture integration technique. For the current distribution method, it is much more difficult and time consuming for the different types of feed pattern and feed position. Induced current approach is used to better approximate the field scattered from a surface. In both methods reflected surfaces should behave like a planar surface locally, that's to say; principal radii of curvatures at the reflection points should be very large compared to wavelength.

### 5.2.1.1. APERTURE INTEGRATION TECHNIQUE

Total field at a point in far zone is the sum of the field radiated by the equivalent sources on  $S_{ap}$  and the field radiation in backward direction. In the aperture integration technique, electrical field distribution in the aperture plane, which is usually located through the focal point, of the reflector due to the feed is first found using “geometrical optics techniques (ray-tracing), GO” or from measurements. Then, this E field is integrated over the aperture to find the near/far zone fields. This is the basic of the basis of the aperture distribution technique.

Incident field due to the feed at a point P on the reflector is:

$$\bar{E}_i = K \frac{e^{-jk_0 R}}{R} \bar{f}_{feed}(\theta', \phi') \quad \text{Equation 5.5}$$

where  $R$  is the distance between the feed and the point P.

Then using this incident electric field, aperture electric field which is at a distance ‘r’ from the reflector is:

$$\bar{E}_{ap}(r) = \frac{R}{r} \times \sqrt{D} \times e^{-jk_0 r} [-\bar{E}_i + 2(\hat{n} \cdot \bar{E}_i)\hat{n}] \quad \text{Equation 5.6}$$

where ‘D’ is the divergence factor which relates the powers between two points, i.e. point P and the point ‘r’ distance away from that point. An equivalent magnetic current source can be written in terms of  $\bar{E}_{ap}$  such as:

$$\bar{J}_{ms} = -\hat{n} \cdot \bar{E}_{ap} \quad \text{Equation 5.7}$$

Finally the fields of the reflector antenna in the near and far zones can be determined using field equivalence principles and Kirchoff’s formula which is a version of the mathematical formulation for Huygen’s-Fresnel formulation:

$$\bar{E}_i(\bar{r}) = \frac{1}{4\pi} \oint \left[ \bar{E}_i \frac{\partial \Psi}{\partial n} - \Psi \frac{\partial \bar{E}_i}{\partial n} \right] ds \quad \text{Equation 5.8}$$

where  $\bar{r}$  is the field point,  $\bar{E}_i$  is the value of the incident field at the surface of the projected aperture ( $\bar{E}_{ap}(r)$ ) and  $\Psi$  is the Green's function.

For the GO techniques to be applicable the changes in the medium over the distances compared to wavelength should be negligible or very small. Between the illuminated and the shadow region of the reflector GO cannot be used. GO cannot be used also for diffraction. GTD (Geometrical Theory of Diffraction) was developed in order to account for diffraction. GO gives reasonably good results when the reflector is electrically large. GO, however, is inadequate for predicting fine detail and for determining spillover and noise temperature. Spillover is a term relating the power radiated by the feed and the power collimated/intercepted by the reflector.

#### 5.2.1.2. INDUCED CURRENT APPROACH (PHYSICAL OPTICS)

In this method, first the induced surface current density on the reflector is found by using the physical optics approximation which bases upon recognizing the incident wave as a plane wave and the reflecting surface as a planar surface locally. The induced surface current density on the reflector:

$$J_s \cong 2\hat{n} \times \bar{H}_{inc} \cong \frac{2}{\eta} [\hat{n} \times (\hat{s}_i \times E_i)] \quad \text{Equation 5.9}$$

where  $\hat{n}$  is the unit vector normal to the surface,  $\hat{s}_i$  is the radial unit vector along the incident ray path,  $E_i$  is the incident electric field and  $\eta$  is the intrinsic impedance of the medium.

This surface current is integrated over the surface of the reflector to get the far zone radiation. The radiated field at the far zone of the reflector due to induced surface current only is as follows:

$$E(r, \theta, \phi) = -j \frac{w\mu}{4\pi r} e^{-jkr} \iint [J_s - (J_s \cdot \hat{a}_r) \hat{a}_r] e^{+jkr \cdot \hat{a}_r} ds' \quad \text{Equation 5.10}$$

where  $r' \cdot \hat{a}_r = x' \sin \theta \cos \phi + y' \sin \theta \sin \phi + z' \cos \phi$

This approach is valid when reflector antenna and radius of curvature of the incident wave is electrically large.

### 5.2.2. APERTURE EFFICIENCY AND DIRECTIVITY

In the designs of reflector antennas aperture efficiency and directivity are very important figure-of-merits. Both these merits primarily depend on the feed pattern and the  $f/d$  ratios of the reflector.

Two components of the electric field can be found [2]:

$$E_\theta = -j \frac{w\mu}{4\pi r} e^{-jkr} \iint \hat{a}_\theta \cdot J_s e^{+jkr'} ds' \quad \text{and} \quad E_\phi = -j \frac{w\mu}{4\pi r} e^{-jkr} \iint \hat{a}_\phi \cdot J_s e^{+jkr'} ds'$$

Equation 5.11

Assuming the feed pattern  $G_f(\theta', \phi')$  is circularly symmetric and linearly polarized in y-direction, total E field in the  $\theta = \pi$  direction, which is forward direction, is given by:

$$E(r, \theta = \pi) = -j \frac{2w\mu f}{r} \left[ \sqrt{\epsilon / \mu} \frac{P_t}{2\pi} \right] e^{-jk(r+2f)} \int_0^{\theta_0} \sqrt{G_f(\theta')} \tan(\theta' / 2) d\theta', [2]$$

Equation 5.12

Directivity in the forward direction is:  $D_0 = \frac{U(\theta = \pi)}{P_t / 4\pi}$  where  $U$  is the power intensity.  $U$  in the forward direction is:

$$U(\theta = \pi) = \frac{1}{2} r^2 \sqrt{\epsilon / \mu} |E(r, \theta = \pi)| \quad \text{Equation 5.13}$$

So substituting the total E field expression in the  $\theta = \pi$  direction into the power intensity expression we get:

$$U(\theta = \pi) = \frac{16\pi^2}{\lambda^2} f^2 \frac{P_t}{4\pi} \left| \int_0^{\theta_0} \sqrt{G_f(\theta')} \tan(\theta' / 2) d\theta' \right|^2 \quad \text{Equation 5.14}$$

Substituting the equation in the directivity formula  $D_0 = \frac{U(\theta = \pi)}{P_t / 4\pi}$ , we get:

$$D_0 = \frac{16\pi^2}{\lambda^2} f^2 \left| \int_0^{\theta_0} \sqrt{G_f(\theta')} \tan(\theta' / 2) d\theta' \right|^2 [2].$$

Using Equation 5.4, we can relate the subtended angle,  $\theta_0$  to the f/d ratio, so the final form of the equation is:

$$D_0 = \left( \frac{\pi d}{\lambda} \right)^2 \left\{ \cot^2 \left( \frac{\theta_0}{2} \right) \left| \int_0^{\theta_0} \sqrt{G_f(\theta')} \tan(\theta' / 2) d\theta' \right|^2 \right\} \quad \text{Equation 5.15}$$

In this expression  $\left( \frac{\pi d}{\lambda} \right)^2$  is the *maximum directivity* when the efficiency is 100%

and the remaining part  $\varepsilon_{ap} = \left\{ \cot^2 \left( \frac{\theta_0}{2} \right) \left| \int_0^{\theta_0} \sqrt{G_f(\theta')} \tan(\theta' / 2) d\theta' \right|^2 \right\}$  is the *efficiency* parts.

Examining  $\varepsilon_{ap}$ , one can notice that it's a function of feed pattern and the subtended angle. So for a given feed pattern all the reflectors that have the same f/d ratio have the same aperture efficiencies.

In general aperture efficiency can be written as:

$$\varepsilon_{ap} = \varepsilon_s \varepsilon_t \varepsilon_p \varepsilon_x \varepsilon_b \varepsilon_r \quad \text{Equation 5.16}$$

where  $\varepsilon_s$  is spillover efficiency,  $\varepsilon_t$  is taper efficiency,  $\varepsilon_p$  is phase efficiency,  $\varepsilon_x$  is polarization efficiency,  $\varepsilon_b$  is blockage efficiency and  $\varepsilon_r$  is random error efficiency over the reflector surface [4]. Spillover efficiency, as explained before, is the ratio of the power radiated by the feed and the intercepted power by the

reflector and for feeds with symmetrical patterns, it is equal to:

$$\epsilon_s = \frac{\int_0^{\theta_0} G_f(\theta') \sin \theta' d\theta'}{\int_0^{\theta_0} G_f(\theta') \sin \theta' d\theta'}$$

Taper efficiency is related with the uniformity of the amplitude distribution of the feed pattern over the surface of the reflector. Tapering reduces the directivity of the antenna and increases the beam width, which are undesirable. It is equal to:

$$\epsilon_t = 32 \left( \frac{f}{d} \right)^2 \frac{\left| \int_0^{\theta_0} \sqrt{G_f(\theta')} \tan(\theta'/2) d\theta' \right|^2}{\int_0^{\theta_0} \sqrt{G_f(\theta')} \tan(\theta'/2) d\theta'}$$

On the other hand tapered aperture-field distribution generally results in lower side-lobe amplitudes, which is desirable.

Phase and polarization efficiencies are related with the phase uniformity and polarization uniformity of the field over the aperture, respectively. Polarization

efficiency,  $\epsilon_x$ , can be stated as:  $\epsilon_x = \frac{P_a - P_x}{P_a} = \frac{P_{co}}{P_a}$  where  $P_a$  is the total radiated

power from the aperture,  $P_{co}$  and  $P_x$  is the power radiated by the co-polarized and cross-polarized aperture fields respectively. Phase efficiency,  $\epsilon_p$ , can be stated as:

$$\epsilon_p = \frac{\left| \int_0^{2\pi d} \int_0^0 E_{ye}(\rho, \phi) \rho d\rho d\phi \right|^2}{\left[ \int_0^{2\pi d} \int_0^0 E_{ye}(\rho, \phi) \rho d\rho d\phi \right]^2}$$

where  $E_{ye}$  is the even part of the aperture field  $E$ .

Cylindrical coordinated have been introduced to carry out the integral [4].

It has been stated that [2], directivity depends on  $\theta_0$  (or  $f/d$  ratio) and the feed pattern ( $G_f(\theta') = G^n_0 \cos^n(\theta')$ ). For different values of  $n$  in the feed pattern expression, some conclusions can be stated as follows:

- Each maximum aperture efficiency is in the neighborhood of 82%. (In practice maximum reflector efficiencies are in the 65-80% range.)
- As  $n$  increases, that means the feed pattern becomes more directive, the reflector half angle,  $\theta_0$  that leads to the maximum efficiency gets smaller.
- When the aperture efficiency versus reflector half angle graph is plotted, it is understood that, all the patterns for each value of  $n$  is almost the same with the others.

It has been stated that, aperture efficiency is primarily depend on spillover and non-uniform amplitude distribution losses. These losses depend primarily on feed pattern. There is a trade-off between these losses. As seen from Figure 5.2, when you are maximizing the spillover efficiency, you minimize the taper efficiency.

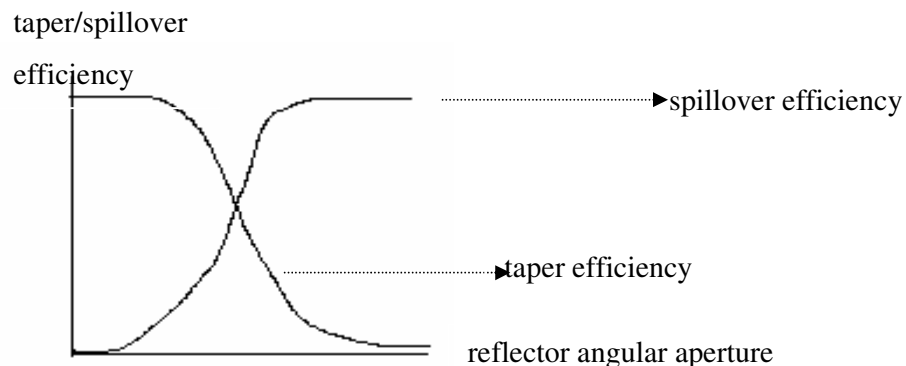


**Figure 5.2** Parabolic reflector taper and spillover efficiencies as a function of reflector angular aperture

High spillover efficiency results in increase in directivity, that's to say the beamwidth of the antenna decrease. On the other hand, tapered aperture field distribution results in lower side-lobe level at the expense of a decrease in the directivity.

### 5.2.3. FEED DESIGN

In the design of an optimum reflector antenna, feed design is one of the most important parameters to be considered. For the feed design, aperture efficiency and low-cross polarization are two main problems. Feed pattern should have the desired distribution over the aperture and very low minor lobes in all the other space. For an ideal feed system, the receiving and the transmitting mode field structures within the focal region should be identical except the direction of propagation. In designing paraboloidal reflectors,  $f/d$  ratio is very important. Referring to Figure 5.1, if  $f/d$  ratio is large, this means there is a less cross-polarization component in the projected aperture, but the disadvantage of selecting the  $f/d$  ratio high is that, spillover efficiency decreases. There has to be a compromise between cross-polarization level and amount of spill-over while selecting the  $f/d$  ratio.

### 5.3. MIR PROGRAM

MIR is a FORTRAN program which is based on physical optics method developed by Prof. Altunkan Hızal and stands for “MICrowave Reflector”. In the scope of this thesis, a reflector antenna is designed with a dual polarized log periodic feed antenna using MIR program.

As input for “MIR”, feed antenna geometry, half lengths of the dipoles and  $R_n$  values, and the magnitude and phases of the currents at the bases of the dipoles are necessary. After the simulations, E and H plane patterns are found and, from the patterns, gains of the reflector at various frequencies are calculated.

MIR program doesn't calculate efficiency of the antenna and gain reduction due to the blockage effect of the feed antenna. A method is developed to calculate this blockage effect and efficiency of the antenna. MIR program is also used in this method.

The minimum gain value requirement of the reflector antenna for each frequency range is given in the following table.

**Table 5.1** Minimum gain requirements for the reflector antenna

f(GHz)	Gmin(dB)
0.4	10
1	15
2	25
4	25
7	25
10	25
12	30
14	30
18	30

User should specify the diameter and the focus of the reflector and the position of the log-periodic antenna which is located in front of the reflector as a feed antenna. The simulations are made as if there is a single polarized log-periodic feed antenna in front of the reflector.

When the  $n^{\text{th}}$  dipole in a log-periodic antenna is active, these elements should be placed at the focus of the parabola. This is the best position for the  $n^{\text{th}}$  dipole, but the feed antenna in this thesis has a very wide band. As  $f$  changes from 0.4 GHz to 18 GHz, best position to place the feed antenna is changing.

At the high end of the antenna, as the frequency is high,  $\lambda$  is small, so the best position for the elements at the high end of the antenna is very sensitive to the distance between the focus and the apex. But at the low end of the antenna as the  $\lambda$  is larger, when you place the antenna which is not very close to the focus point, you make a mistake which is not very big in terms of  $\lambda$ . So the antenna is placed in front of the reflector, considering the best position for the shorter dipoles. Then the patterns at the low frequencies are tried to be corrected by changing  $f$  and  $D$  of the reflector.

Final design parameters of the reflector antenna are given in Figure 5.3. Diameter of the antenna is 1650 mm; focal point of the antenna is 675 mm away from the antenna so the  $f/d$  ratio of the antenna comes out to be 0.4.  $Z_1$  is the distance between the apex of the antenna and the rim of the reflector and

$Z_1 = f - \frac{D^2}{16f} = 422.9166\text{mm}$ . AF is the distance between the apex of the log-periodic antenna and the focal point and it is 15 mm.

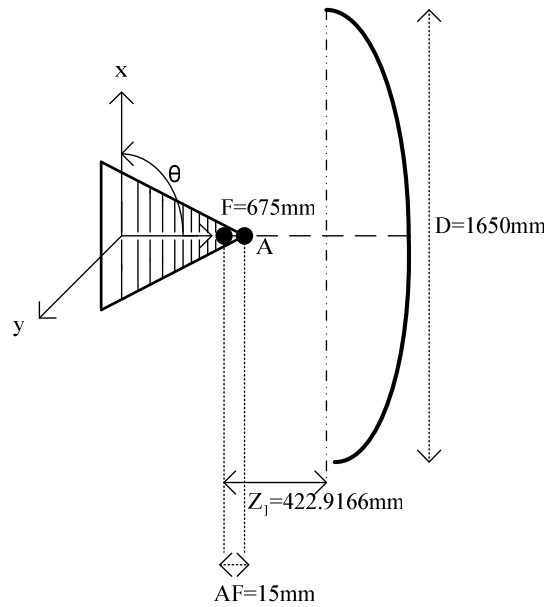


**Figure 5.3** Scaled down version of the reflector antenna designed using “MIR”

Inspecting of Figure 5.3, maximum of the field of the feed antenna appears at  $\theta = 0^\circ$  while maximum of the E and H plane patterns of the reflector antenna appears at  $\theta = 180^\circ$ .

### 5.3.1. EFFICIENCY AND BLOCKAGE EFFECTS OF A REFLECTOR ANTENNA

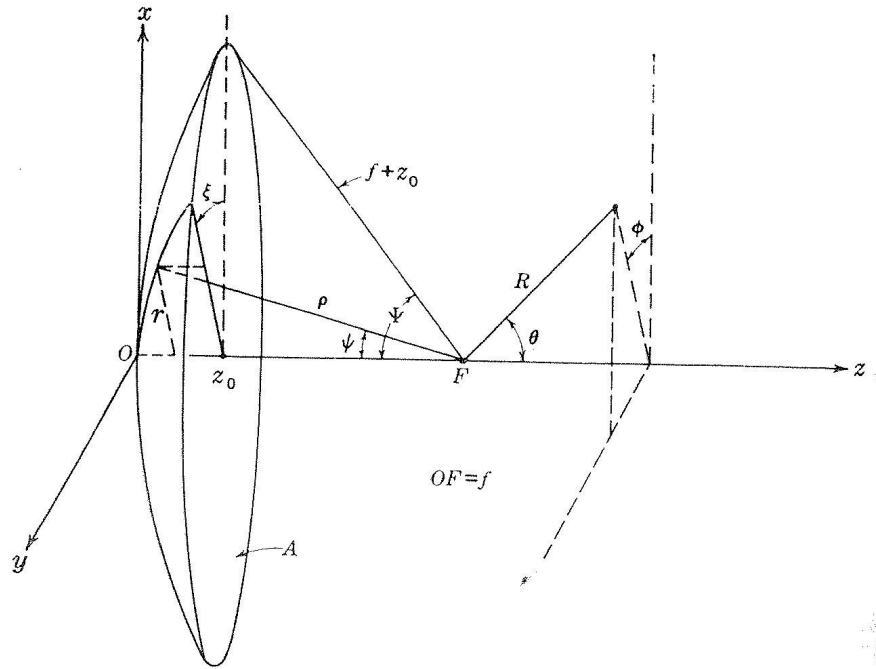


**Figure 5.4** Geometrical parameters for the paraboloidal reflector [18]

As explained in Section 5.2.2, gain of a reflector antenna can be formulated as

$$G = \left( \frac{\pi \cdot D}{\lambda_0} \right)^2 \eta_a \quad \text{Equation 5.17}$$

where  $\eta_a$  is the aperture efficiency. Aperture efficiency can be written as:

$$\eta_a = \frac{1}{4\pi^2} \text{Cot} \left( \frac{\Psi_0}{2} \right)^2 \cdot \left| \int_0^{2\pi} d\xi \int_0^{\Psi_0} \sqrt{Gf(\Psi, \xi)} \cdot \tan \left( \frac{\Psi}{2} \right) d\psi \right|^2 \quad [18] \quad \text{Equation 5.18}$$

where  $\sqrt{Gf(\Psi, \xi)}$  is the directive gain function of the feed and  $\Psi_0$  is the subtended angle of the reflector.

When we concentrate on the directive gain function of the feed;

$$\sqrt{Gf(\Psi, \xi)} = \sqrt{Gf(0,0)} \cdot \frac{\sqrt{E_\Psi^2 + E_\xi^2}}{\sqrt{E_\Psi^2(0,0) + E_\xi^2(0,0)}} = \sqrt{Gf(0,0)} \cdot F(\Psi, \xi) \quad \text{where}$$

$\sqrt{Gf(0,0)}$  is the maximum gain of the field along  $\Psi = 0$  and  $\xi = 0$ .  $F(0,0) = 1$

can be noticed in the equation above [18]. Also,  $\sqrt{E_\Psi^2(0,0) + E_\xi^2(0,0)} = 1$

Equation 5.18 can be written in the following form:

$$\eta_a = \frac{1}{4\pi^2} \text{Cot} \left( \frac{\Psi_0}{2} \right)^2 \cdot Gf(0,0) \cdot I_a^2 \quad \text{where} \quad I_a = F(\Psi, \xi) \cdot \int_0^{2\pi} d\xi \int_0^{\Psi_0} \tan \left( \frac{\Psi}{2} \right) d\psi \quad [18]$$

Equation 5.19

Using Equation 5.19, Equation 5.17 can be written as:

$$G = \left( \frac{\pi \cdot D}{\lambda_0} \right)^2 \cdot \eta \cdot \frac{1}{4\pi^2} \text{Cot} \left( \frac{\Psi_0}{2} \right)^2 \cdot Gf(0,0) \cdot I_a^2 \quad \text{Equation 5.20}$$

### 5.3.1.1. CURVE FIT TO $F(\Psi, \xi)$

Our aim is to find the efficiency of the reflector antenna. For this purpose, first  $F(\Psi, \xi)$  should be found. To find it  $\Psi$  and  $\xi$  components of the electric field should be found.

In the MIR program, one can see the field values in the output of the program, mir.out. For 0.4 GHz, examining the output file, one can fill the following table as follows:

**Table 5.2** Values of the electrical fields for different  $\Psi$  and  $\xi$  angles.

$\Psi$	$\xi=0^\circ$		$\xi=30^\circ$		$\xi=60^\circ$		$\xi=90^\circ$	
	$ E_\Psi ^2$	$ E_\xi ^2$	$ E_\Psi ^2$	$ E_\xi ^2$	$ E_\Psi ^2$	$ E_\xi ^2$	$ E_\Psi ^2$	$ E_\xi ^2$
$0^\circ$	1	0	0.7498	0.25	0.25	0.7498	0	1
$25^\circ$	0.699	0	0.534	0.216	0.184	0.672	0	0.909
$50^\circ$	0.227	0	0.180	0.145	0.0672	0.488	0	0.690
$65^\circ$	0.069	0	0.056	0.104	0.0218	0.3664	0	0.527

The subtended angle of the designed reflector antenna is  $62.85^\circ$ . So the E field values are taken from the output file at some frequencies up to  $\Psi = 65^\circ$ . Next from Table 5.2, values of  $|F(\Psi, \xi)|$  should be found. Results are given in the following table:

**Table 5.3** Values of the field magnitudes,  $|F(\Psi, \xi)|$  for different  $\Psi$  and  $\xi$  angles.

$\Psi$	$\xi=0^\circ$	$\xi=30^\circ$	$\xi=60^\circ$	$\xi=90^\circ$
$0^\circ$	1	1	1	1
$25^\circ$	0.836	0.866	0.925	0.953
$50^\circ$	0.476	0.57	0.745	0.8306
$65^\circ$	0.2626	0.4	0.623	0.7259

Entries of the Table 5.3, gives the field magnitudes,  $|F(\Psi, \xi)|$ , for different  $\Psi$  and  $\xi$  angles.

Let,  $F(\Psi, \xi) = C_0(\xi) + C_1(\xi)\Psi + C_2(\xi)\Psi^2 + C_3(\xi)\Psi^3$  and

$$C_x(\xi) = A_0^{(x)} + A_1^{(x)}\xi + A_2^{(x)}\xi^2 + A_3^{(x)}\xi^3.$$

$$C_0(\xi) = 0$$

There are 16 equations obtained from Table 5.3 with 16 unknowns and when the unknowns are solved by MATLAB<sup>®</sup>, arbitrary  $C_x(\xi)$  functions and later  $F(\Psi, \xi)$  can be found.

To calculate the blockage effect of the antenna, the following figure can be thought:

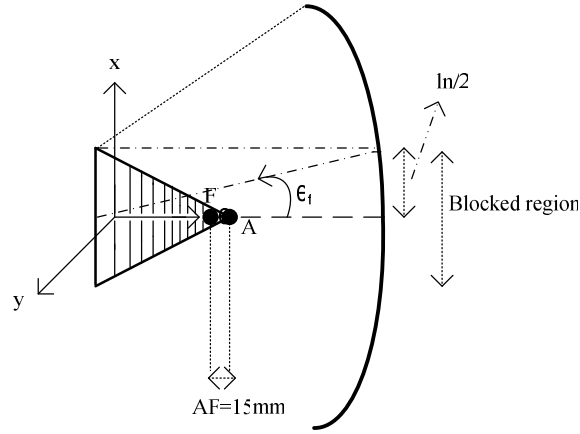


**Figure 5.5** Blocked region of the reflector antenna

When the inner integral given in Equation 5.18 is evaluated from  $\theta_f$  to  $\Psi_0$  instead of 0 to  $\Psi_0$ , blockage effect of the log periodic antenna is taken into account. For the designed reflector antenna and the feed configuration,  $\theta_f$  is calculated as  $9.687^\circ$ . Using MATLAB<sup>®</sup> program, the gains of the reflector with efficiencies considering no blockage and blockage effects are calculated and these gains are compared with the gain calculated from the Krauss's formula. These results are given in Chapter 6.

# **CHAPTER VI**

## **IMPLEMENTATIONS, MEASUREMENTS AND SIMULATIONS OF LPDA AND REFLECTOR ANTENNA**

### **6.1. INTRODUCTION**

In this chapter all measurements about single and dual polarized log-periodic antennas and simulation results about reflector antenna will be given. The measurements are done at the “Anechoic Chamber” at ASELSAN<sup>®</sup> Inc. Top view of anechoic chamber and antenna measurement set-up are given in the following figures:

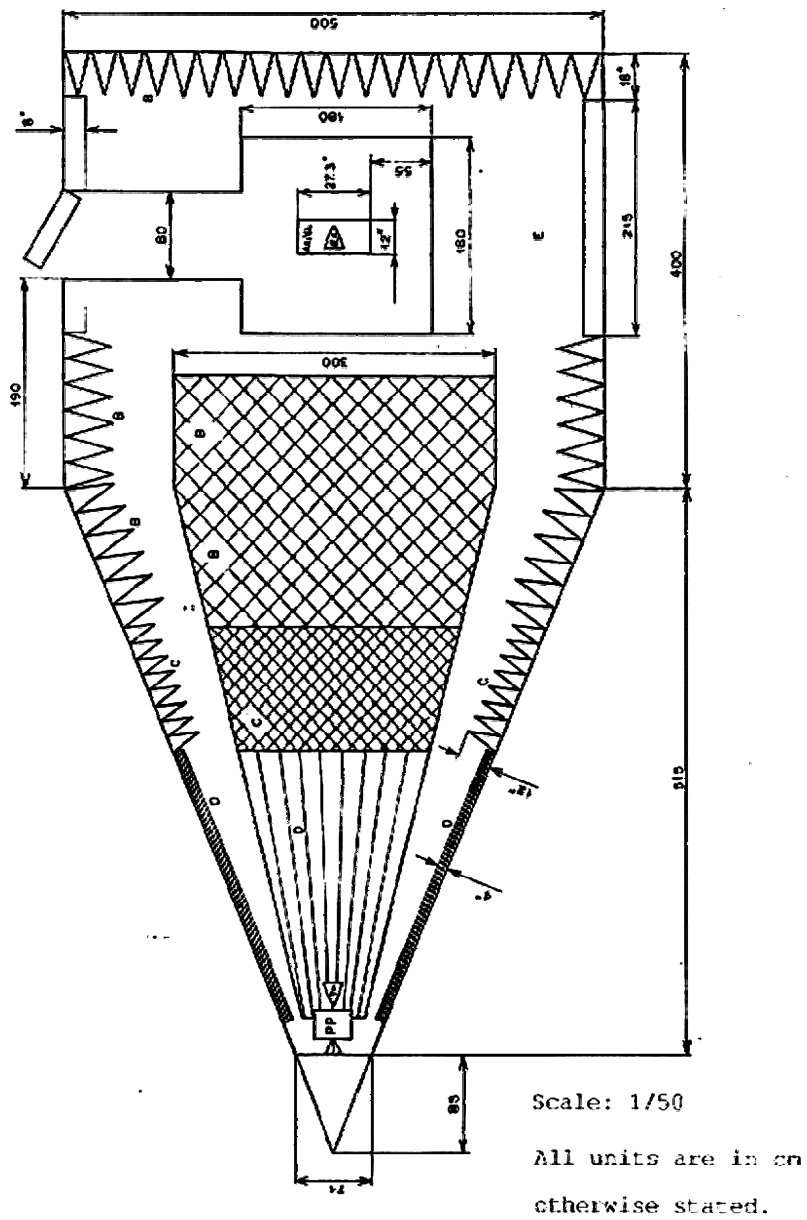
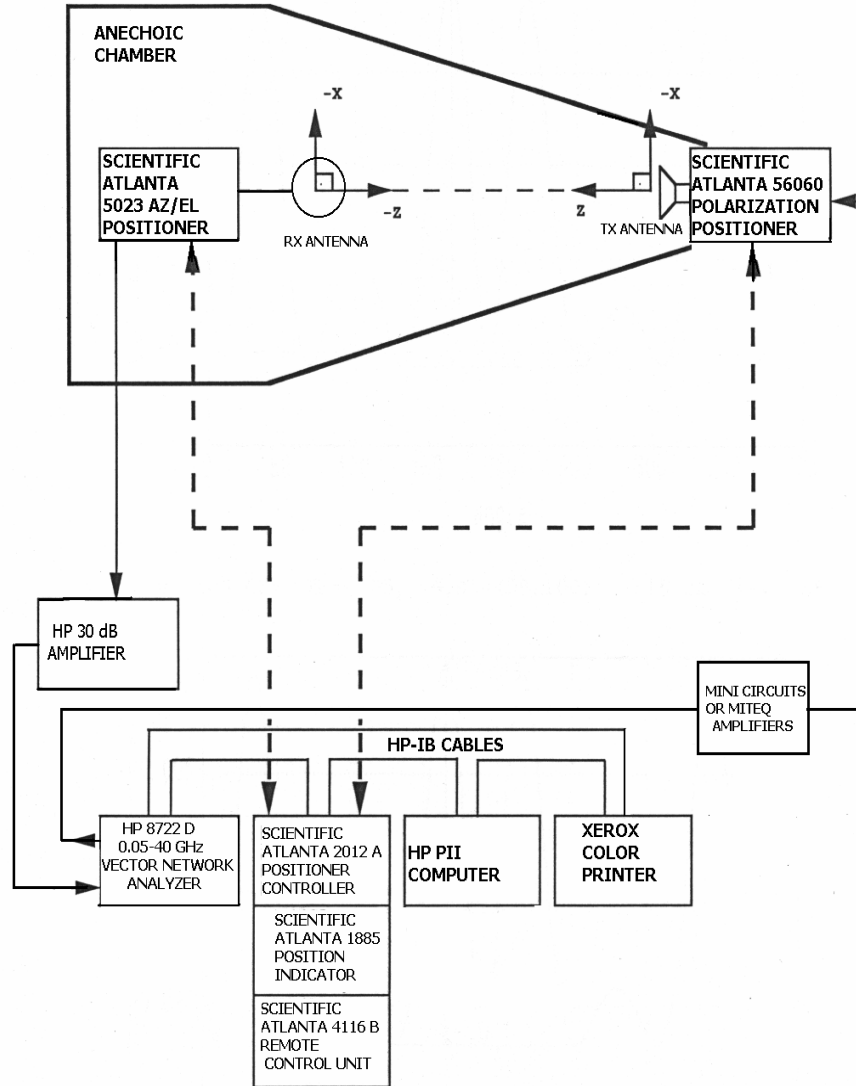


Figure 6.1 Top View of the Anechoic Chamber in ASELSAN® Inc. [9]



**Figure 6.2** Antenna Measurement Setup in Anechoic Chamber

The VSWR measurements of antennas are made using HP 8722 D Vector Network Analyzer.

Before production and testing of dual polarized log-periodic antenna, first, production and measurements of a single polarize log periodic antenna are done. After the results of the single antenna are found satisfactory, dual polarized antenna is constructed and tested.

## 6.2. MEASUREMENTS OF A SINGLE POLARIZED LOG-PERIODIC ANTENNA

The photograph of the manufactured single polarized log-periodic antenna is given in the following figure:

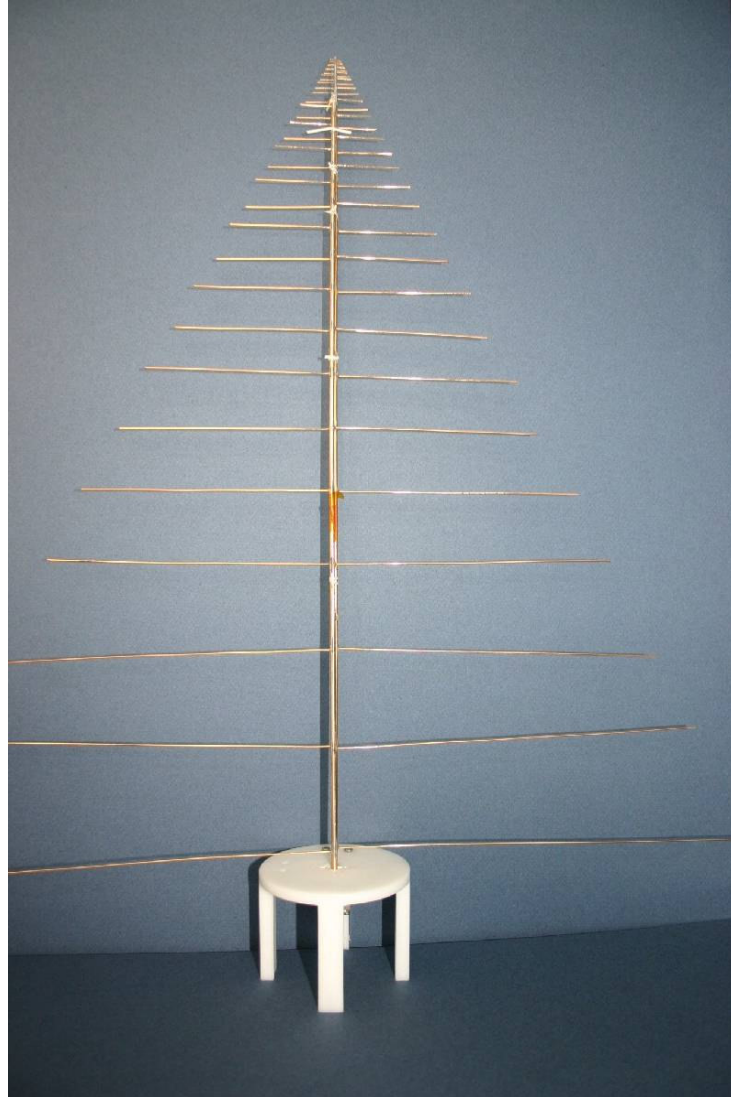


**Figure 6.3** First production of single polarized log periodic antenna

The detailed drawing of this antenna is given in Figure 4.19. The input return loss of the antenna is given in the following chart:

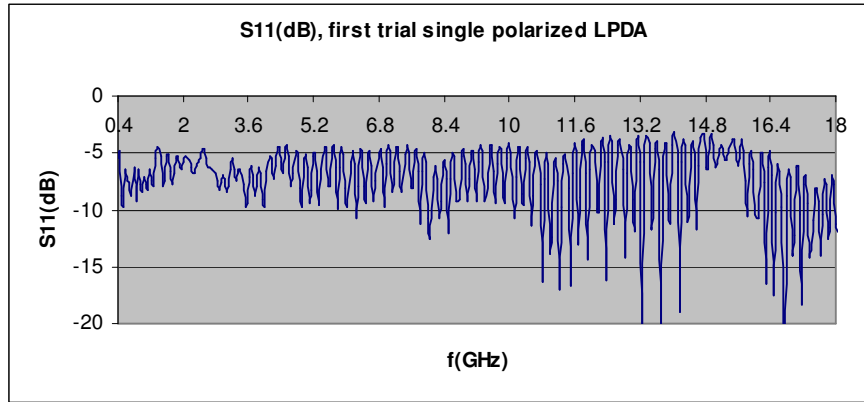


**Figure 6.4** Input Return Loss of the Antenna given in Figure 6.3

In the Figure above, since the S11 of the antenna is not so satisfactory, first, it is tried to be improved. When we concentrate on the top part of the Figure 4.19, the coaxial cable of the antenna is constructed as in the following figure:

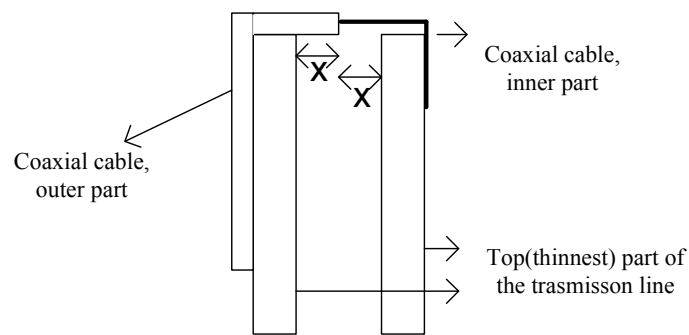


**Figure 6.5** Coaxial cable construction on the top part of the log-periodic antenna

Examining Figure 6.5, and based on some theoretical and experimental results, it can be stated that, shield of coaxial cable should be removed in the middle of the transmission lines and the central conductor of the coax should be extended to the other feeder line. When the coaxial cable is constructed as in Figure 6.5, then the dipoles on the different sides of the transmission lines can be fed by a 180 degree phase difference and the energy is beamed in the direction of shorter elements without any shifting in the pattern of the antenna.

At the expense of shifting the pattern of the antenna, the top part of the coaxial cable is modified as in Figure 6.6, i.e., shield of the coax is tried to be made longer. By this way the inductive effect of the central conductor is tried to be minimized.

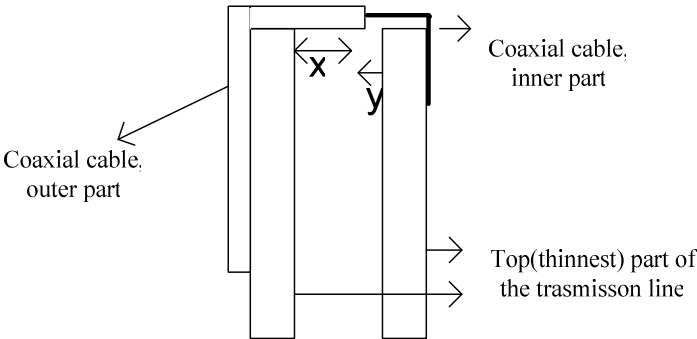


**Figure 6.6** Modification of the coaxial cable construction given in Figure 6.5

In the realization of the antenna, this modification is done by a small metal piece as shown in Figure 6.7.

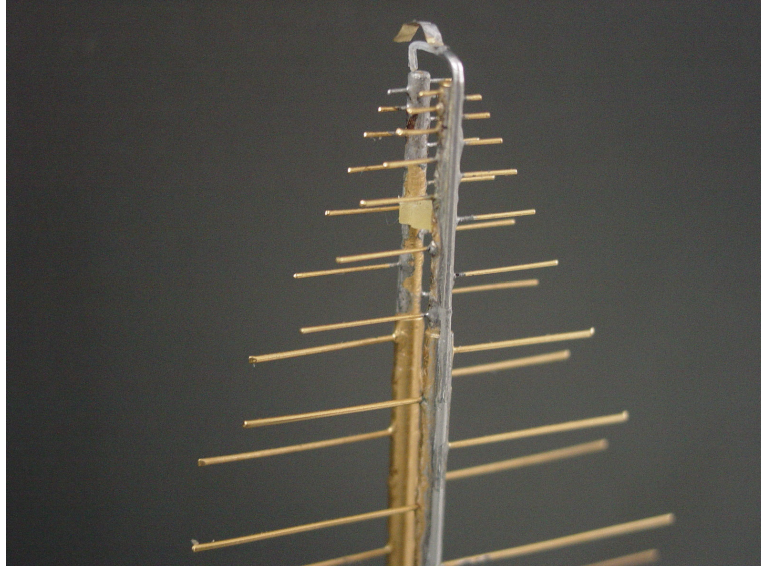


**Figure 6.7** Zoom to the tip of the tuned antenna with a small piece of metal

This tuning, improves the  $S_{11}$  as seen in Figure 6.8.

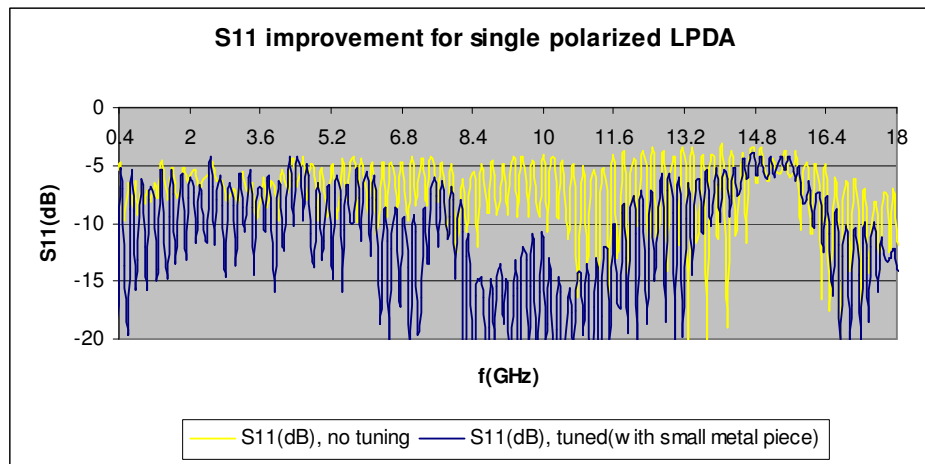
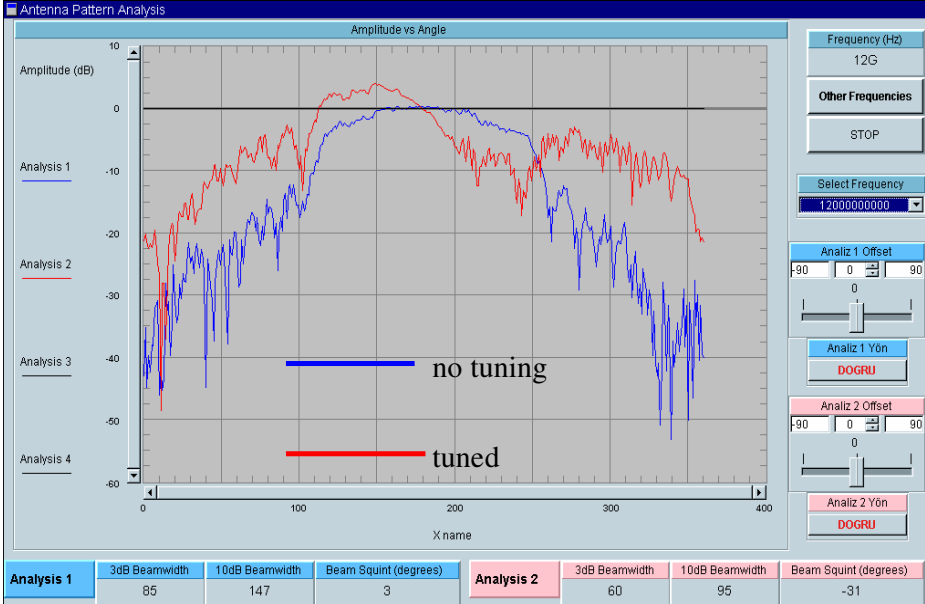


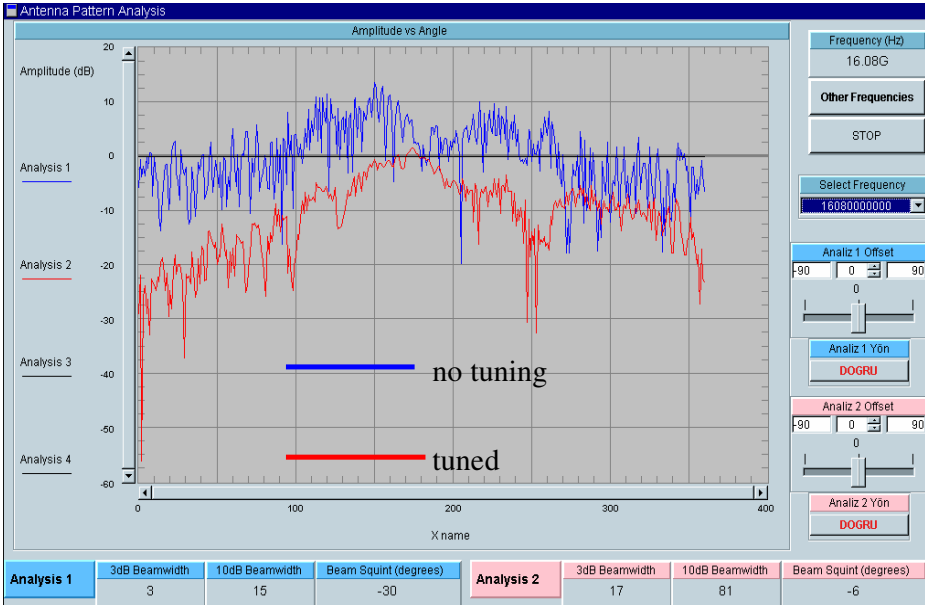
**Figure 6.8**  $S_{11}$  improvement with small piece of metal

When the construction of coaxial cable is as in Figure 6.5, at some frequencies, pattern does not occur because of the poor  $S_{11}$ . When the antenna is tuned as in Figure 6.7,  $S_{11}$  improves. As a result of this, the pattern occurs, but with a shift at

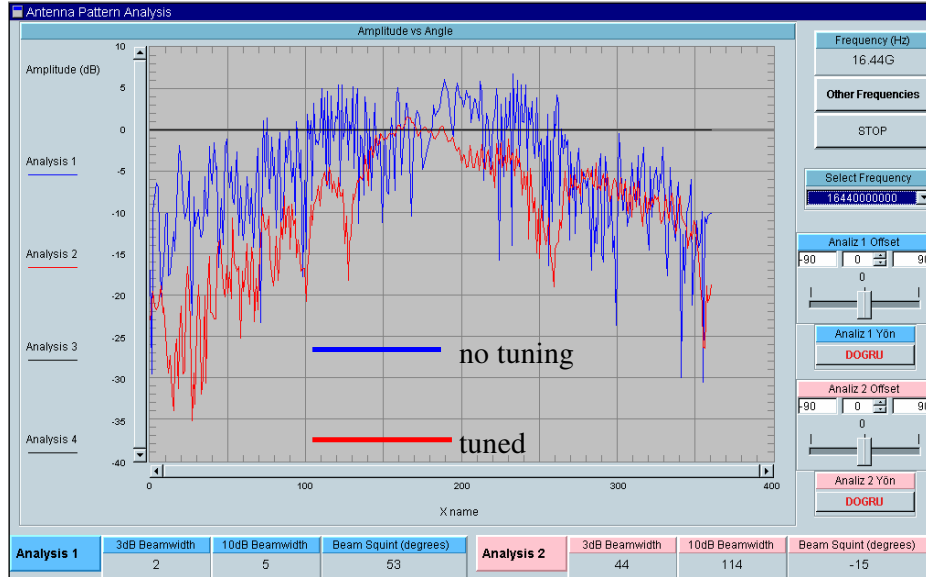
some frequencies, as expected. The comparison of the H plane patterns at some frequencies are as follows:



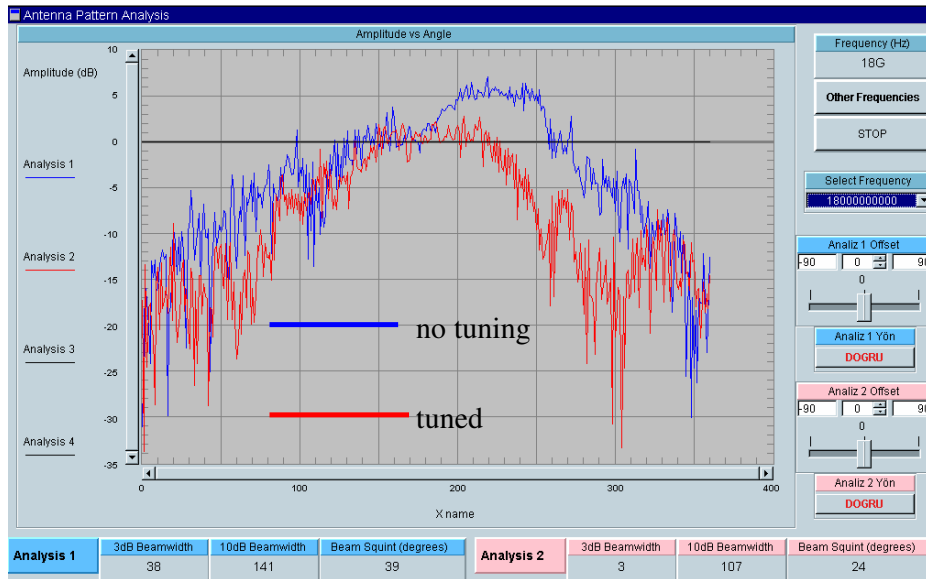
(a)



(b)



(c)



(d)

**Figure 6.9** Comparison of the H plane patterns when the coaxial cable construction differs in Figure 6.5 and Figure 6.6 at frequencies 12 GHz (a), 16.08 GHz (b), 16.44 GHz (c) and 18 GHz (d).

Examining the Figure 6.9, although the antenna is tuned with a small metal piece, the radiation patterns are not found to be so satisfactory. This may be result of the fact that the thinnest transmission lines are so far away, approximately  $0.3 \lambda$  at 18 GHz, from each other as seen in Figure 4.19.

So in the next step, the thinnest parts of the transmission line are made thinner and closer to each other as seen in Figure 4.20. Better results are expected. The photographs of the modified single polarized log-periodic antenna are given in the following figures:



**Figure 6.10** Thinnest part of the antenna.

The small piece given in Figure 6.10 is the smallest part of the whole antenna. The longest dipole in Figure 6.10 corresponds to 5.67 GHz, therefore, this part of the antenna is said to be the most critical part of the whole antenna. This part is attached to the top part of the antenna, after the previous thin part is cut from the antenna, as seen in the following. Detailed drawing of the following figure is given in Figure 4.20.

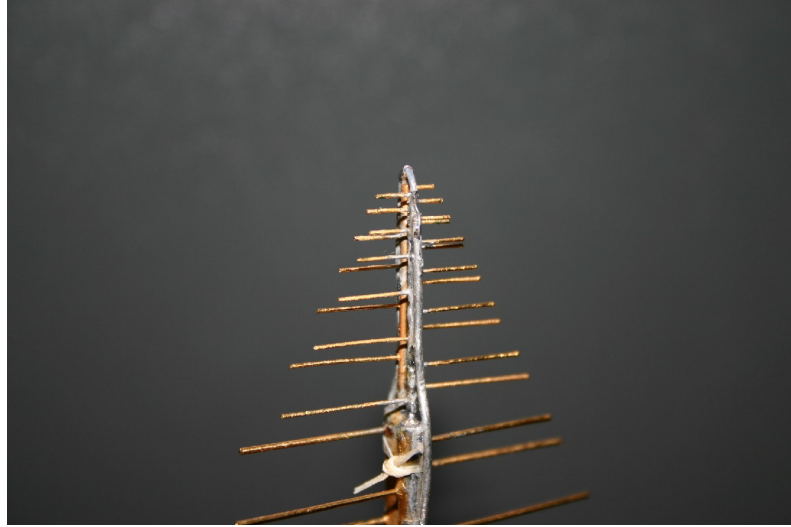
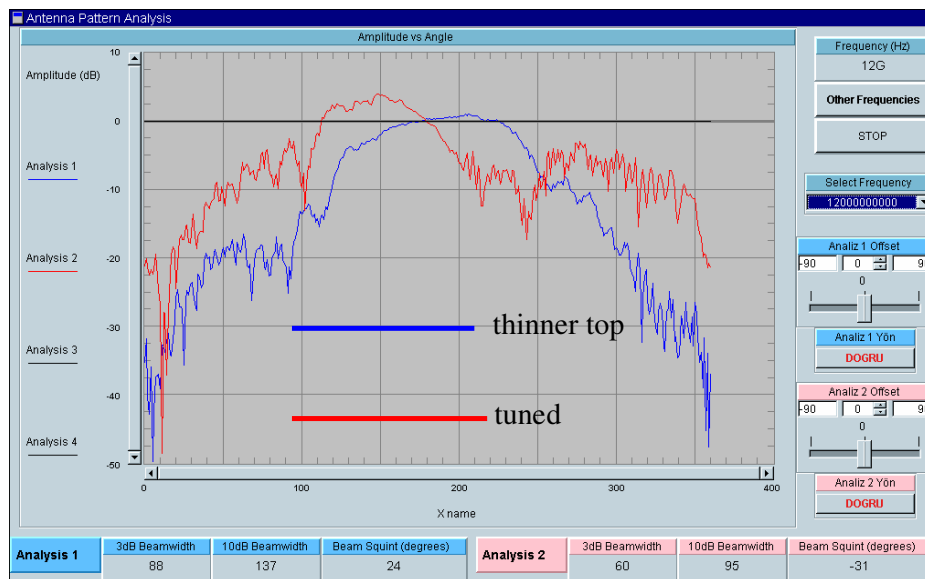
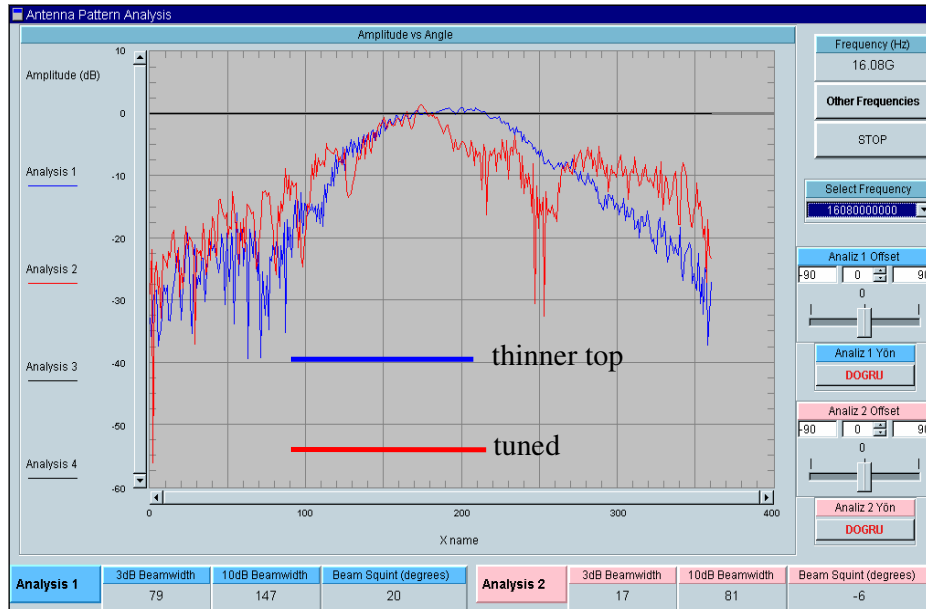


**Figure 6.11** Modified form of the thinnest part of the antenna

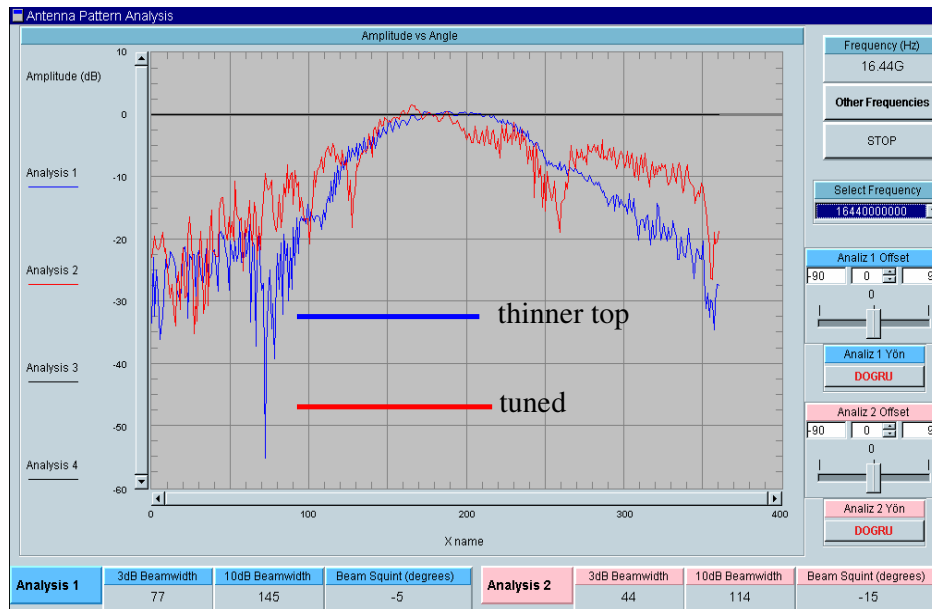
When the electrical test results of the antenna given in Figure 6.11 are performed, satisfactory results of the single polarized LPDA are obtained. The comparison of the H plane patterns of the antennas given in Figure 6.7 and Figure 6.11 at some frequencies are as follows:



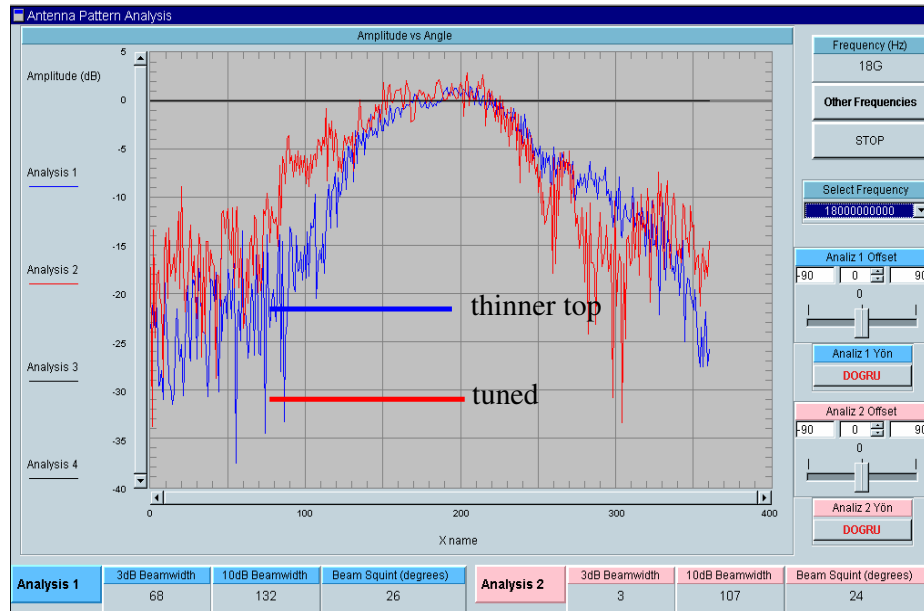
(a)



(b)



(c)



(d)

**Figure 6.12** Comparison of the H plane patterns when the top parts of the antennas are different as seen in Figure 6.7 and Figure 6.11 at frequencies 12 GHz (a), 16.08 GHz (b), 16.44 GHz (c) and 18 GHz (d).

Input return loss comparison for the antennas given in Figure 6.7 and Figure 6.11 are as follows:

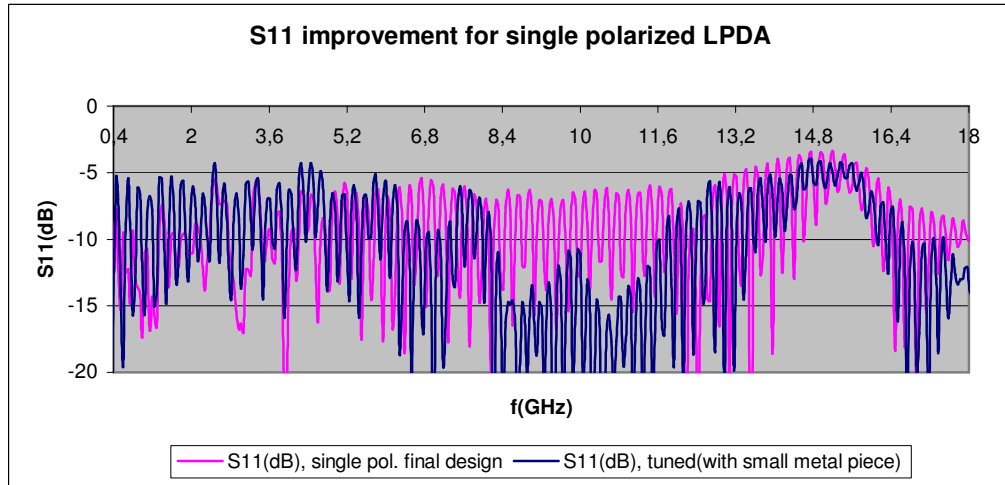


**Figure 6.13**  $S_{11}$  comparison between the tuned antenna and the final design of the single polarized antenna

After the test results of the final design of single polarized log-periodic antenna are found satisfactory, next step is to produce the dual polarized log-periodic antenna.

### 6.3. MEASUREMENTS OF THE DUAL POLARIZED LOG-PERIODIC ANTENNA

Dual polarized log periodic antenna is constructed by combining two single polarized log periodic antennas whose electrical tests are found satisfactory. In the production of the antenna, 2 smallest dipoles are thrown away. Because when the top and the thinnest transmission line parts are made closer as in Figure 6.11, the frequency that corresponds to smallest dipole rises to 27.98 GHz. When two dipoles from the top are thrown away the last remaining dipole corresponds to 21.75 GHz which is considered to be enough for the scope of this thesis. Besides, when the two smallest dipoles are thrown away, elements in the top part of the

antenna become sparser, thus it is easier to construct a dual polarize log periodic antenna and the risk of contact between the elements of the cross polarized antennas is minimized.

The photographs and drawings of the manufactured dual polarized log-periodic antennas are given in the following figures:

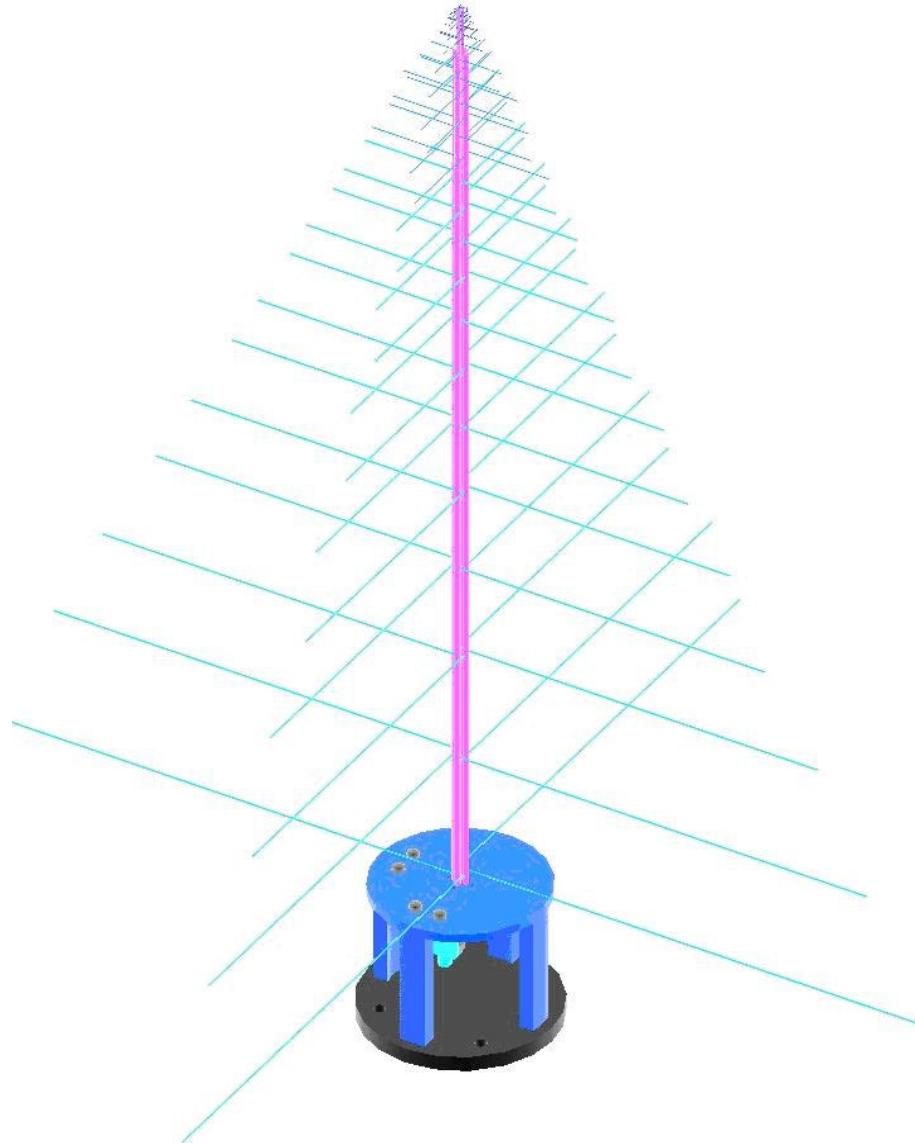


**Figure 6.14** Full drawing of 0.4-18 GHz dual polarized LPDA

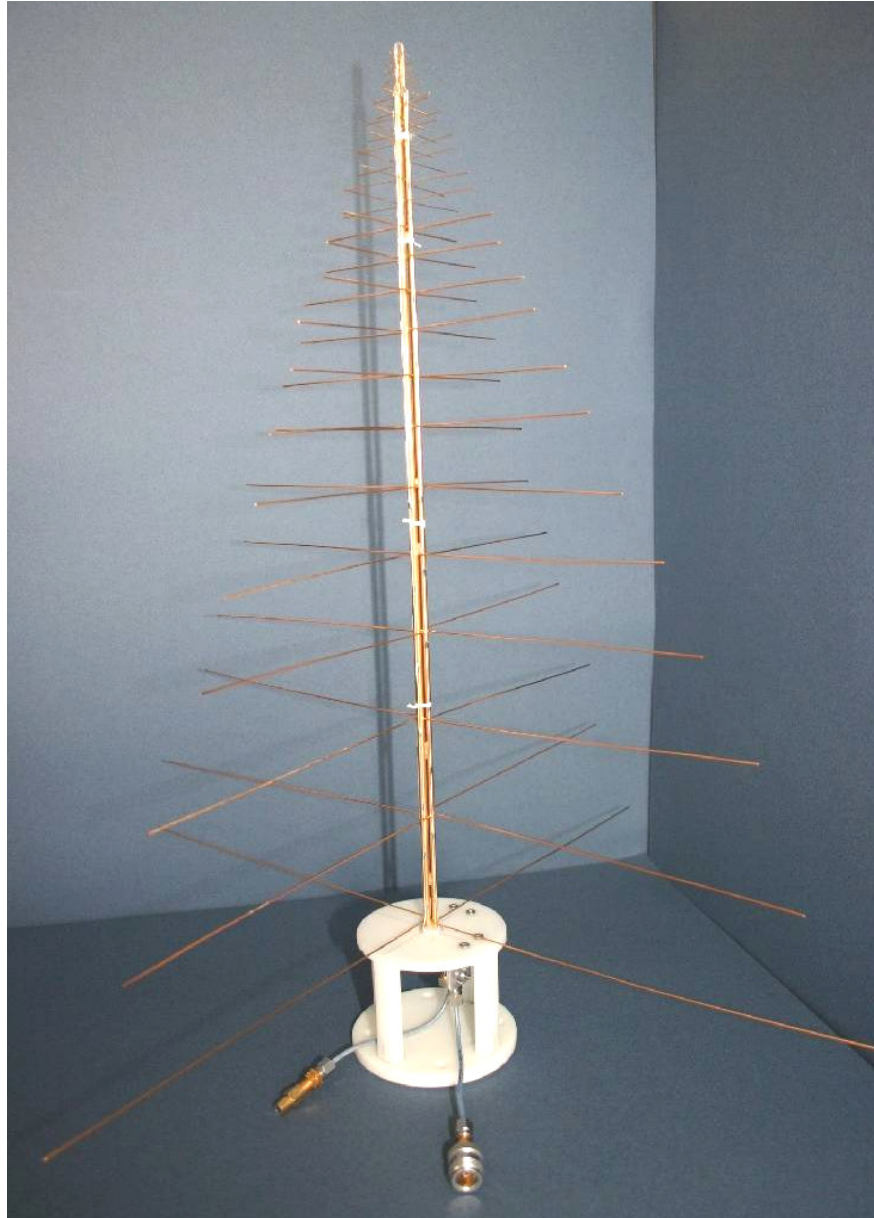


**Figure 6.15** Full photo of 0.4-18 GHz dual polarized LPDA

The input return loss of the antenna measured from the two connectors (Vertical, Horizontal) is as follows:

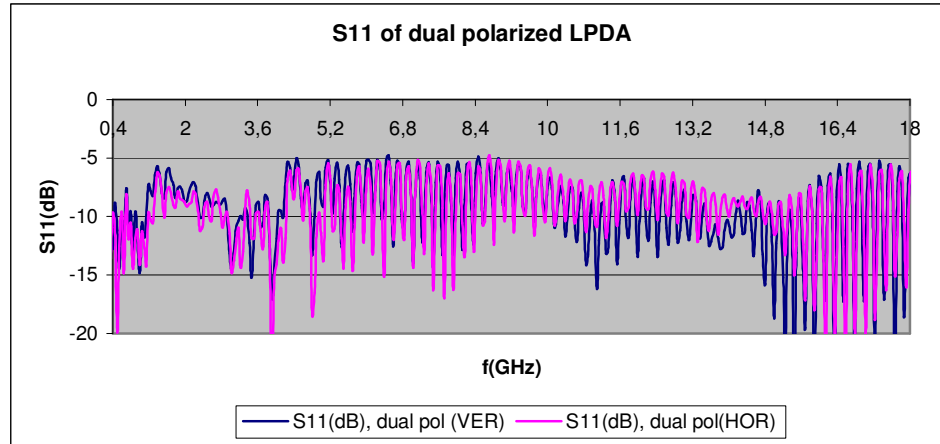


**Figure 6.16** Return loss of dual polarized log periodic antenna

When this return loss is compared with the one of the single polarized log periodic antenna, one can notice that  $S_{11}$  of the dual polarized log periodic antenna is much better. Especially between 13 GHz and 16 GHz,  $S_{11}$  of the antenna is much better, even dropping below -10 dB at some frequencies. Since the input impedance of the antenna is taken as  $100\Omega$ , theoretically  $S_{11}$  is calculated as -9.54 dB, thus the result given in Figure 6.16 is quite satisfactory. This may be the result of better assembling process. The comparison can be observed in the following figure:

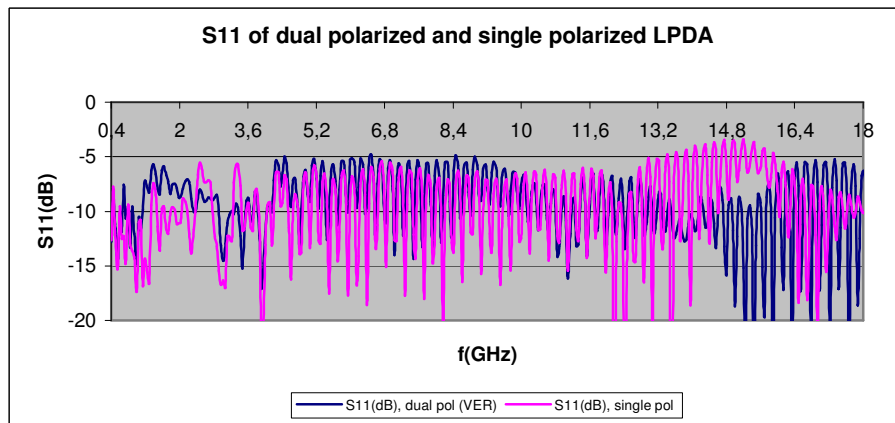


**Figure 6.17** Comparison of the return losses of dual polarized and single polarized log periodic antennas

In the following figures one can see the drawing and the photo of the top, thinnest part of the antenna which is the most crucial and difficult to construct part of the antenna. The risk of contact between the coax cable which is mounted on the transmission line and the dipoles of the cross polarized antenna is very high so the antenna should be constructed very carefully.

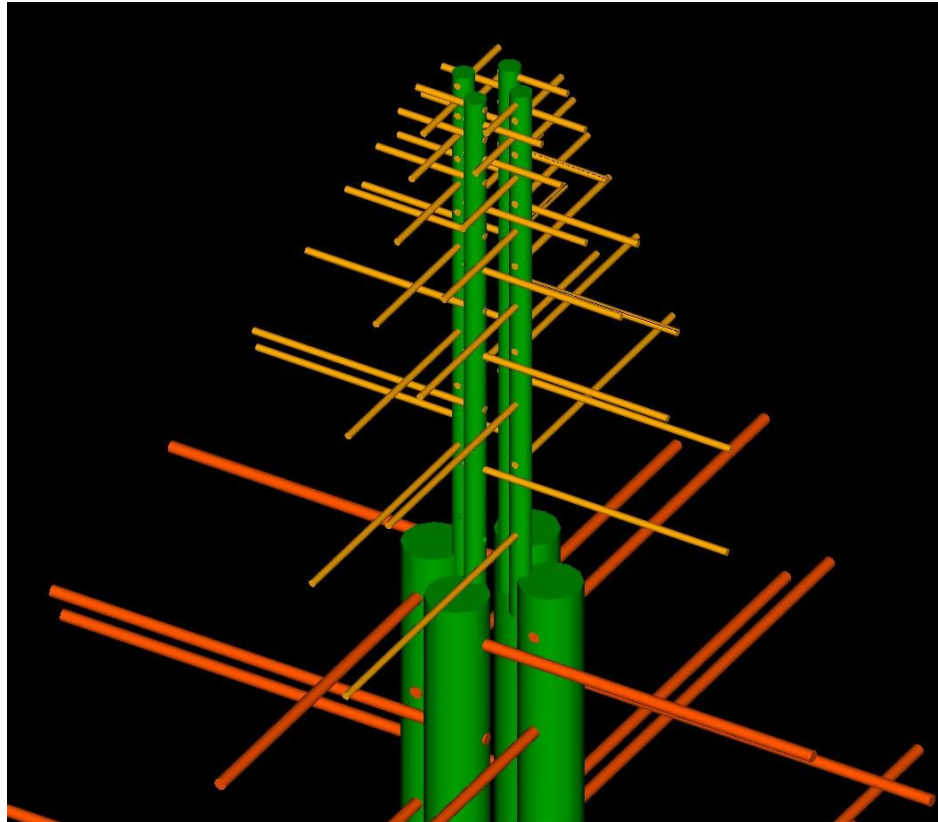


**Figure 6.18** Top and smallest part of the full drawing given in Figure 6.14

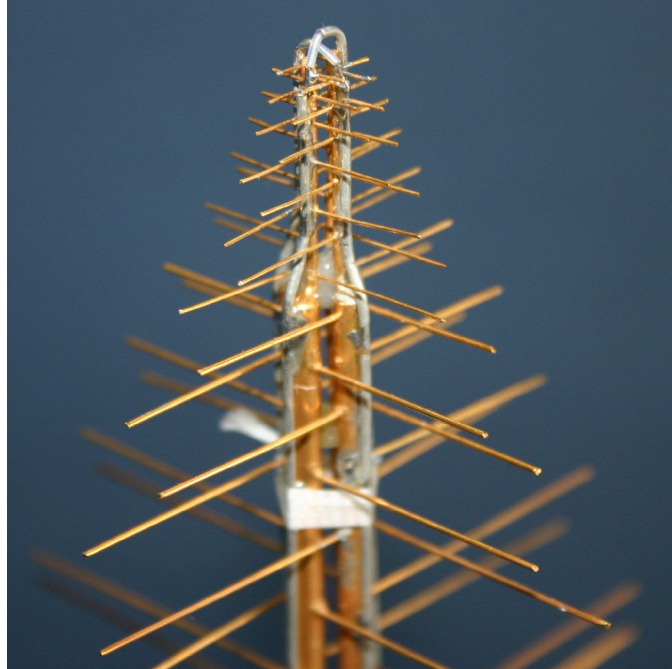


**Figure 6.19** Practical realization of the smallest part of the antenna given in Figure 6.18

Figure 6.20 shows the two connectors of the antenna. When the antenna is measured from one port, the other port is terminated with  $50 \Omega$  to obtain minimum reflection from that port.



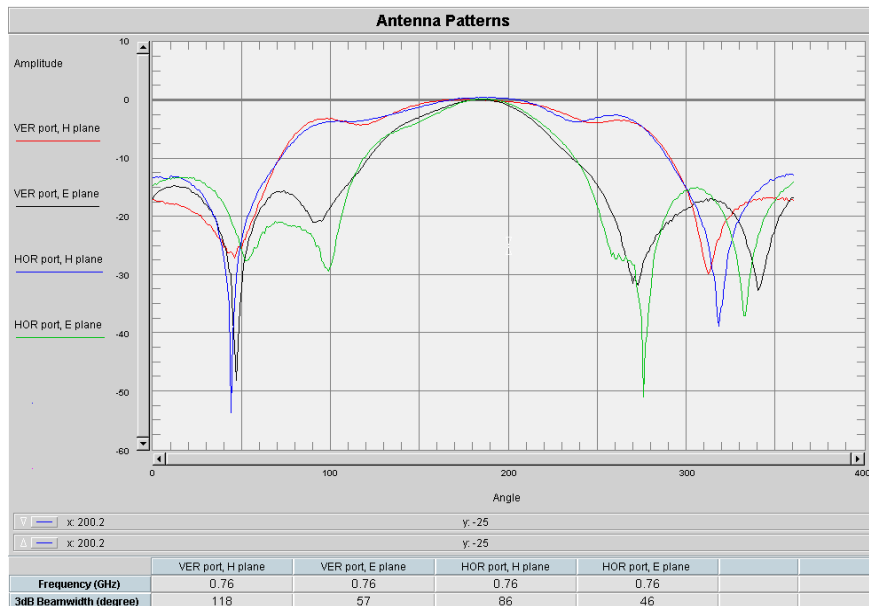
**Figure 6.20** Connectors at the bottom of the antenna

### 6.3.1. RADIATION PATTERNS OF DUAL POLARIZED LOG-PERIODIC ANTENNA

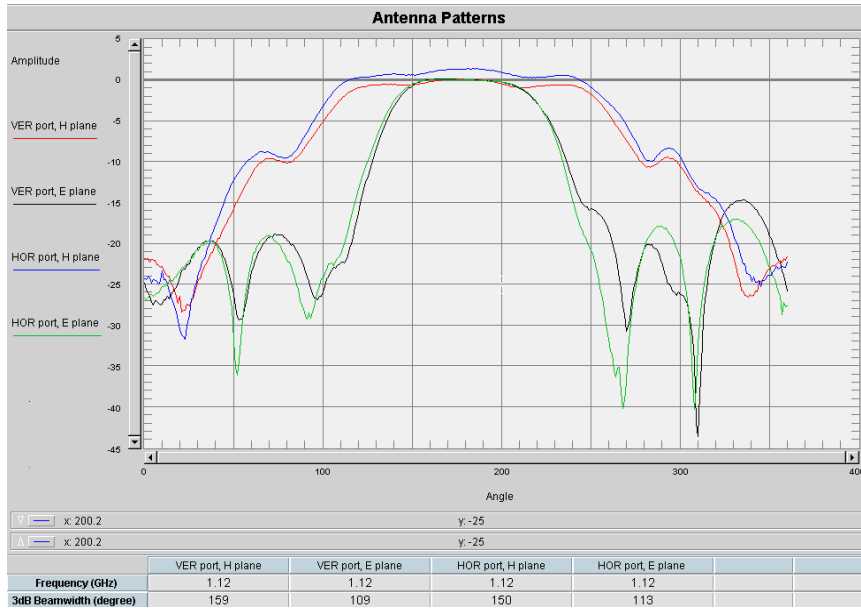
In this section all the co and cross polarized radiation patterns of the designed antenna will be given.

#### 6.3.1.1. 0.4-4 GHZ FREQUENCY BAND

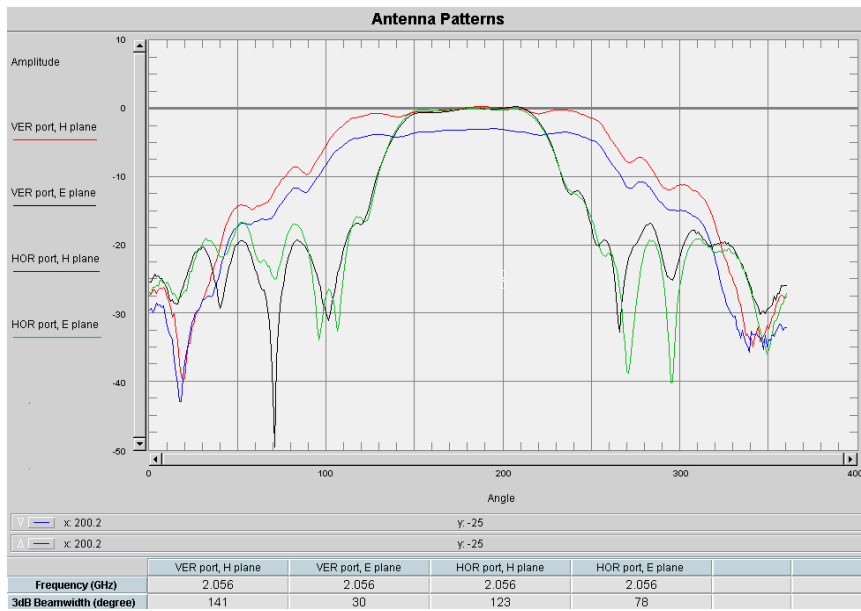
In the following figures E and H plane patterns which are measured from both vertical and horizontal ports of the antenna between the frequency band of 0.4-4 GHz.



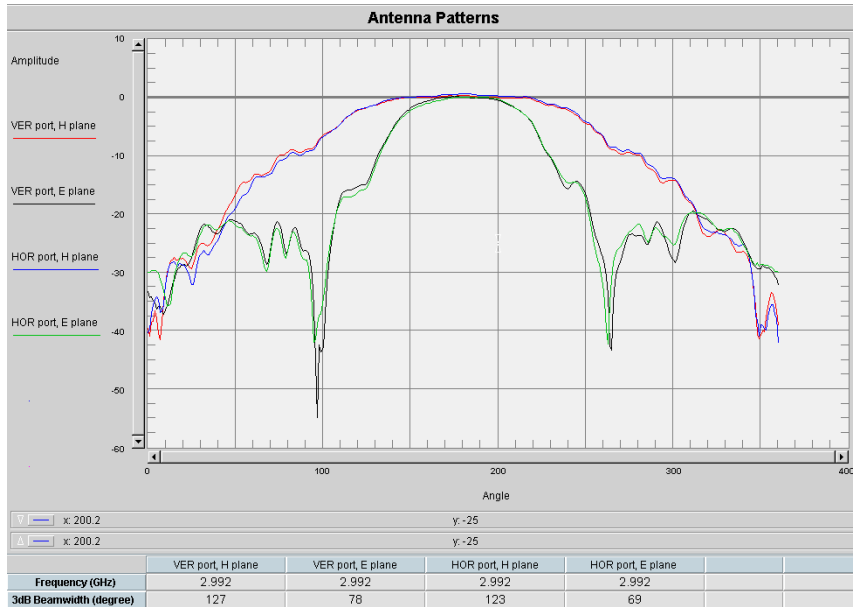
(a)



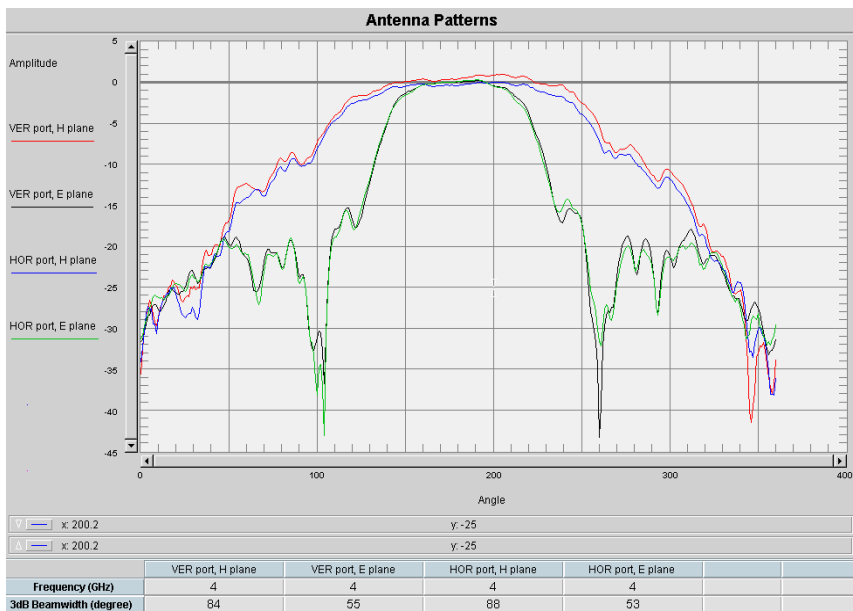
(b)



(c)



(d)



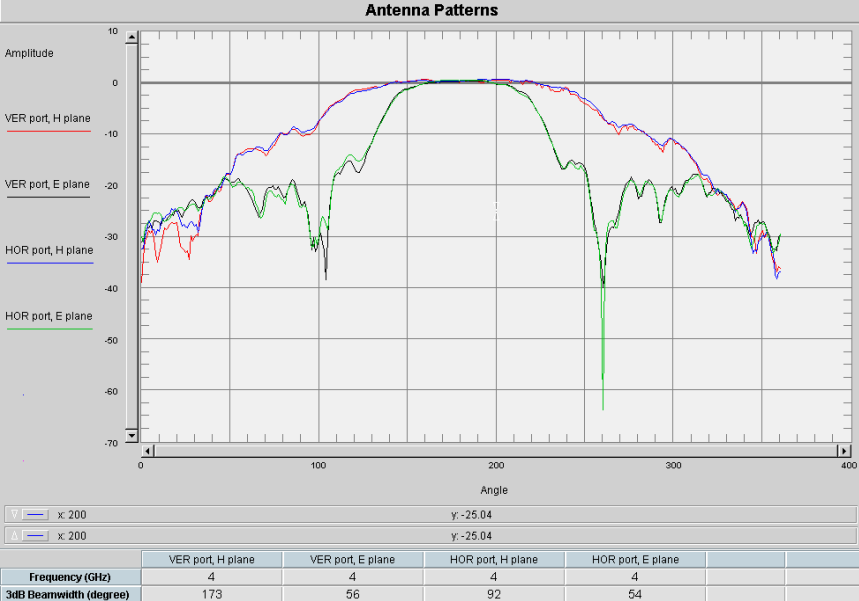
(e)

**Figure 6.21** E and H plane patterns of dual polarized log periodic antenna measured from two ports of the antenna at frequencies 0.76 GHz (a), 1.12 GHz (b), 2.056 GHz (c), 2.992 GHz (d) and 4 GHz (e) respectively

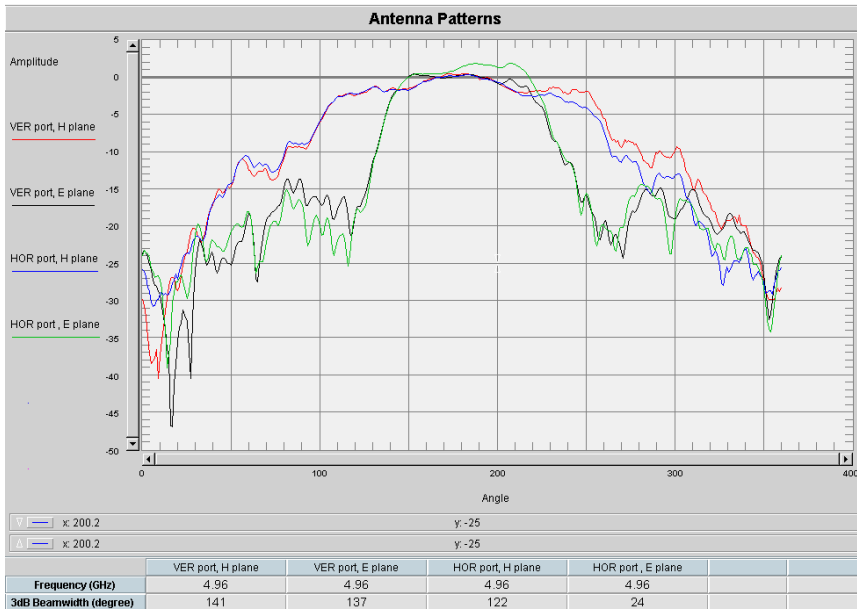
Inspecting the patterns in Figure 6.21, one can notice that patterns measured from two output ports are quite similar. In Figure 6.21(c), the pattern named HOR port, H plane, has a maximum signal level below 0 dB. This is a calibration error, since while the pattern is measured, the AUT and the source antenna is aligned and a through response calibration is performed. As a result at all frequencies, the maximum signal level is taken as the reference, and this reference is 0 dB.

**6.3.1.2. 4-12 GHZ FREQUENCY BAND**

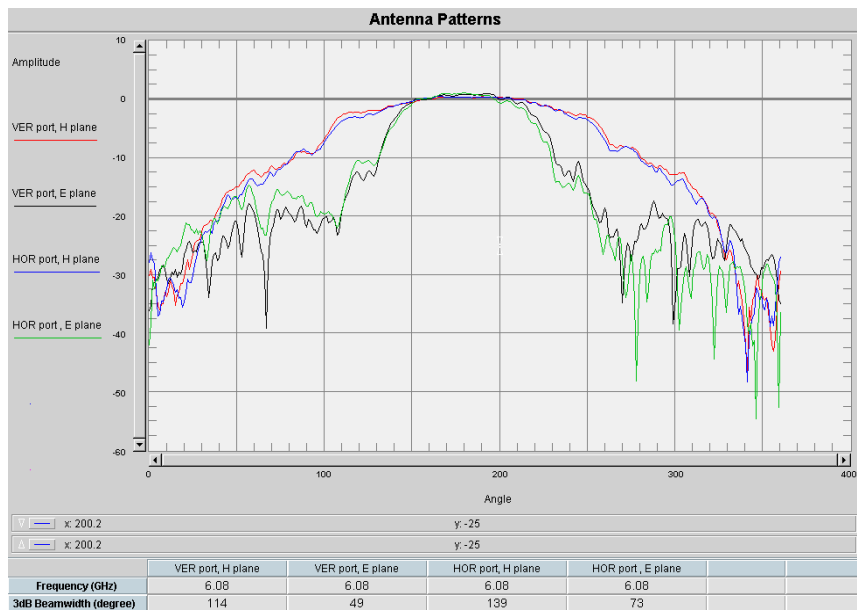
E and H plane patterns of the antenna between the frequency band of 4-12 GHz are given in the following figures.



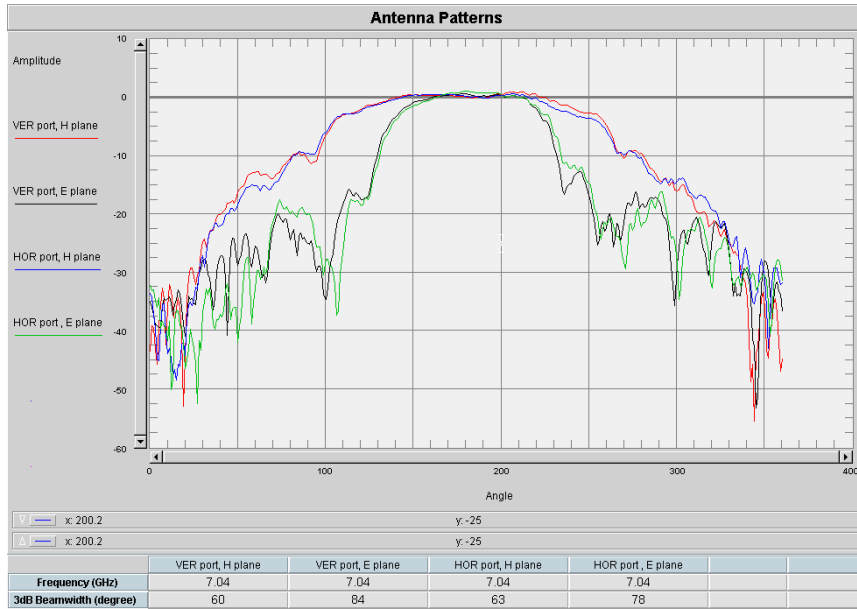
(a)



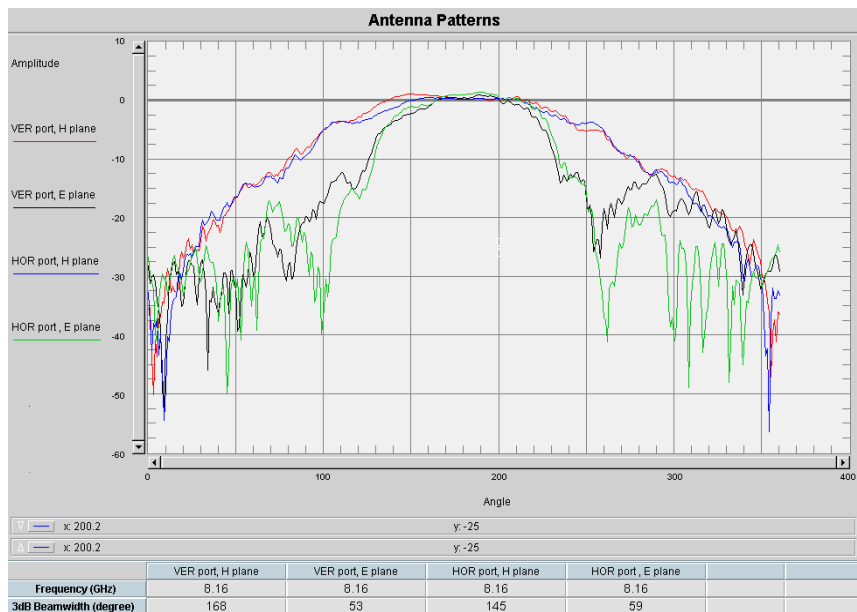
(b)



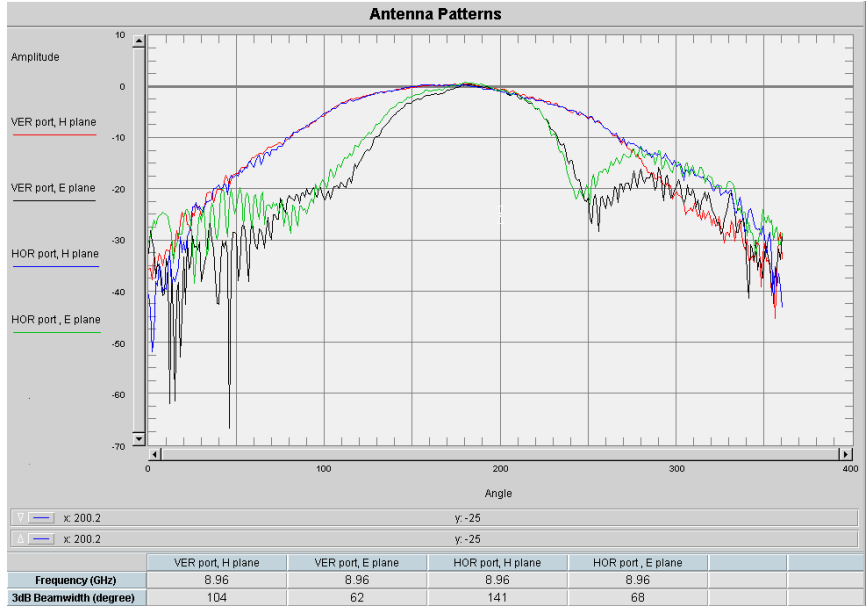
(c)



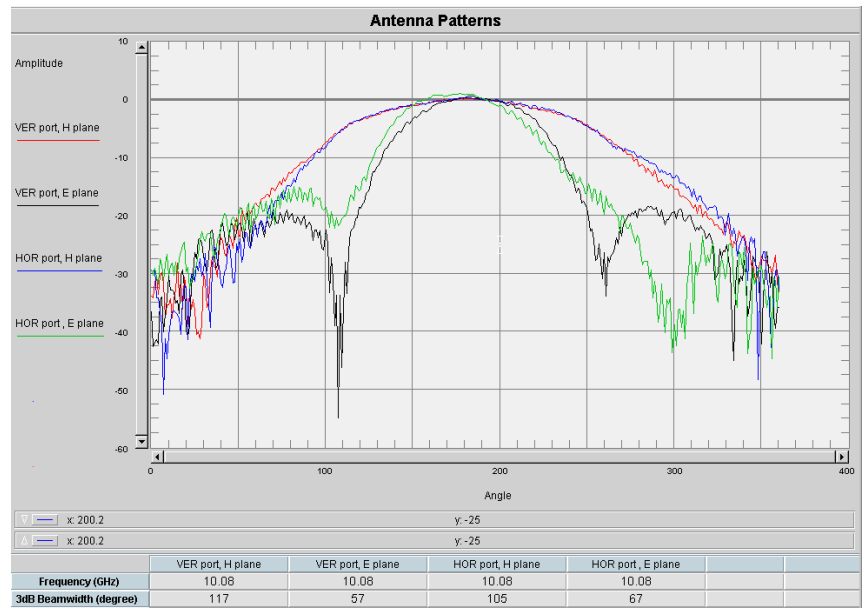
(d)



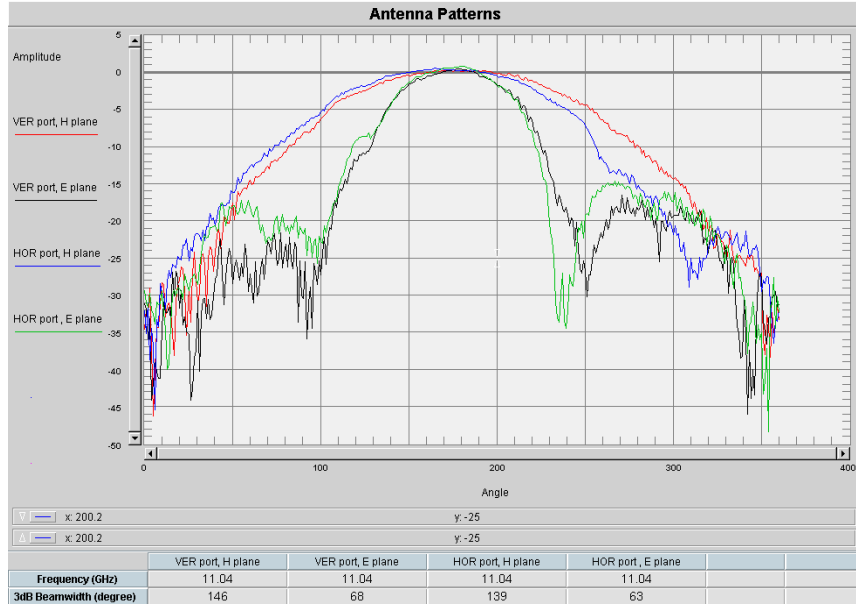
(e)



(f)



(g)



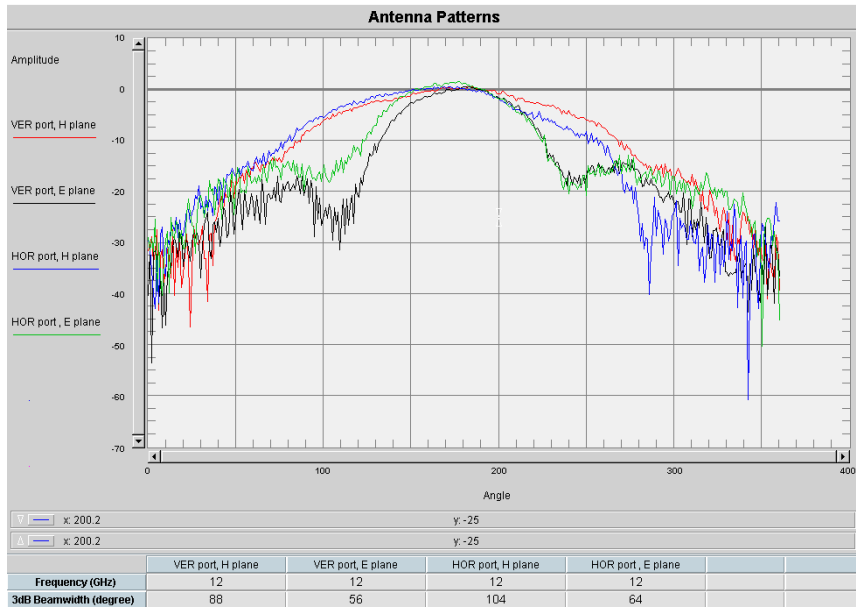
(h)

**Figure 6.22** E and H plane patterns of dual polarized log periodic antenna measured from two ports of the antenna at frequencies 4 GHz (a), 4.96 GHz (b), 6.08 GHz (c), 7.04 GHz (d), 8.16 GHz (e), 8.96 GHz (f), 10.08 GHz (g) and 11.04 GHz (h) respectively

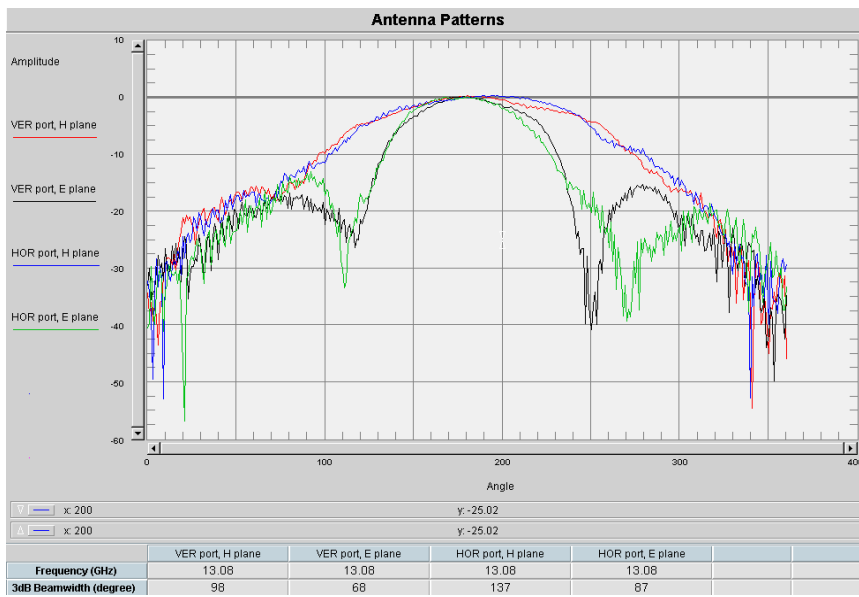
Inspecting the patterns in Figure 6.22, patterns measured from the two ports of the antenna are quite similar and there are no big deteriorations in the patterns up to 12 GHz.

### 6.3.1.3. 12-18 GHZ FREQUENCY BAND

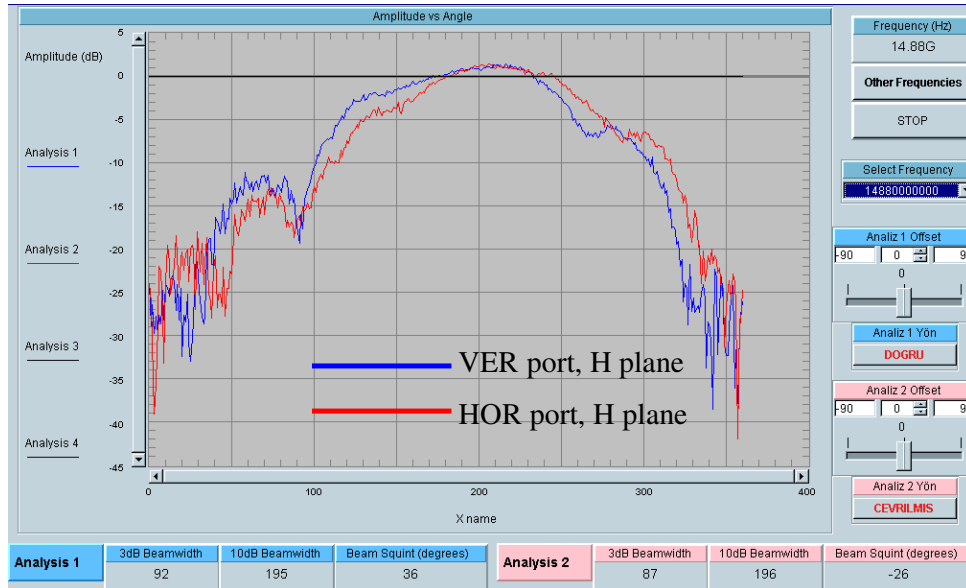
E and H plane patterns of the antenna between the frequency band of 12-18 GHz are given in the following figures.



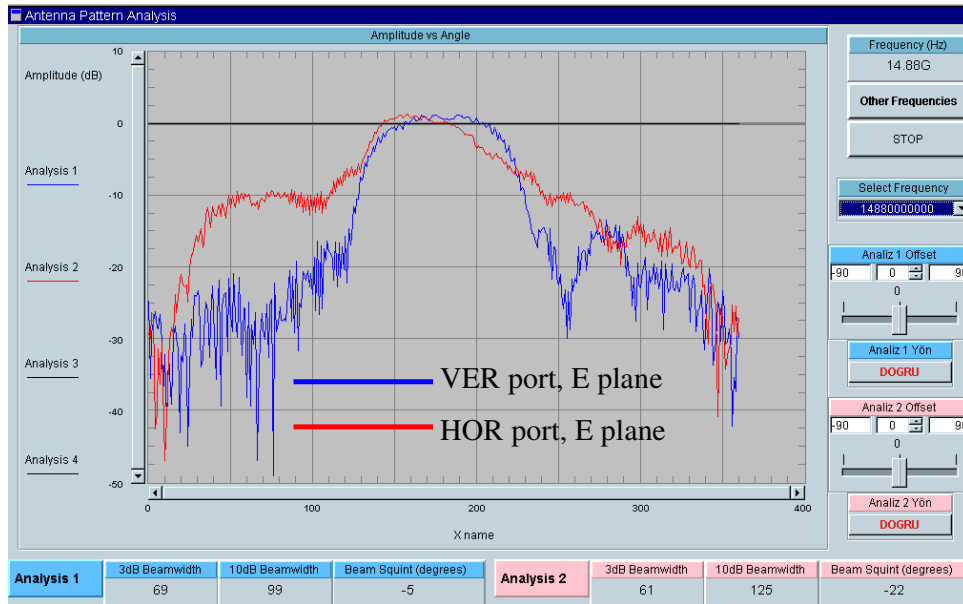
(a)



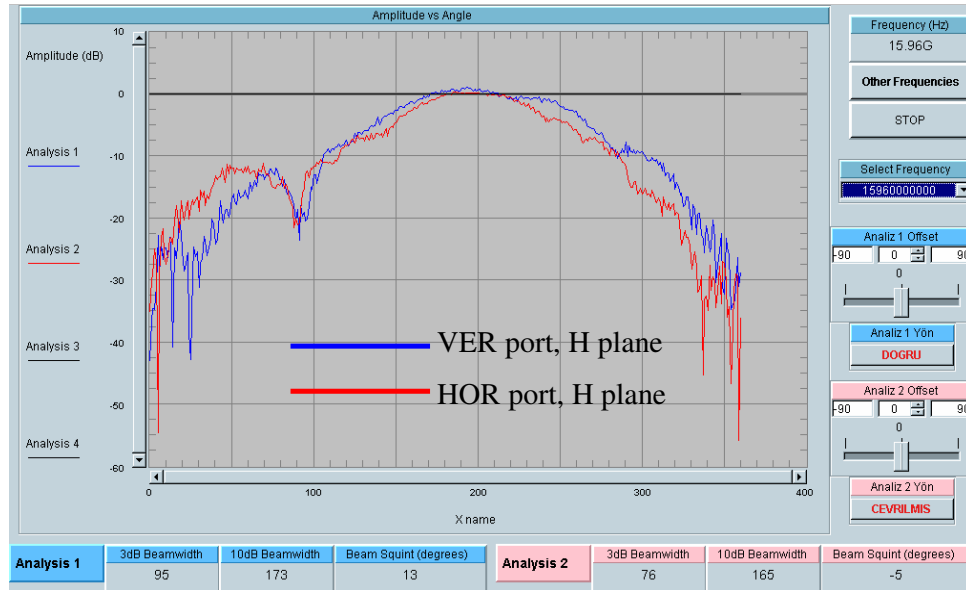
(b)



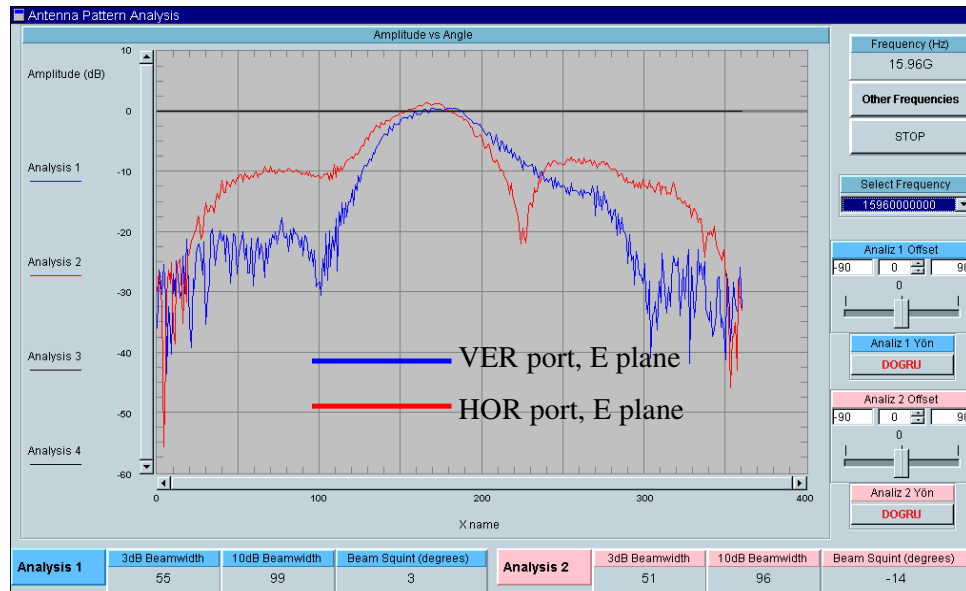
(c-1)



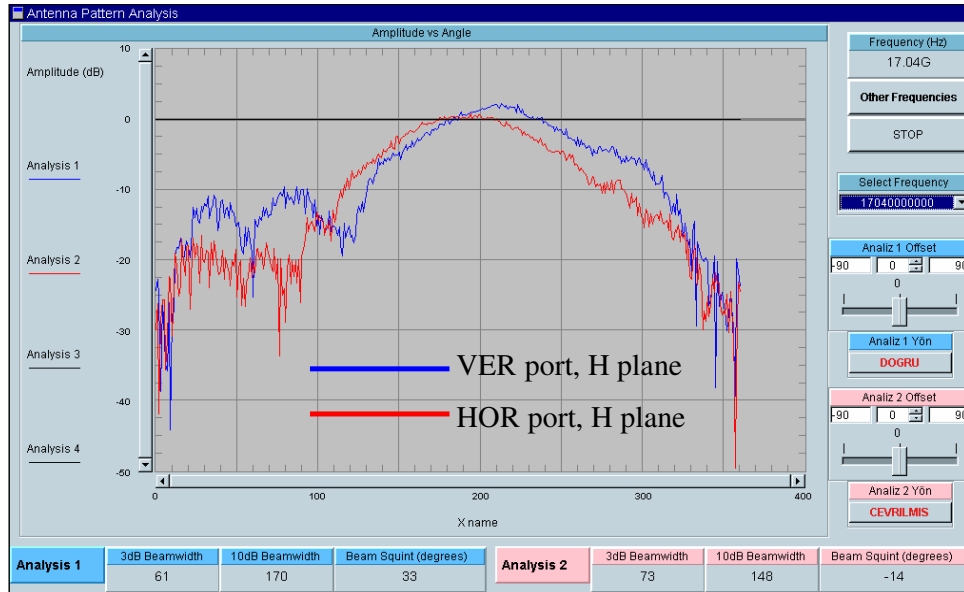
(c-2)



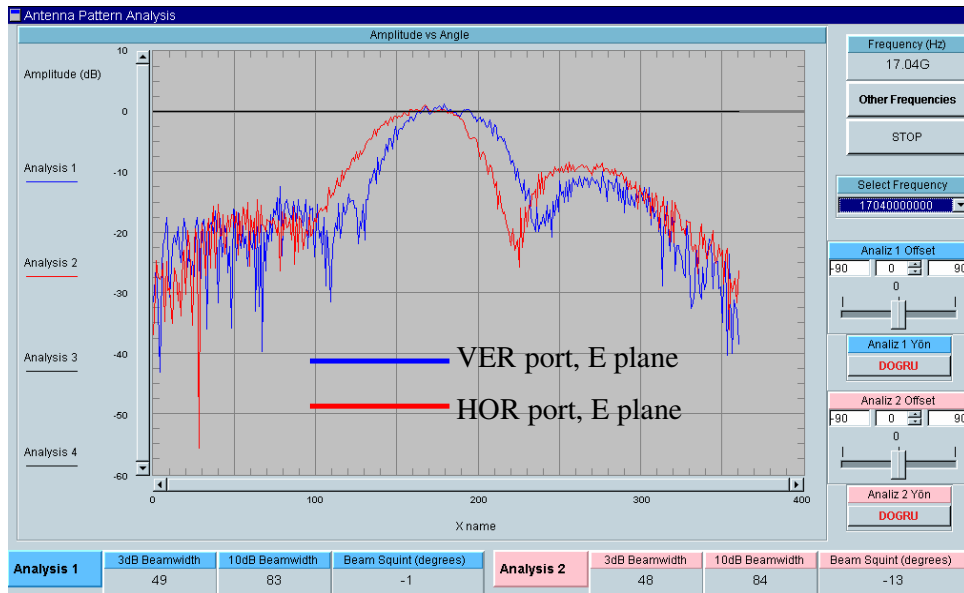
(d-1)



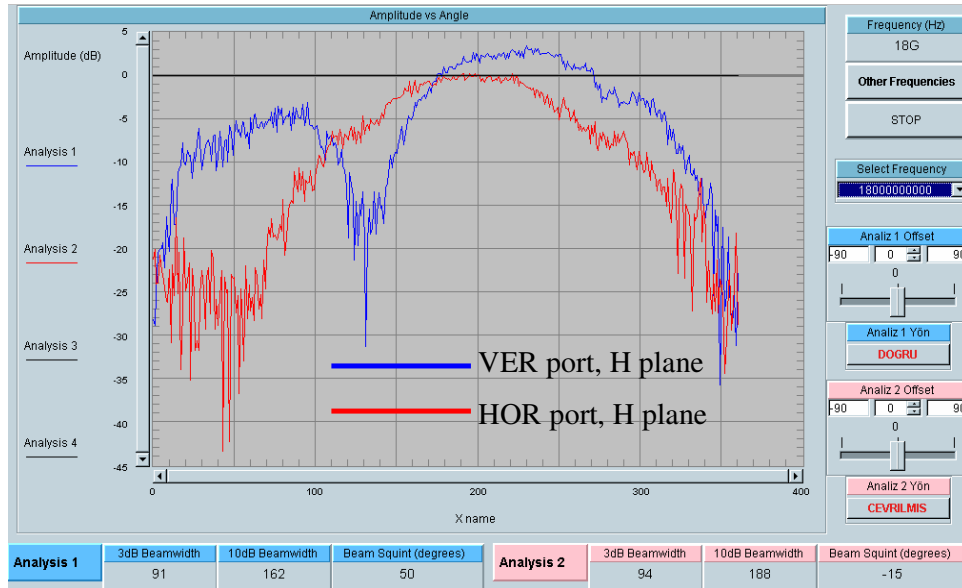
(d-2)



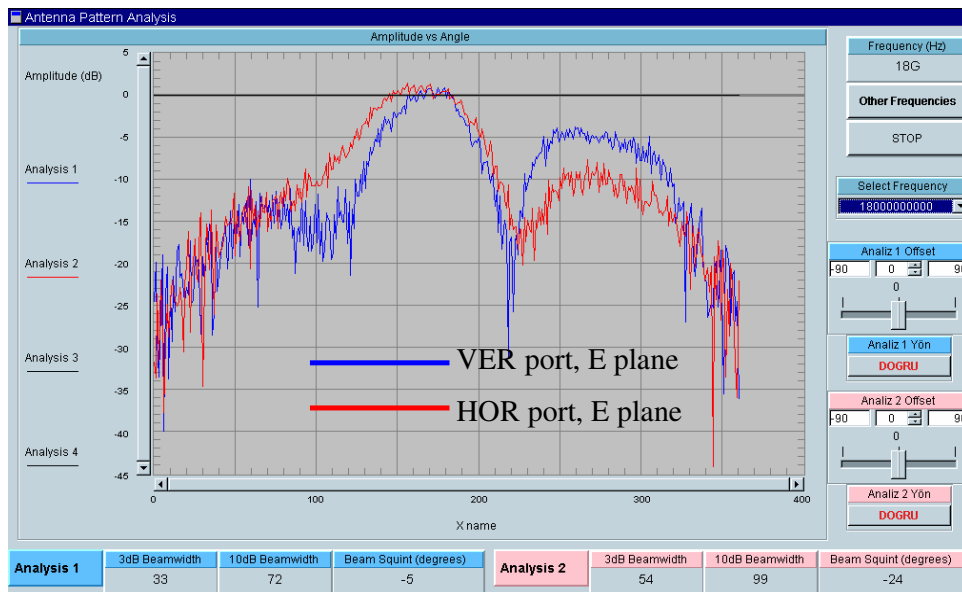
(e-1)



(e-2)



(f-1)



(f-2)

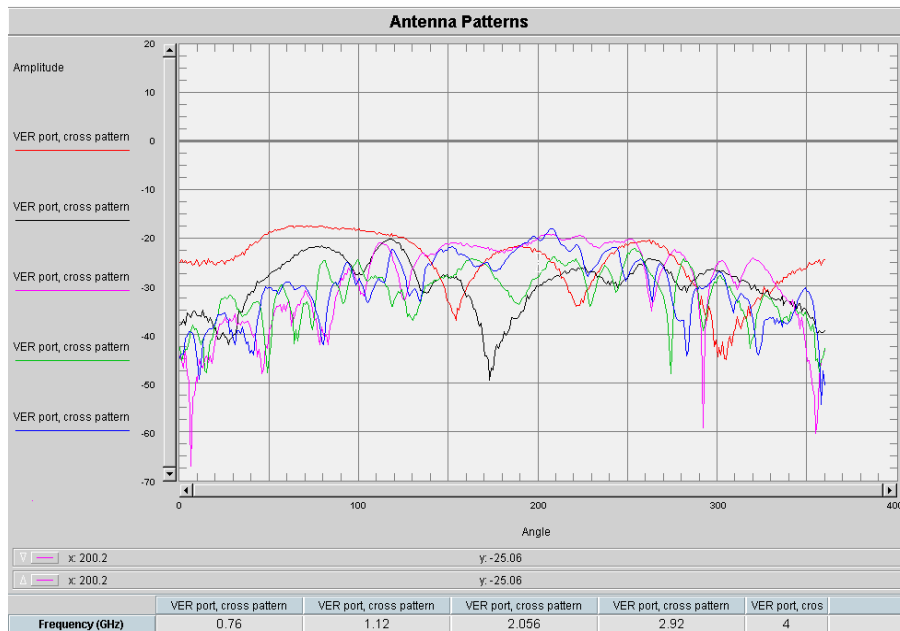
**Figure 6.23** E and H plane patterns of dual polarized log periodic antenna measured from two ports of the antenna at frequencies 12 GHz (a), 13.08 GHz (b), 14.88 GHz (c-1, c-2), 15.96 GHz (d-1, d-2), 17.04 GHz (e-1, e-2) and 18 GHz (f-1, f-2) respectively

Shifting especially in the H-plane patterns of the antenna at some frequencies can be observed in Figure 6.23. This is because of the phenomenon explained using Figure 6.5. The spacing between the transmission lines is 1.68 mm; therefore the outer conductor of the transmission line should be removed at 0.84 mm, which is a very small distance to be measured accurately.

At some frequencies such as 18 GHz, H-plane patterns are quite different. This may be due to the small difference between the feeds of the two orthogonal antennas

#### 6.3.1.4. CROSS POLARIZED RADIATION PATTERNS

To give an idea about the cross polarized patterns of the antenna, measurement results of vertical port of the antenna are given in the following figures:



(a)



In Figure 6.24(a), cross polarized patterns at 0.76 GHz, 1.12 GHz, 2.056 GHz, 2.92 GHz and 4 GHz are given. Cross patterns at frequencies 5.12 GHz, 6,08 GHz, 7.04 GHz, 8 GHz, 9.12 GHz and 10.08 GHz are given in Figure 6.24(b) and finally in Figure 6.24(c), cross polarized patterns at 12 GHz, 13.08 GHz, 14.28 GHz, 15 GHz, 16.08 GHz and 18 GHz are given

Inspecting Figure 6.24, cross pattern level increases with frequency. Below 12 GHz cross polarization level is less than -10 dB.

#### 6.4. SIMULATIONS OF THE REFLECTOR ANTENNA DESIGNED USING MIR

Using the currents at the bases of dipoles and the dimensions of the LPDA, MIR can calculate the incident field of the reflector, in other words pattern of the LPDA. At few frequencies HPBW values calculated from the MATLAB<sup>®</sup> and the MIR program are compared. The results are as follows:

**Table 6.1** Comparison of HPBW's calculated using MATLAB and MIR program

<b>MATLAB<sup>®</sup></b>					
<b>f(GHz)</b>	0,4	4	10	14	18
<b>E plane_HP BW(degree)</b>	68	80	80	74	72
<b>H plane_HP BW(degree)</b>	134	148	150	136	130
<b>MIR</b>					
<b>E plane_HP BW(degree)</b>	69,5	76	79	73	76
<b>H plane_HP BW(degree)</b>	135	142	150	136	134

Inspection of Table 6.1 shows that outputs of the two programs are sufficiently similar.

E and H plane patterns of the designed reflector antenna are simulated at various frequencies such as 0.4 GHz, 1 GHz, 2 GHz, 4 GHz, 7 GHz, 10 GHz, 12 GHz, 14 GHz and 18 GHz. At these frequencies gains of the antenna are also calculated. The simulated E and H plane patterns at some frequencies are given in the following figures:

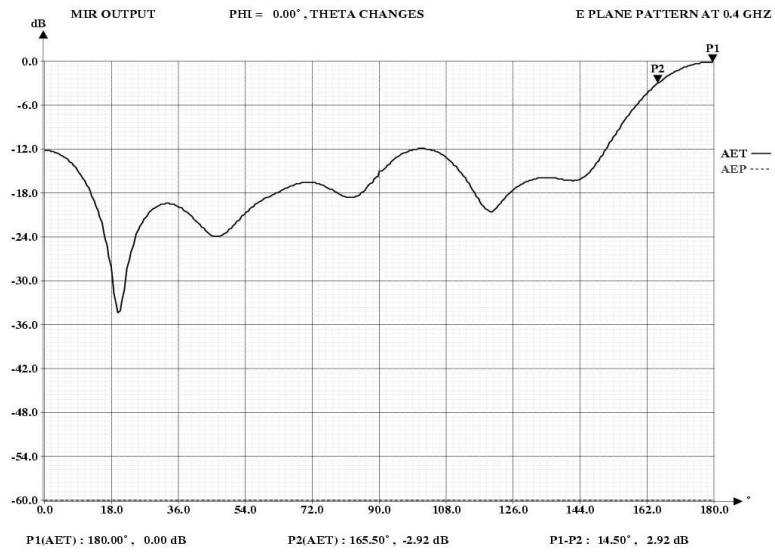


Figure 6.25 Simulated E plane pattern at 0.4 GHz

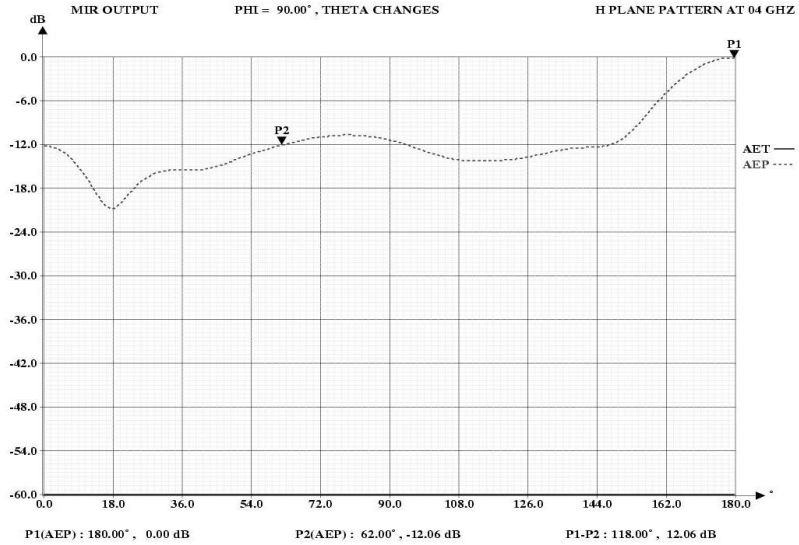
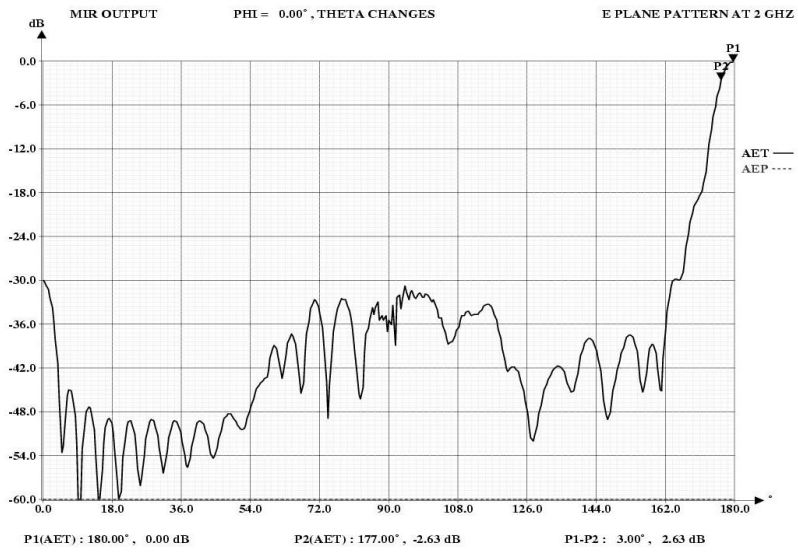
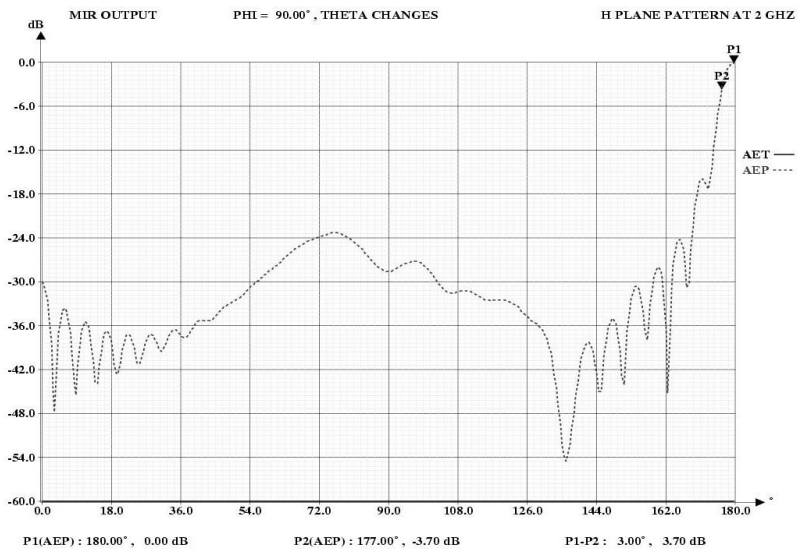


Figure 6.26 Simulated H plane pattern at 0.4 GHz



**Figure 6.27** Simulated E plane pattern at 2 GHz



**Figure 6.28** Simulated H plane pattern at 2 GHz

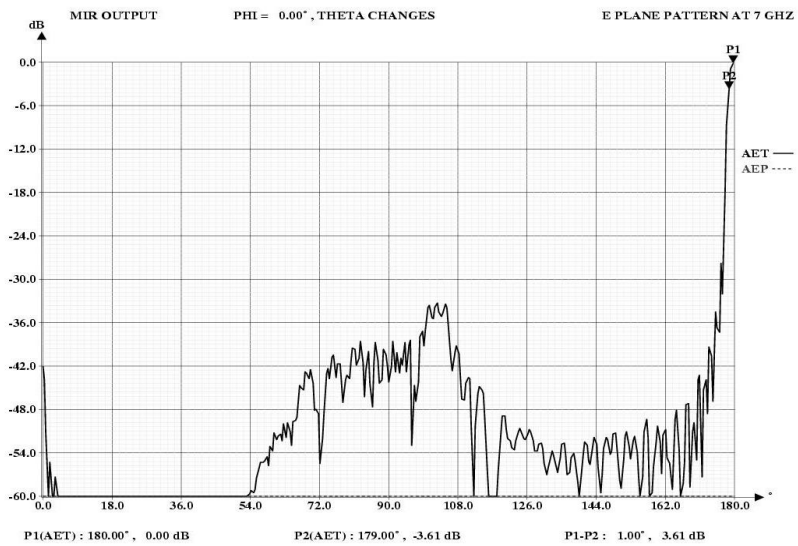


**Figure 6.29** Simulated E plane pattern at 7 GHz

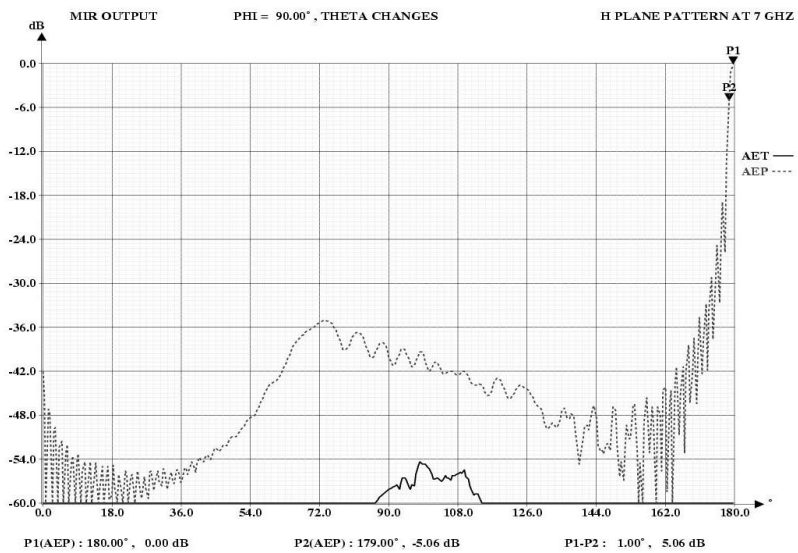


**Figure 6.30** Simulated H plane pattern at 7 GHz

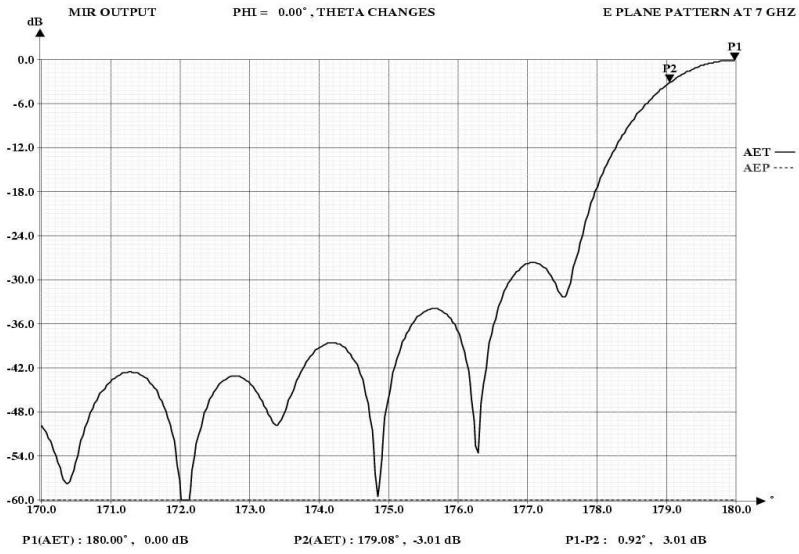


**Figure 6.31** Zoomed simulated E plane pattern at 7 GHz

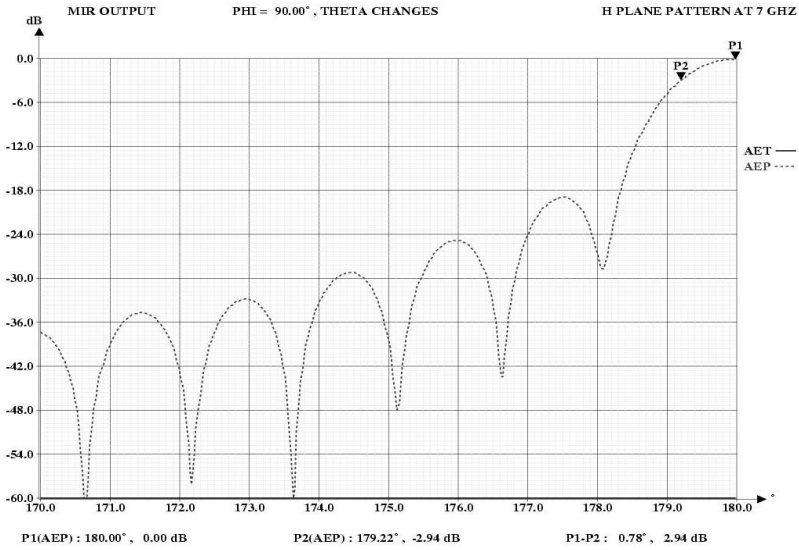


**Figure 6.32** Zoomed simulated H plane pattern at 7 GHz

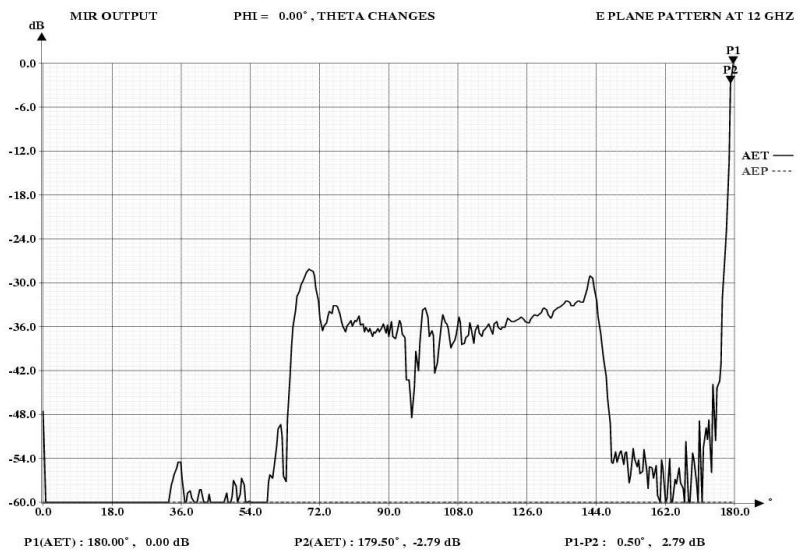


**Figure 6.33** Simulated E plane pattern at 12 GHz

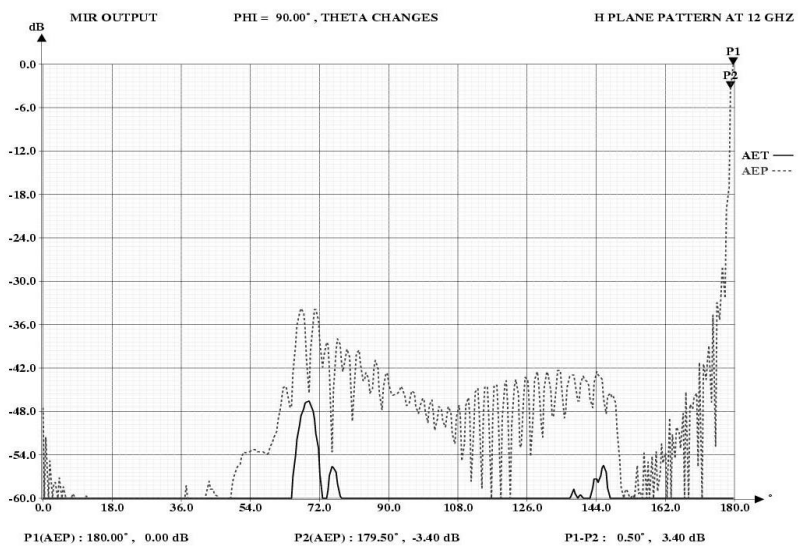


**Figure 6.34** Simulated H plane pattern at 12 GHz

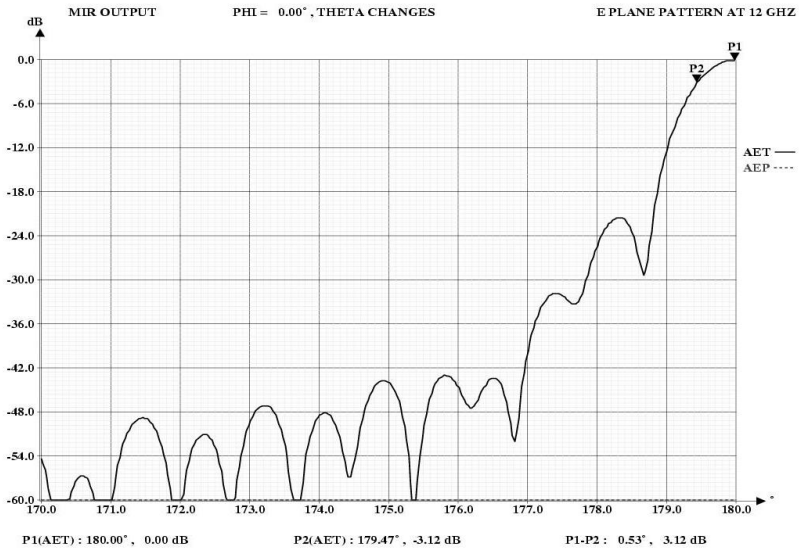


**Figure 6.35** Zoomed simulated E plane pattern at 12 GHz

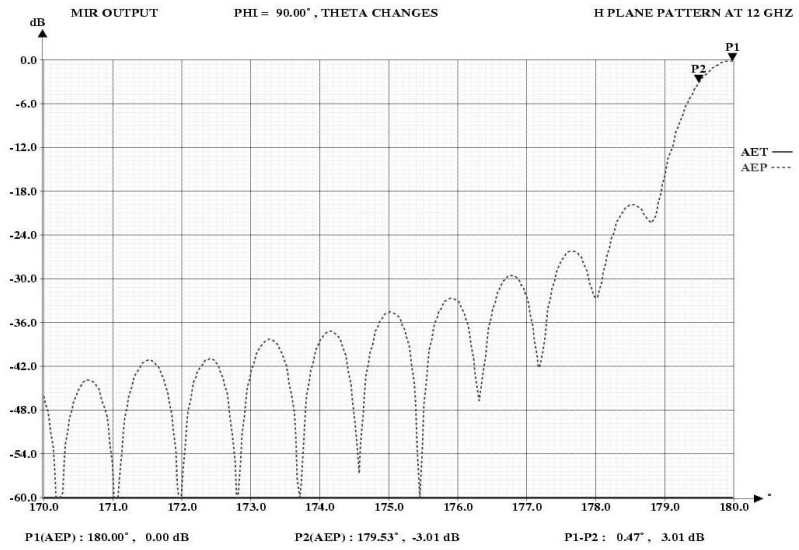


**Figure 6.36** Zoomed simulated H plane pattern at 12 GHz

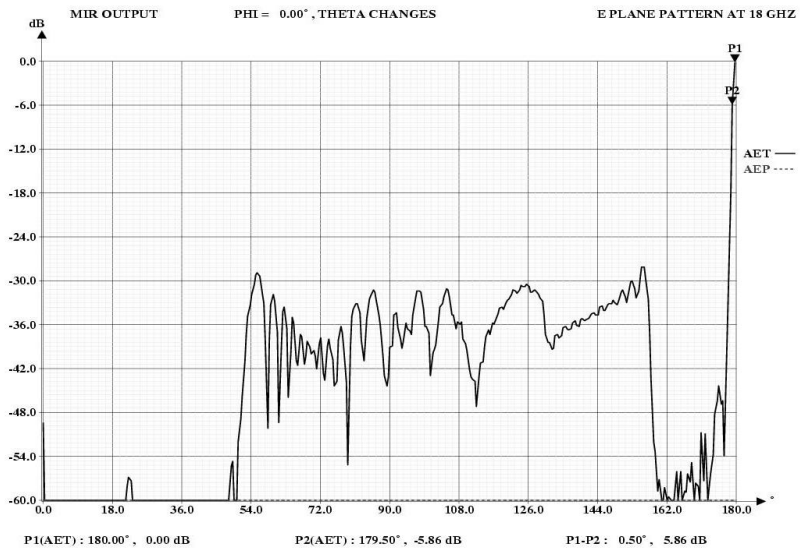


**Figure 6.37** Simulated E plane pattern at 18 GHz

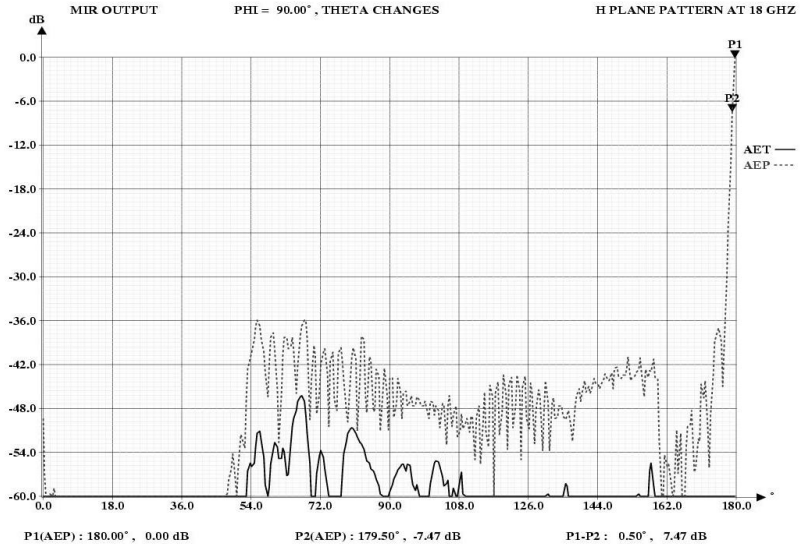


**Figure 6.38** Simulated H plane pattern at 18GHz

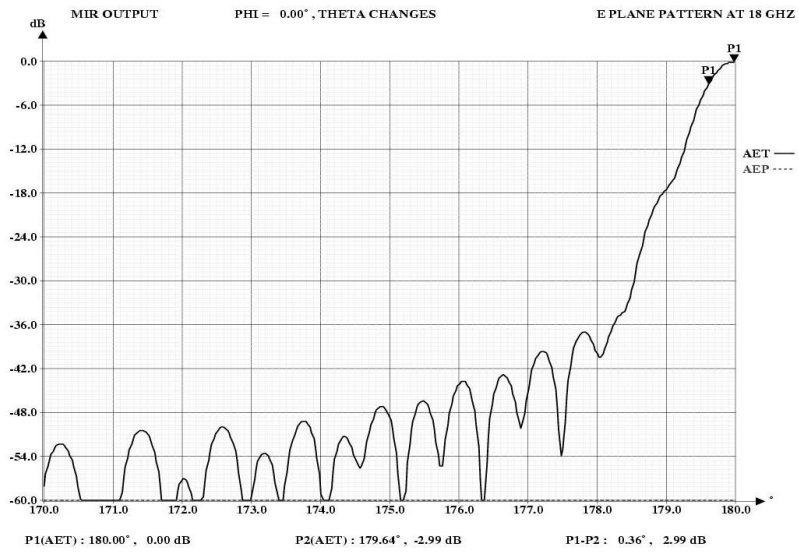


**Figure 6.39** Zoomed simulated E plane pattern at 18 GHz

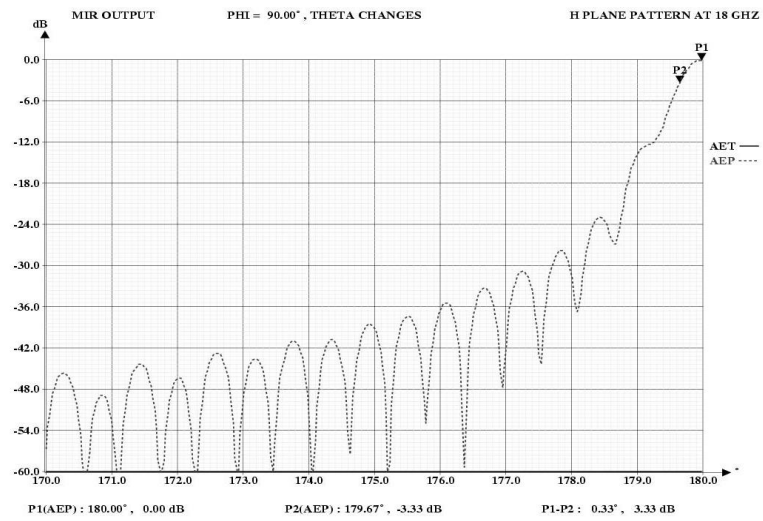


**Figure 6.40** Zoomed simulated H plane pattern at 18 GHz

Side lobe, back lobe levels, half power beam widths of the patterns are given in the following table:

**Table 6.2** Summary information about the simulated patterns

	f(GHz)	0.4	1	2	4	7	10	12	14	18
<b>E plane</b>	1st SLL(dB)	-11.8	-20.6	-29.8	-34.5	-27.9	-18.9	-21.5	-35.1	-37.1
	BL(dB)	-11.8	-22.2	-30	-36.9	-42	-42	-47	-48	-49
	HPBW(degree)	29.4	12.1	6.4	3.2	1.84	1.58	1.04	0.92	0.72
<b>H plane</b>	1st SLL(dB)	-10.6	-17.3	-30.2	-17.5	-18.9	-19.3	-19.7	-16.8	-22.8
	BL(dB)	-12.1	-22.1	-30	-36	-42	-44	-48	-47.9	-49
	HPBW(degree)	27.6	11.1	5.4	2.8	1.58	1.12	1.4	0.82	0.64
<b>Gain(dB)</b>	(Kraus)	16.02	23.82	29.71	35.6	40.5	42.6	43.4	46.3	48.48

In the table above, gain is calculated using Kraus's formula. The gain of the reflector within the frequency band is as following:

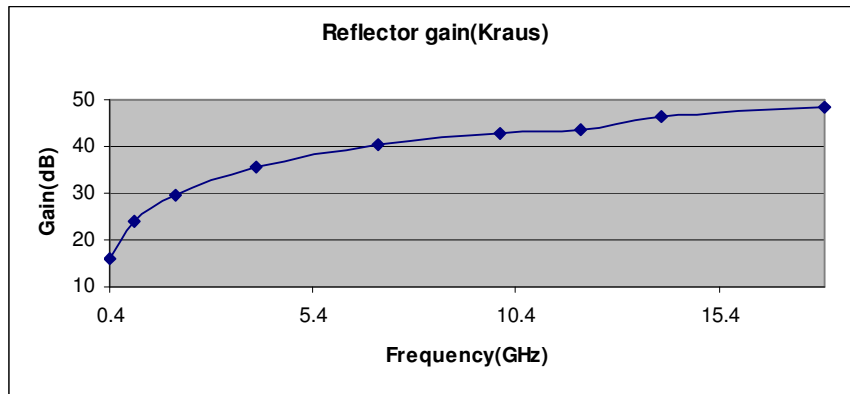


**Figure 6.41** Gain of the reflector antenna calculated using Kraus's formula

### 6.4.1. EFFICIENCY AND BLOCKAGE CALCULATIONS

These calculations are made at frequencies of 0.4 GHz, 2 GHz, 7GHz, 12 GHz and 18 GHz.

Values of the electrical fields and  $|F(\Psi, \xi)|$  for different  $\Psi$  and  $\xi$  angles which are given at Table 5.2 and Table 5.3 for 0.4 GHz, are also calculated at the frequencies of 2 GHz, 7 GHz, 12 GHz and 18 GHz using MIR program.

Using this information, efficiency of the reflector antenna considering no blockage and blockage effects are calculated using MATLAB<sup>®</sup>. The results are given at the following table:

**Table 6.3** Gains and efficiencies considering blockage and no blockage effects

f(GHz)	Reflector gain(Kraus)(dB)	$\eta_a$	$\eta_b$	GA(dB)	GB(dB)
0.4	16.02	0.4916	0.4618	13.714	13.4421
2	29.714	0.4049	0.3815	26.8619	26.592
7	40.484	0.4572	0.4296	38.259	37.9893
12	43.487	0.3712	0.3495	42.0366	41.7746
18	48.483	0.4262	0.4001	46.1578	45.8838

In the table above, first column shows the frequencies at which these calculations are made. Second column shows the gains which are calculated from the simulated E and H plane patterns using Kraus's gain formula.  $\eta_a$  shows the efficiency considering no blockage in front of the reflector. GA (dB) shows the gain calculated using this efficiency.  $\eta_b$  shows the efficiency considering blockage in front of the reflector. GB (dB) shows the gain calculated using this efficiency. In the following table, gain reduction due to efficiency calculation and blockage effect can be seen.

**Table 6.4** Gain loss due to efficiency and blockage effects

f(GHz)	loss due to efficiency(dB)	loss due to efficiency+blockage(dB)
0.4	2.306	2.5779
2	2.8521	3.122
7	2.225	2.4947
12	1.4504	1.7124
18	2.3252	2.5992

In Table 6.4, second column shows the gain reduction of the reflector, when there is no blocked region in front of it. Last column shows the gain reduction when the effect of the blocked region is taken into account. In this case efficiency of the antenna drops a little bit further as can be noticed from Table 6.3.

In the following figure gain of the reflector antenna calculated from the Krauss's formula considering 100% efficiency and gain considering the gain reduction due to real efficiency and blockage effects are given.

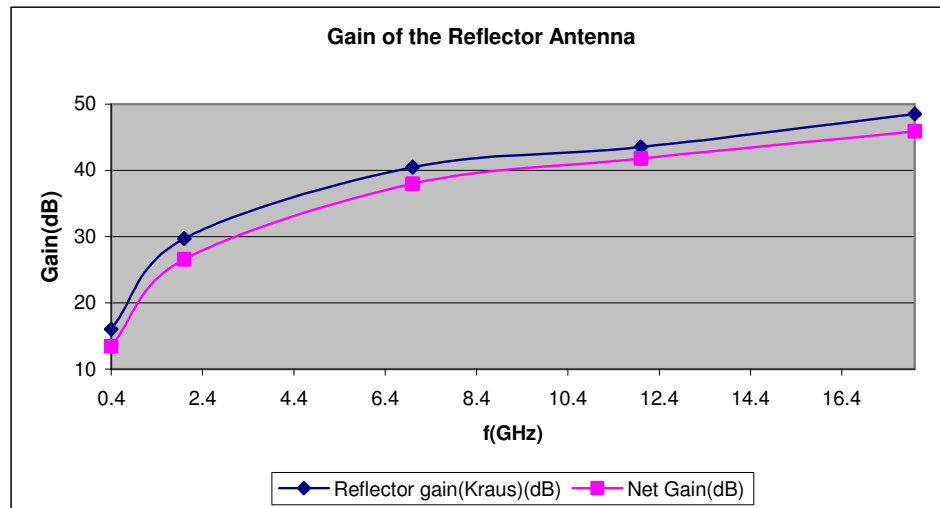


**Figure 6.42** Gain of the reflector calculated from the Kraus's formula and net gain after the losses due to efficiency and blockage are taken into account

Final technical drawing of the reflector antenna together with the feed can be seen in the following figure:

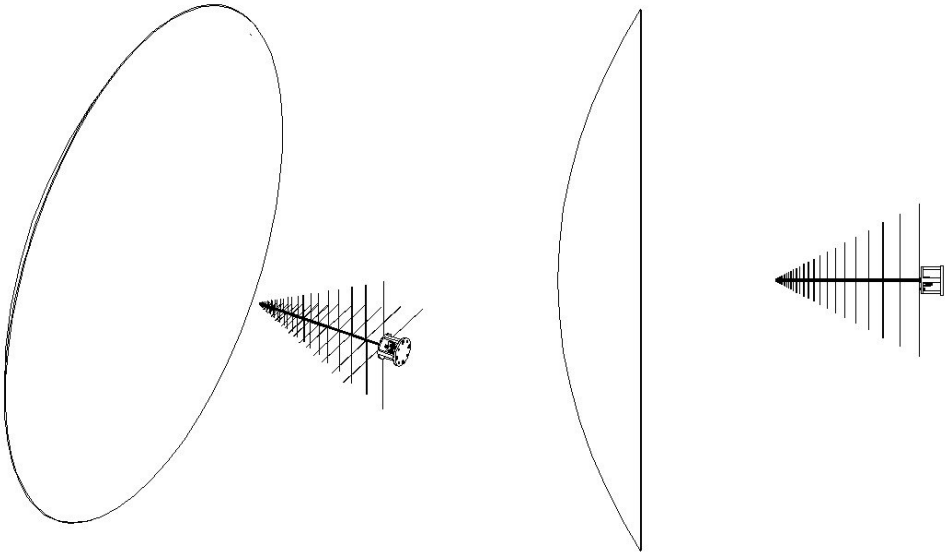


**Figure 6.43** Perspective and side views of the reflector antenna together with feed

## CHAPTER VII

### CONCLUSIONS

In this thesis, a reflector antenna covering a frequency range of 0.4-18 GHz band with required gain characteristics is designed and simulated. As the feed of the reflector, a dual polarized LPDA is designed, simulated and constructed.

First step of the design process was to determine the design approach. Admittance matrix approach for the LPDA's was introduced. The aim of this step was to find the currents at the bases of the dipoles of the LPDA. To achieve this aim, mutual coupling between the linear elements of the LPDA was investigated and programmed in addition to the admittance matrix approach; then a method was developed. Simulations were made with MATLAB<sup>®</sup> and FORTRAN. The results of the both programs were compared with each other to check the consistency of the programs. Then the results of this method were compared with several examples given in the literature [1], [2], [3], [6], and [7].

Next, single polarized LPDA was designed. Using the design parameters and the simulation program written in MATLAB<sup>®</sup>, currents of the LPDA were found. This is one of the most crucial parts of this thesis since absolute values and the phases of the currents were used together with the physical dimensions of the LPDA to simulate the reflector antenna.

Construction of a dual polarized LPDA is another important part of the thesis. Before production of the dual polarized LPDA, considering the necessary parameters for it, a single polarized prototype LPDA was constructed. First, the results of the electrical tests were not so satisfactory. This led the attention to be focused on the thinnest part of the transmission line and the feeding section of the antenna. Transmission lines of the antennas should be closer than  $0.3 \lambda$ . Otherwise  $S_{11}$  of the antenna and thus the pattern of the antenna doesn't give satisfactory results. In this thesis, final forms of the thinnest transmission lines are

0.15  $\lambda$  apart from each other. As an other observation, transmission lines shouldn't be so thick compared to the dipole thickness at the high frequency range. 0.9 mm transmission lines are used with the thickness of 0.3 mm dipoles in the LPDA designed in the scope of this thesis. Attention should be paid to the feeding section as well. The shield of the coax should be removed in the middle of the transmission lines; otherwise shifting in the pattern occurs.

After all the necessary improvements were done in the prototype LPDA, dual polarized LPDA was constructed. The antenna should be constructed very carefully since the risk of contact between the coaxial cables, which is mounted on the transmission lines and the dipoles of the cross polarized antenna, is very high. It was noticed that, better assembling process in the high frequency region of the antenna is very important. Two single polarized LPDA, having the same dimensions as the final form of the prototype antenna are combined to have a dual polarized LPDA. Due to the better assembling process, return loss of dual polarized LPDA is better than the prototype single polarized antenna. Improvement of the  $S_{11}$  is approximately 5 dB between 13-16 GHz frequency region.

All the electrical measurements were done in anechoic chamber and successful results were obtained. Performance is compared with few commercial products and the performance was found to be even better in some frequencies.

Finally, the currents at the bases of the dipoles and the dimensions of the LPDA are used to simulate the reflector antenna in the MIR program. In this FORTRAN program, incident field of the feed, pattern of the LPDA, can be found also. This simulated pattern in MIR was compared with the pattern obtained from MATLAB<sup>®</sup>, and HPBW's obtained from two program are sufficiently similar. This shows the consistency between the two programs written in MATLAB<sup>®</sup> and FORTRAN.

As a critical point in the design of the reflector antenna, active element in the LPDA should be placed in the focus of the reflector. But since the active region of the feed antenna changes with frequency, user should choose where to place the

antenna. Since the pattern is more sensitive to the displacement of the dipole from the focus at the high frequency range in the LPDA, smallest dipole should be placed at the focus of the reflector. Otherwise a null appears at the center of the pattern at high frequency.

When the diameter of the reflector is doubled, gain of it increases 6 dB. The diameter of the reflector is selected such that the gain of the reflector satisfies the gain value constraints. To be sure of the specified gain values are achieved, efficiency and blockage effect calculations for the reflector antenna at various frequencies are done and the gain reductions due to these effects are taken into account. Efficiency of the designed antenna is found approximately 45% at most of the frequencies.

As a future work, the reflector antenna which was designed and simulated can be constructed and measured to see if the simulation results are consistent with measurement results or not. LPDA was constructed using cylindrical transmission lines and dipoles, and all the mutual coupling calculations were made on these cylindrical structures. But during the construction process, it was noticed that it's very difficult to drill very small holes on the transmission lines, for the dipoles. Special drilling techniques like electron bombarding which are expensive should be used. If the transmission lines and the dipoles are cut from a metallic sheet, that's to say they are rectangular prism, with small thickness, instead of cylinder, the production process can be very easy and cheap. But in this process all the mutual coupling calculations should be changed according to the new structure of the dipoles. In the design process, when cylindrical transmission lines are used, characteristic impedance of the feeder line should be greater than  $105.6 \Omega$ . When the dipoles are cut from the sheet, the feeder impedance can be lower since the transmission lines are not cylinder as well and they are less prone to contact to each other.

## REFERENCES

- [1] Kraus, John D. and Marhefka Ronald J., *Antennas for All Applications*, 3rd edition
- [2] Balanis, Constantine A. (2002), *Antenna Theory Analysis and Design*, 2nd edition
- [3] Markov, G. (1965), *Antennas*
- [4] Collin, Robert E. (1985), *Antennas and Radiowave Propagation*, International Student Edition
- [5] Carrel, Robert Louis. (1961), *Analysis and Design of the Log-Periodic Dipole Antennas*, PH.D. Dissertation, Elec. Eng. Dept., University of Illinois, Ann Arbor,MI
- [6] Walter, Joachim. (1970), 'Solution of Maxwell's Equations for Log-Periodic Dipole Antennas', IEEE Transactions on Antennas and Propagation, Vol.AP-18, No:6
- [7] Stutzman, Warren L. and Thiele Gary A. (1981), *Antenna Theory and Design*
- [8] Jordan, Edward C. and Balmain, Keith G. (1968), *Electromagnetic Waves and Radiating Systems*, 2nd edition
- [9] Erzin, Salih Serhat. (1991), *Range Evaluation of the Anechoic Chamber in Aselsan® Inc.*, MSc Dissertation, Electrical&Electronics Engineering , Middle East Technical University, Ankara

- [10] Isbell, D.E. (1960), 'Log Periodic Dipole Arrays', IRE Transactions on Antennas and Propagation
- [11] Vito, Giuseppe and Stracca Giovanni B. (1973), 'Comments on the Design of Log-periodic Dipole Antennas', IEEE Transactions on Antennas and Propagation, Vol.AP-21
- [12] Vito, Giuseppe and Stracca Giovanni B. "Further Comments on the Design of Log-periodic Dipole Antennas", IEEE Transactions on Antennas and Propagation, Vol.AP-21, No:3, September, 1974
- [13] Kyle Robert H. (1970), 'Mutual Coupling Between Log-Periodic Antennas', IEEE Transactions on Antennas and Propagation, Vol.AP-21, No:3
- [14] Abd El-Samie Mostafa and Yacout El-Moazzen, 'Log-Periodic Dipole Antenna', Electrical Engineering department Alexandria University, Egypt, A.R.E.
- [15] Johnson, Richard C., (1993), *Antenna Engineering Handbook*, 3rd edition
- [16] Love A.W. 'Reflector Antennas', IEEE Press
- [17] Milligan T. (1985), *Modern Antenna Design*
- [18] Samuel S., (1984) *Microwave Antenna Theory and Design*
- [19] Rugde A.W., Milne K., Olver A.D., Knight P., (1982), *The Handbook of Antenna Design*, Volume 1
- [20] Lo Y.T. and Lee S.W., (1988), *Antenna Handbook Theory Applications and Design*

- [21] Johnson R.C. and Jasik H., (1987), *Antenna Applications Reference Guide*
- [22] Hall L., (1984), *The ARRL Antenna Book*, 14th edition
- [23] Connor F.R., (1975), *Antennas*, 2nd edition
- [24] Johnson R.C., (1991), *Designer Notes for Microwave Antennas*
- [25] IEE Conference Publications, *Antennas & Propagation (Part 1: Antennas)*,  
(1981)

## APPENDIX A

### MATLAB<sup>®</sup> CODE WHICH CALCULATES THE CURRENTS AT THE BASES OF DIPOLES AND E AND H-PLANE PATTERNS OF A LPDA

```
%design of 0.4-18 GHz log-periodic antenna
%calculates the currents at the bases of LPDA and E&H
%plane patterns of LPDDA

%tau= 0.865
%sigma=0.08
%alpha=22.87 derece...
%ln=0.46413m (the longest dipole )
%shortest dipole=0.00446 meter
%number of elements: 31

clear all;

eta=377; %ohm, for free space

h=zeros(31,1); %half length of the dipoles
                %first entry is the smallest distance
hmax=0.232065; %meter (half of the longest dipole)
tau=0.865;
for q=1:31,
    h((32-q),1)=hmax*tau^(q-1);
end
h;

dim=zeros(31,1); %diameters of the dipoles from
%shortest to longest
for p=1:31,
    if (p<=13)
        dim(p,1)=0.0003; %meter
    elseif (p>13)&(p<22)
        dim(p,1)=0.0005;
    else
        dim(p,1)=0.0008;
    end
end
end
dim;
```

```

tau=0.865;
spacing=zeros(31,1); %R1,R2... values from shortest to
%longest
spmax=0.4421;
for s=1:31,
    spacing((34-s),1)=spmax*tau^(s-1);
end
spacing;

sp=zeros(30,1);
sp=diff(spacing); %spacings between two dipoles
%starting from the shortest one

ZA=zeros(31,31);

    for a=1:31

        for b=1:31

            if (a==b)
                ZA(a,b)=MutCoup2(h(a),h(a),(dim(a)/2));

            elseif (a<b)
                sptot=0;
                for n=a:(b-1)
                    sptot=sptot+sp(n);
                end

                ZA(a,b)=MutCoup2(h(a),h(b),sptot);

            end

            ZA(b,a)=ZA(a,b);

        end

    end

    ZA

YA=inv(ZA)
Zc=141.26; %ohm
Yc=1/Zc %characteristic admittance of the %transmission
line

% YN2*2 line matrices. Transmission line %admittances %
will be calculated
lambda= 0.3; %meter
B=2*pi/lambda;

```

```

l=zeros(30,1);
length=0.44421;    %length=R29
tau=0.865 ;
for m=1:30
    l((31-m),1)=length*tau^(m-1)-length*tau^m
end

l;

Yn=zeros(30,4);
for a=1:30
    for k=1:2
        if k==1
            Yn(a,k)=Yc/(j*sin(B*l(a)))*cos(B*l(a));
            Yn(a,k+3)=Yn(a,k);
        else
            Yn(a,k)=Yc/(j*sin(B*l(a)));
            Yn(a,k+1)=Yn(a,k);
        end
    end
end

%31*31 overall YN matrix is as follows:

YNmatrix=zeros(31,31);

for a=1:30
    for b=1:2
        YNmatrix(a,a+b-1)=YNmatrix(a,a+b-1)+Yn(a,b);
    end
    for b=1:2
        YNmatrix(a+1,a+b-1)=YNmatrix(a+1,a+b-
1)+Yn(a,b+2);
    end
end
YNmatrix;

Zl=10000; %load impedance is opened
Yl=1/Zl;
    YL=zeros(31,31);
    YL(31,31)=Yl;

% Combined Y matrix is:

Ycombined=YA+YNmatrix+YL

Is=1 %amper;

```

```

M=zeros(31,1);
M(1,1)=Is;

V= inv(Ycombined)* M;

% Final result: currents at the base of the dipoles %of
LPDA(first entry corresponds to smallest dipole)

I= YA*V

lamda= 0.3; %f=1GHz
k=2*pi/lamda;

theta=linspace(0,2*pi,361);
phi=linspace(0,2*pi,361);

E_theta=0;
E_phi=0;
r=10; %meter

%E plane pattern, xz plane, phi=0;

for a=1:31,
E_theta=E_theta+((j*eta)/(2*pi*r*sin(k*h(a))))*exp(-
j*k*r)*(I(a)*exp(j*k*spacing(a).*sin(theta)).*...
((cos(k*h(a)).*cos(theta))-cos(k*h(a)))./sin(theta));
end

E_theta(1)=0.001;
E_theta(181)=0.001;
E_theta(361)=0.001;
figure(1)
t1=20*log10(abs(E_theta)/max(abs(E_theta)));
%t1=20*log10(abs(E_theta));
polar(theta,t1-min(t1));
Title('E plane pattern');

%H plane pattern, xy plane, theta=90;
for a=1:31,
E_phi=E_phi+((j*eta)/(2*pi*r*sin(k*h(a))))*exp(-
j*k*r)*(I(a)*exp(j*k*spacing(a).*cos(phi)).*(1-
cos(k*h(a))));
end

figure(2)
t2=20*log10(abs(E_phi)/max(abs(E_phi)));
polar(phi,t2-min(t2));
Title('H plane pattern');

```

## APPENDIX B

### MATLAB<sup>®</sup> CODE WHICH CALCULATES SELF AND MUTUAL IMPEDANCES OF LINEAR ELEMENTS

```
function Mut=MutCoup2(h,l,s) % h,l are the half %length
of the dipoles, s is the
lamda=0.3; %meter
k=2*pi/lamda;
d=0;
g=0;
b=((j*k*30)/((sin(k*h))*(sin(k*l))));

for t=-10000:10000
    z=l*t/10000;
    g=g+b*((exp(-j*sqrt((k*s)^2+(k*z+k*d-
k*h)^2))/sqrt((k*s)^2+(k*z+k*d-k*h)^2)...
    +exp(-
j*sqrt((k*s)^2+(k*z+k*h)^2))/sqrt((k*s)^2+(k*z+k*h)^2)-
2*cos(k*h))*...
    exp(-
j*sqrt((k*s)^2+(k*z)^2))/sqrt((k*s)^2+(k*z)^2))*...
    sin(k*(l-abs(z)))*2*l/20000;
end
g;
z=0;
x=b*((exp(-j*sqrt((k*s)^2+(k*z+k*d-
k*h)^2))/sqrt((k*s)^2+(k*z+k*d-k*h)^2)...
    +exp(-
j*sqrt((k*s)^2+(k*z+k*h)^2))/sqrt((k*s)^2+(k*z+k*h)^2)-
2*cos(k*h))*...
    exp(-
j*sqrt((k*s)^2+(k*z)^2))/sqrt((k*s)^2+(k*z)^2))*...
    sin(k*(l-abs(z)))*l/20000;

Mut=(g-x)
```

## APPENDIX C

### FORTRAN CODE WHICH CALCULATES SELF AND MUTUAL IMPEDANCES OF LINEAR ELEMENTS

```
C  MUTUAL IMPEDANCES WITH RESPECT TO THE CENTER POINTS
C  OF TWO PARALLEL DIPOLES
C  DISPLACED BY D/LAMDA, SEPARATED BY S/LAMDA AND
C  HALF LENGTHS H/KAMDA AND L/KAMDA .
C  SINUSOIDAL CURRENT DISTRIBUTIONS ARE ASSUMED.
C -----
C  IMPLICIT REAL*8 (A-H,O-Z)
C  INTEGER    GD1
C  PARAMETER  (GD1=82)
C -----
C  CHANGE GD1 IN THE SUBROUTINE GAUSS_LEGENDRE ALSO !
C  CHANGE GD12 IN THE SUBROUTINES GAUSS_LEGENDRE AND
C  XIWILE ALSO !
C -----
C  GD1 = # OF GAUSS POINTS (EVEN) ; positive values only !
C -----
C  INTEGER    I, GAUSS
C -----
C23456
C  REAL*8    T(GD1),W(GD1),
C  *          F, G, HL, LL, KH, KL, KS, KD, TKH
C  COMPLEX*16 ZM
C  COMMON    /PRMTS/KH,KL,KS,KD,TKH
C  DATA     PI/3.141 592 653 589 793 238 462 D0/
C -----
C  OPEN(UNIT=1,FILE='para.inp',BLANK='NULL',STATUS='OLD')

OPEN(UNIT=7,FILE='para.out',STATUS='UNKNOWN',FORM='FORMATTED'
)
C -----
C  TWOPI    = PI + PI
C -----
C  READ (1,*) HL, LL, SL , DL
C  READ  H/LAMDA, L/LAMDA, S/LAMDA , D/LAMDA
C  READ (1,*) GAUSS
C -----
```

```

WRITE(7,90)
90 FORMAT (/39X,'GAUSS DATA'/39X,10('=')//)
IF(MOD(GAUSS,2).NE.0) GAUSS = GAUSS - 1
CALL GAUSS_LEGENDRE (GAUSS, T, W)
WRITE(7,91) GAUSS
WRITE ( 7, 92 ) (T(I),W(I), I=1,GAUSS)
91 FORMAT (/39X,'GAUSS =',I3//24X, 'T(I)', 30X , 'W(I)//)
92 FORMAT (5X,D30.12,5X,D30.12)

```

C -----

```

KH = TWOPI*HL
KL = TWOPI*LL
KS = TWOPI*SL
KD = TWOPI*DL
TKH = DCOS(KH)
TKH = TKH + TKH
CNST = 30.0D0*KL/(DSIN(KH)*DSIN(KL))
X12 = 0.0D0
R12 = 0.0D0
DO 10 I = 1, GAUSS
WI = W(I)
TI = T(I)
DO 10 II = 1,2
IF(II.EQ.2) TI = - TI
X = KL * TI
CALL FUNC(X,F,G)
X12 = X12 + WI * F
R12 = R12 + WI * G
10 CONTINUE
X12 = CNST * X12
R12 = CNST * R12
ZM = DCMPLX(R12, X12)
WRITE(7,80) HL, LL, SL, DL, R12, X12
80 FORMAT(/5X,'HL=',F4.2,2X,'LL=',F4.2,2X,'SL=',F4.2,2X,'DL=',F4.2//
* 5X,'R12 =',E10.4, 5X, 'X12 =',E10.4)

```

C -----

```

CLOSE(UNIT=1,STATUS='KEEP')
CLOSE(UNIT=7,STATUS='KEEP')
WRITE(*,*) 'END OF EXECUTION : SEE para.out'
STOP
END

```

C23456 -----

```

SUBROUTINE FUNC(X,F,G)
IMPLICIT REAL*8 (A-H,O-Z)
REAL*8 F,G,CD,KH,KL,KS,KD,TKH,KS2,KR1,KR2,KR0
COMMON /PRMTS/KH,KL,KS,KD,TKH
KS2 = KS**2
KR1 = DSQRT(KS2+(X+KD-KH)**2)
KR2 = DSQRT(KS2+(X+KD+KH)**2)
KR0 = DSQRT(KS2+(X+KD)**2)

```

```

CD = DSIN(KL-DABS(X))
F = CD * (DCOS(KR1)/KR1+DCOS(KR2)/KR2-TKH*DCOS(KR0)/KR0)
G = CD * (DSIN(KR1)/KR1+DSIN(KR2)/KR2-TKH*DSIN(KR0)/KR0)
RETURN
END

```

```

C -----
C FOR THE GAUSS-LEGENDRE QUADRATURE NUMERICAL
INTEGRATION SCHEME

```

```

C ABSICCAS AND WEIGTHS ARE GENERATED IN THIS SUBROUTINE
C

```

```

SUBROUTINE GAUSS_LEGENDRE(GAUSS, T, W)
IMPLICIT REAL*8 (A-H,O-Z)
INTEGER GAUSS, GD1, GD12, N_r, N_r2, I_1
PARAMETER (GD1=82)
PARAMETER (GD12=164)
REAL*8 T(GD1),W(GD1),XI(GD12), WI(GD12)

```

```

C
N_r2 = GAUSS
N_r = N_r2 + N_r2
CALL XIWILE(-1.0D0, 1.0D0, N_r, XI, WI)
I_1 = N_r2 + 1
DO 11 I=I_1, N_r
T(I-I_1+1) = XI(I)
11 W(I-I_1+1) = WI(I)
RETURN
END

```

```

C -----
SUBROUTINE XIWILE(X1, X2, Nwx, X, W)
IMPLICIT REAL*8 (A-H,O-Z)
INTEGER GD12, Nwx, M, I, J
PARAMETER (GD12=164)
REAL*8 X(GD12), W(GD12)

```

```

C
Acc3 = 3.0D-14
M = (Nwx + 1) / 2
Xm = 0.5D0 * (X2 + X1)
XL = 0.5D0 * (X2 - X1)
DO 1 I=1,M
Z=COS(3.141592653589793238D0*(I-0.25D0)/(Nwx+0.5D0))
10 P1 = 1.0D0
P2 = 0.0D0
DO 2 J=1, Nwx
P3=P2
P2=P1
2 P1 = ((2.0D0*J-1.0D0)*Z*P2-(J-1.0D0)*P3)/J
PP = Nwx*(Z*P1-P2)/(Z*Z-1.0D0)
Z1 = Z
Z = Z1-P1/PP
IF(DABS(Z-Z1).GT.Acc3) GO TO 10

```

```
X(I) = Xm-XL*Z
X(Nwx+1-I) = Xm + XL*Z
W(I) = 2.0D0*XL/((1.0D0-Z*Z)*PP*PP)
1 W(Nwx+1-I) = W(I)
RETURN
END
```

C

---

## APPENDIX D

### MATLAB<sup>®</sup> CODE WHICH CALCULATES MUTUAL IMPEDANCES BETWEEN ORTHOGONAL ELEMENTS

```
I=1;
s=0;
a=0.006;
l=0.367;
lambda=0.3; %meter
k=100;
g=[0:k/2-1 k/2+1:k-1];
for m=0:k-1
    for n=1:k-1
        E=((((a*cos(2*pi*m/k))-(l/2))*exp(-
j*(2*pi/lambda)*sqrt((a*sin(2*pi*m/k))^2+(-
l/2+l*g(n)/k)^2+...
(a*cos(2*pi*m/k)-(l/2))^2))/sqrt((a*sin(2*pi*m/k))^2+(-
l/2+l*g(n)/k)^2+(a*cos(2*pi*m/k)-(l/2))^2)...
+((a*cos(2*pi*m/k))+(l/2))*exp(-
j*(2*pi/lambda)*sqrt((a*sin(2*pi*m/k))^2+(-
l/2+l*g(n)/k)^2+(a*cos(2*pi*m/k)...
+(l/2))^2))/sqrt((a*sin(2*pi*m/k))^2+(-
l/2+l*g(n)/k)^2+(a*cos(2*pi*m/k)+(l/2))^2)-
2*(a*cos(2*pi*m/k))...
*cos((2*pi/lambda)*l/2))*exp(-
j*(2*pi/lambda)*sqrt((a*sin(2*pi*m/k))^2+(-
l/2+l*g(n)/k)^2+(a*cos(2*pi*m/k))^2))...
/sqrt((a*sin(2*pi*m/k))^2+(-
l/2+l*g(n)/k)^2+(a*cos(2*pi*m/k))^2))/(-
l/2+l*g(n)/k))*I*sin((pi*g(n)/k)));
        s=s+E;
    end
end
-j*30/(2*pi)*s/(k*k)
```

## APPENDIX E

### TEST REPORT OF MECHANICAL STRENGTH OF THE LOG PERIODIC ANTENNA

ASELSAN HABERLEŞİM GÜVENLÜĞÜ VE GİZLİLİK BÖLÜMÜ COMMUNICATIONS DIVISION		ÜRÜN KALİTESİ MÜDÜRLÜĞÜ DENETİM İSTEK FORMU	
STOK NO:	DENETİMİ YAPACAK BÖLÜM:		
TANIM: Anten	EKLER:		
DENETİM NEDENİ / AÇIKLAMA: Kaynak mukavemetinin belirlenmesi			
MALZEMENİN BULUNDUĞU YER: Malzeme elden teslim edilmiştir.	MİKTAR:		
İSTENEN DENETİM: Kaynak mukavemetinin belirlenmesi	DENETLENECEK MİKTAR:	İLGİLİ DOKÜMAN / STANDARD:	
DENETİM İSTEYEN (BÖLÜM / KİŞİ): NST/MTM (ALİ LAFCI)	ONAYLAYAN: [Signature]	TARİH: 17/06/2004	İMZA:
DENETİM SONUCU (DOKÜMAN/STANDARD DEĞERİ, ÖLÇÜLEN DEĞER, SONUÇ): Malzeme kırık olduğundan uzun olan ilk dört çubuğa test uygulanabilmistiği. Sonuç: 14-15 kg uygulandığında malzemenin koptuğu tespit edilmiştir.			
EKLER:			
DENETLEYEN: A. RAMAZAN	ONAYLAYAN: D. AKSOY	TARİH: 18.06.2004	İMZA: [Signature]

90'

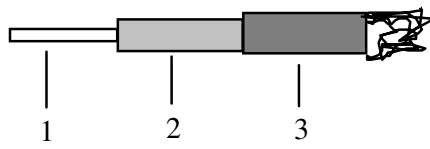
## APPENDIX F

### SPECIFICATION OF THE COAXIAL CABLE USED IN THE CONSTRUCTION OF LPDA

#### MATERIAL SPECIFICATION

**Manufacturer** : MICRO-COAX  
**Manufacturer`s Specification** : Semi-rigid coaxial cable  
(MICRO-COAX SEMI-RIGID COAXIAL  
CABLE CATALOGUE 1996)  
**Manufacturer`s Type Number** : UT -034-TP

#### Cable Construction



**1 Center Conductor** : SPCW , wire ,  $\varnothing$  mm = 0.2  
**2 Dielectric** : PTFE ,  $\varnothing$  mm = 0.66  
**3 Outer Conductor** : TIN / COPPER,  $\varnothing$  mm = 0.86

#### Electrical Data

**Impedance** : 50 OHM  
**Impedance tolerance** :  $\pm 1.5$  OHM  
**Capacitance** : 95.1 pF/m  
**Corona Extinction Voltage** : 750 volt rms at 60 Hz  
**Voltage Withstanding** : 2000 volt rms at 60 Hz  
**Moding Frequency** : 155 GHz

#### \*Attenuation :Typical values at 20 °C

<u>f (GHz)</u>	<u>Attenuation dB /100 ft</u>
0.5	34.0
1.0	48.3
5.0	110.4

10.0	158.6
20.0	229.1

**\* Power : Typical values at 20 °C**

<u>f (GHz)</u>	<u>Power watts CW</u>
0.5	30.5
1.0	21.5
5.0	9.5
10.0	6.6
20.0	4.6

\* : For detailed information ,see manufacturer's Catalogue

**Temperature range** : -40 °C to +125 °C

**Mechanical Data**

**Min. inside bending radius** : 1.27 mm  
**Weight** : 0.31 kg / 100m